Molecular Fluorescent Reporters for Force and Smart Surfaces for Sensing Cell-Surface Interaction

by

Mariya Barch

Submitted to the Department of Chemistry
in partial fulfillment of the requirements for the degree of

Doctor of Philosophy

at the

MASSACHUSETTS INSTITUTE OF TECHNOLOGY

September 2009

Author ... .
Department of Chemistry
August 21, 2009

Certified by ....
Paul Matsudaira
Professor of Biology and Biological Engineering
Thesis Supervisor

Certified by ... .
Matthew Lang
Professor of Mechanical Engineering and Biological Engineering
Thesis Supervisor

Accepted by .. ..
Robert W. Field
Chairman, Department Committee on Graduate Students

This doctoral thesis has been examined by a committee of the Department of Chemistry as follows:

Professor Moungi Bawendi ____
Professor of Chemistry
Thesis Committee Chair

Professor Paul Matsudaira ____
Professor of Biology and Biological Engineering
Supervisor

Professor Matthew Lang ____
Professor of Mechanical Engineering and Biological Engineering
Supervisor

Professor Alice Ting ____
Professor of Chemistry
Thesis Committee Member

Molecular Fluorescent Reporters for Force and Smart Surfaces for Sensing Cell-Surface Interaction

by

Mariya Barch

Submitted to the Department of Chemistry
on August 21, 2009, in partial fulfillment of the
requirements for the degree of
Doctor of Philosophy

Abstract

Molecular sensors are powerful because they make it possible to adapt the measurement to the sample instead of a sample to an instrument. Many reporter are available for measuring the chemical properties of a sample, but no purpose-built molecular sensors exist to report a sample's mechanical properties. To address recent interest in the mechanical coordinate of molecular interactions, we developed a prototype molecular sensor, calibrated its force-fluorescence relationship, and adapted the sensor to a cell adhesion assay. This thesis focuses on the considerations for combining force measurement with the environmental and distance sensitivity offered by fluorescence to measure cell-surface adhesion. We showed that DNA can be used as a scaffold to build a sensor molecule, that fluorescence can be used as a reporter of a threshold force, and that introducing cells to the sensor molecules changes the fluorescence properties. Because Cy3 experiences an enhanced intensity sensitivity when conjugated to DNA, the reporter's FRET signal was occluded and we instead activated the sensor complex as a novel, all-fluorescent means of reporting cell-surface proximity. This method for reporting cell-surface separation is significant because it simplifies measurements in thicker and more complex materials interesting to cell-substrate interaction studies.

Thesis Supervisor: Paul Matsudaira
Title: Professor of Biology and Biological Engineering

Thesis Supervisor: Matthew Lang
Title: Professor of Mechanical Engineering and Biological Engineering

Acknowledgments

I am deeply grateful to my advisor, Paul Matsudaira, for sharing with me his vision that has guided this exciting project. His always-open door and support gave me boundless opportunities both creatively and intellectually; I am grateful. I have also been blessed with the opportunity to work under the mentorship of Matthew Lang, who graciously accepted me into his lab and asked questions that will long guide me scientifically. I would like to thank Moungi Bawendi, for chairing my committee and throughout offering critical advice that has guided my experiments. I would also like to thank Alice Ting, for keeping me on my toes and on top of the authors of the literature.

I have been fortunate to work in lab with a wide range of expertise. The following people have always been available to help with experiments and answer questions at any hour of the day or night: David Appleyard, Lera Baru, Bob Burger, Carlos Castro, James Evans, Yelena Freyzon, Alec Robertson, Sangjin Ryu, David Shechner, Winston Timp, and Ben Zeskind. In particular, I thank Ricardo Brau and Peter Tarsa, with whom I worked closely and learned a lot about the scientific process from beginning to end. I would like to thank all the members of the Matsudaira and Lang lab for the many scientific discussions that have been educational and stimulating.

I have been blessed with great friends who have been with me to share the highs and lows of graduate school. The sense of humor, wisdom, and support of the following people created a much needed life-balance: Tai Sakuma, Michael Goldberg, Manas Mittal, Sarah Barkow, Christian Gonzalez, Alexander Barnes, the kids of E15.

I would like to thank my sister, Rena, whose character is truly inspirational. I am grateful to Hubert, from whom I learn something new every day. His patience, support, and LaTeXprowess have seen me the whole way through; I am fortunate to have had him in my life over these years. Finally, I would like to thank my parents, who have never told me what to do and always been supportive and encouraging. Their sacrifices gave me this opportunity to come to MIT. It has been a really special experience and I am endlessly grateful.

This thesis is dedicated to my grandfather, Adolf Levitanus.

Contents

List of Figures

List of Tables

Chapter 1

Introduction to optical methods for force measurement

Biological reporters have significantly improved the throughput, and more importantly access, to many physical and chemical characteristics of a system. Such molecular sensors have allowed us to visualize otherwise undetectable changes such as ion concentration, spatial distribution, polarity, hydrophobicity, and charge, among others. In the last 15 years, mechanical measurements brought a better understanding of their significance in biological questions. These new measurements motivated the development of metrics for characterizing a system mechanically. However, currently, relatively specialized instruments are required to address the mechanical properties of a system. One solution is to develop molecular reporters for these mechanical changes. In addition to improving throughput and access to a system's mechanical characteristics, such molecules would provide another dimension of information to supplement the physical and chemical processes we can already capture with available molecular reporters. Thus, in order to characterize the mechanical coordinate of a chemical reaction, we need to make sensors for force that integrate with conventional imaging methods.

The objective of this work is to develop force sensors that can be integrated with conventional microscopy techniques. By creating such sensors it is possible to image the distribution of force within a sample without the need for specialized force mea-

suring equipment. It is also possible to access force information in more complicated samples that are experimentally difficult to adapt to the requirements imposed by the instruments typically used to measure force, such as with three dimensional samples, for instance.

This work describes a prototype force sensor based on a DNA hairpin structure. To couple the sensed mechanical changes with microscopy, the molecule reports changes via fluorescence. The relevant scales for such a reporter are nanometer distances, and picoNewton forces. These scales are compatible with molecular interactions. A population of molecules can thus report a bulk molecular process; a population of reporters amplifies the molecular response to a level of signal detectable to conventional contrast schemes. The sensing exploits secondary structure of base pairing between complementary strands of DNA. The molecule can adopt two conformations, one with and one without secondary structure. The measurement is thus discrete, a force is reported if its magnitude is above a particular threshold. The reporter can therefore be used to measure a specific threshold force as determined by the thermodynamic stability of higher order molecular structures. More specifically, the sensor can measure the spatial distribution or population levels of the presence of a force of a set magnitude. This molecule cannot however yield a continuous force measurement based on the strength of energy transfer.

To confirm the ability of our molecular sensor to report force, we applied it in a cell adhesion assay. An advantage to this application is that the forces involved in adhesion are well studied and offer a platform for comparison. Furthermore, molecular sensors would allow mechanical measurements on cells to extend easily into three dimensions, an area that has been experimentally difficult to pursue because of either computational complexity associated with extracting quantitative information or the specificity of the method to two dimensions.

1.1 Fluorescence Sensitivity

Fluorescence microscopy is our choice for detection and imaging; fluorescent molecules provide a high contrast and high resolution method for collecting both spatial and temporal information within the cell. Several types of fluorescent molecules are readily available and have been adapted to many applications. Organic dyes have been modified and tuned for specific color, reactivity, and affinity for different solvents and environments. Fluorescent proteins make up another class of fluorescent reporter and can be modified with mutations that tune color and maturation rate. Inorganic molecules, such as quantum dots, have benefitted from optimized coating thickness, color and functionality variability. The range of photostabilities, colors, and conjugation properties has made fluorescent reporters a powerful means of addressing many biochemical reporting needs.

An additional advantage is that numerous fluorescent molecular reporters have been developed for biochemical sensing. For instance, sensing of metal ion concentrations [62], pH [11], chemical modifications [79], polarity [19], and hydrophobicity [68], among others. This versatility comes from the fact that the emission of a fluorophore can be recorded in several ways. Among them are emission peak wavelength (color), emission intensity, and energy transfer (a time resolved measurement) to an appropriate acceptor of the energy (as in a Förster resonance energy transfer (FRET) pair). In the energy transfer measurements, high FRET efficiencies correspond to a separation smaller than the Förster radius (5.3nm for Cy3 and Cy5) and decrease with distance as $\frac{1}{r^6}$. This dependence allows FRET-based sensors to report separation distances below the resolution of light microscopy. Examples of FRET reporters include indicators of phosphorylation state and Ca^{2+} concentrations [79, 62]. We take advantage of the reporting properties of fluorescence to create mechanical sensors that are minimally invasive and provide a direct measure of force.

1.1.1 Environment

Many fluorescent dyes experience a change in the orientation of dipole moment upon electronic excitation and their emission intensity, quantum yield, and lifetime are thus sensitive to microenvironement imposed factors such as polarity, pH, and viscosity. Other environmentally dependent pathways of relaxation that lead to lower fluorescence intensities (or non-radiative relaxation) include solvent mediated relaxation and intramolecular charge transfer (or twisted intramolecular charge transfer). The latter is made possible by a twist or rotation in the molecule's conformation in the excited state. The charge separation is associated with an increase in dipole moment, thus (twisted) intramolecular charge transfer is favored in polar environments, leading to lowered fluorescence intensities.

Luminescence, the light emission from a molecule, can be divided into two processes, phosphorescence and fluorescence. Phosporescence is a slow (milliseconds), weak emission process that results from non-spin-allowed (triplet) states. Alternatively, fluorescence, is a much brighter and faster (nanoseconds) process that results from spin allowed (singlet) states[1]. A fluorescent dye, often with an aromatic structure, requires an external energy source to promote an electron to an excited electronic state. Vibrational states are thermally accessible to the electron, and internal conversion (picoseconds) brings the electron to the lowest vibrational level within the electronic excited state. As a result, all electrons relax from the same vibrational level. Loss of energy, be it to internal conversion or solvent effects, leads to lower energy emission, resulting in the Stoke's shift. Consequently, the Stoke's shift is sensitive to environmental factors that contribute to energy losses on this scale.

Fluorescence spectra can also report environmental changes. Absorption is a femtosecond process and thus insensitive to collisions with quencher molecules, which in solution, occur on a much slower scale. The absorption is thus a measure of only

[1]The spin allowance refers to the ground state electron having the opposite spin than the excited state electron. Triplet states are accessed when spin conversion accompanies internal conversion (intersystem crossing). Transitions from triplet states to ground singlet states are spin-forbidden. As a result, molecules in triplet states become inaccessible to excitation-emission cycles.This is the suspected pathway for Oxygen-mediated collisional quenching.

the solvent shell immediately in contact with the dye molecule. The electronic coupling in the longer-lived static quenching complexes affect the fluorescent molecule's absorption spectrum. On the longer time scales associated with fluorescent dye emission (10-400ns), diffusion-limited (ns) collisions with quencher molecule can change the intensity of the emission spectrum. Furthermore, most fluorophores have larger dipoles in the excited state than the ground state and thus influence the dipoles of surrounding molecules more strongly. When solvent molecules reorient (10-100 picoseconds) during the excited state of the fluorophore (nanoseconds), the electron returns to an initially slightly different ground state. The extent of difference in energy is reflected in the Stoke's shift.

Another fluorescence property, sensitive to environmental conditions, is quantum yield. Quantum yield is the ratio of the number of photons absorbed by a fluorescent molecule to the number emitted. Quantum yield decreases when non-radiative relaxation processes compete with fluorescence emission in the excited state. Quantum yield is related to the fluorescence lifetime, the time a fluorophore spends in the excited state. When non-radiative relaxation competes with emission, the fluorescence lifetime decreases. Both of these properties are sensitive to environmental conditions, which may introduce competing non-radiative decay pathways.

1.1.2 Distance

A more general environmentally-sensitive phenomenon, fluorescence quenching, is a measure of fluorescence decrease relative to a reference. Sources of quenching include reactions in the excited state, ground state complex formation, energy transfer, molecular rearrangements, and collisional quenching. Fluorescence quenching only records the emission intensity ratio and thus can only report on relative intensity differences between two sets of conditions. Quenching is a good environmental indicator because it requires molecular contact (2Åseparations) and is thus sensitive to very short range interactions. Some molecular interactions lead to enhanced fluorescence, and are reported as positive quenching values.

Quenching commonly occurs in two forms. In one case, a fluorescent molecule

interacts with a quenching species in the ground state and, this interaction interferes with the excitation. This process is called static quenching and results from electronic coupling to molecules that yield non-fluorescent complexes. The second type of quenching results from non-radiative processes competing with fluorescence emission from the excited state. This type of quenching is dynamic quenching, and results from short-lived molecular contacts largely guided by diffusion processes that occur on timescales comparable to the fluorescence lifetime.

An example of an environmentally specific quenching process is the quenching due to unfavorable partitioning of fluorescent dye. As previously mentioned, quenching requires molecular contact. Consequently, factors affecting the probability and rate of molecular contact affect quenching. Such processes include steric shielding and charge interactions. The steric properties of the environment can structurally shield dyes from access by quenchers. It has previously been observed that fluorophores on surfaces of proteins, experience less quenching than those that are free in solution. This type of shielding likely extends to the surface of a covers lip. The polarity of the immediate environment must be considered. Another good example of steric shielding is the intercalation and partial intercalation of dyes into DNA. Here, the DNA shields intercalated dyes from collisional quenching to the extent that the dye is intercalated into the DNA[45].

Quenching can occur by several mechanisms. These mechanisms include: charge transfer complexes, electron transfer to scavengers, and singlet to triplet transitions, Förster-based quenching, contact-quenching, self processes such as intercharge twist, and collisional. For some of these processes the set of quenchers is broad (electron transfer: amines, acrylamides, metals, protons; intersystem crossing: oxygen, halogens, heavy atoms). For others, the quencher properties uniquely identify a few molecules (Förster-based quenching: an acceptor dye with spectral excitation overlap) [45].

Fluorescence resonant energy transfer (FRET) occurs when the emission spectrum of a donor overlaps with the absorption spectrum of an acceptor molecule, which may or may not be fluorescent. When the spectral overlap requirement is satisfied, the

donor and acceptor molecules couple to one another by a dipole-dipole interaction. The extent of FRET depends on three things: the amount of spectral overlap, the distance between the donor and acceptor species, and the relative orientation of the donor and acceptor transition dipoles. The spectral relationship is defined by the set of dyes, and the orientation of transition dipoles is set by the structural relationship between the two dyes and is often taken as an average value calculated for freely rotating dyes. The distance sensitivity, yields a "spectroscopic ruler" with about 10nm sensitivity, depending on the choice of dyes. The following equation relates the distance to the extent of energy transfer:

$$\text{EnergyTransfer} = \frac{1}{1 + \frac{r^6}{R_0^6}} \tag{1.1}$$

The 50% energy transfer distance is the Förster radius (typically 2-6nm). In images, FRET is usually reported as a ratio relative to a reference per pixel. This ratio can be of the donor in the presence and absence. Alternatively, with separately controlled excitation and emission filters, FRET can be reported as a ratio of intensities collected at the acceptor emission wavelength for excitation at donor vs acceptor wavelengths.

Fluorescence can be registered on several detector types. A sensitive detection method used for many of the techniques described above is the use of photomultiplier tube (PMT). PMT's generate current proportional to the light intensity (the number of photons) the PMT receives. These photons are translated into electrons and the charge into a quantifiable value. An alternative detection source is the charge coupled device (CCD). Microscopes equipped with CCD cameras can access spatial resolution with decent sensitivity.

The sensitivity of any of the fluorescent properties described above can be activated to report molecular processes. The choice of property depends on the time scale of the molecular process and the means of detection. In the experiments described in the following chapters, the requirement for spatial resolution rendered fluorescence microscopy ideal. With this detection scheme, we have some spectral control over excitation and emission and can return a two dimensional intensity array as a

quantitative map of molecular interaction, relative to a well defined reference. While intensity is the only available information given a set of excitation and emission wavelengths, it contains sensitivity contributions from all the processes outlined above. As an example, with clever experimental design, the intensity can be very sensitive to environmental changes that yield spectral shifts.

1.2 Force measurement

To investigate the mechanical coordinate of chemical reactions we are developing mechanical reporters that take advantage of thermodynamic properties of molecules and report by the same means. The forces a mechanical reporter can sense are in return directly correlated to the forces necessary to disrupt a thermodynamically stable interaction. To establish a system of scale, it is important to note that the interactions of interest occur on nanometer length scales, the corresponding relevant forces are on the order of picoNewtons, and the mechanical loads at these length scales are typically pN/nm magnitudes. The Gibbs free energy corresponding to the thermodynamic stability of interactions disrupted by these forces and the melting temperature vary. Within a living cell, k_BT is about 4pN/nm. The theory relating mechanical and thermodynamic principles of molecules follows.

In Newtonian mechanics, all forces can be modeled by some linear combination of mass, spring, and dashpot components and force is described by the familiar relationship F=ma. Table 1.1[2] summarizes some common sources of external forces. For molecular scale interactions, the forces with significant effects on molecules are elastic, viscous, thermal, and electrostatic. We propose mechanical sensor molecules to span the same range and start by reporting picoNewton force magnitudes. To target these magnitudes and tune sensing within this range, our sensors are based on thermodynamically stabilized interactions; each reporter adopts its conformation as a result of a favorable thermodynamic interaction (ie. hydrogen-bonding, hydrophobicity, charge) the more stable interactions require more work (force) to disrupt and

[2]Table adapted from reference[35]

Table 1.1: Examples of Forces Acting on Molecules

Type of Force	Magnitude (pN)
Collisional	$10^{-12} - 10^{-9}$
Gravity	10^{-9}
Magnetic	10^{-6}
Centrifugal	10^{-3}
Elastic	$1 - 100$
Viscous	$1 - 1000$
Electrostatic and Van der Waals	$1 - 1000$
Thermal	$100 - 1000$
Covalent	$10,000$

change the conformation. We generalize these forces as the work necessary to yield a predetermined mechanical separation (that we report with FRET) to explain the effect force has on the energy landscape of molecular events. The following section describes the equations relating force and energy stability as they are outlined in [15].

1.2.1 Energetics of force

To describe the effects of the above-mentioned forces within the realm of traditional chemical experiments, we can incorporate an extra work term into the first law of thermodynamics.

$$dE = dq_{rev} + dw_{rev} \tag{1.2}$$

$$= TdS - PdV + \int F \cdot dx \tag{1.3}$$

Here, F is an applied force and **dx** is a small distance in a chosen direction. Since work is not a state function, it is important that experiments maintain equilibrium. Equilibrium conditions will be assumed in the subsequent discussion.

The mechanics of single molecules can be related to bulk thermodynamic experiments through the ergodic hypothesis. While bulk experiments average over large populations of molecules sampling a variety of conformations, single molecule experiments average over time the conformations a single molecule can sample. Given a long enough length of time, under the same conditions, a single molecule will sample

the same probability distribution of conformations as an ensemble of molecules at one instant of time.

A Legendre transform yields the corresponding Gibbs free energy relationship, which depends on parameters more easily controlled in standard laboratory settings.

$$dG = -SdT + VdP + Fdx \tag{1.4}$$

Because temperature and pressure are easy to control, experiments can be done at constant temperature and pressures. As a result, the Gibbs free energy of a mechanically induced transition can be measured by integrating under the reversible force-extension curve.

$$G = \int_{x_1}^{x_2} F\mathbf{d}x \tag{1.5}$$

Similarly, enthalpy and entropy can be expressed in terms of force, by applying the relationship: G=H-TS. For these thermodynamic equations to apply, it is important that the described stretching events are reversible and that the relaxation curve reproduces the extension curve. When a molecule is stretched both the applied force and the distance change are positive. As a result, the work required to stretch the molecule is positive and so is the Gibbs free energy.

When an applied force causes a transition to occur, such that one stable species is converted into another. The effect of this force on the free energy of the reaction can be described by adding a force term to the zero-force free energy.

$$\triangle G(F) = \triangle G^0 - F(x_B - x_A) + k_B T \ln \frac{[B]}{[A]} \tag{1.6}$$

Here, [A] and [B] are single molecule properties and refer to the probabilities of populating a particular state, rather than the concentrations of each species. G^0 is the standard state free energy. At equilibrium,

$$\triangle G^0 - F\triangle x = -k_B T \ln K_{eq} \tag{1.7}$$

Where K_{eq} would be 1 at the critical force necessary to induce the transition. The transition from state A to state B is accompanied by a spontaneous change in length between the two points upon which the force is applied. The spontaneous increase in length corresponds to an increase in free energy. For a 100% efficient or reversible process, relaxation is accompanied by a spontaneous decrease in length and thus a decrease in the free energy.

Experimentally, as a molecule of DNA is stretched along its length or is unzipped along its base pairs, The force necessary to increase the $\triangle$x separation increases as $\triangle$x increases, because as the molecule is stretched fewer conformational states are available for it to sample and the entropy is decreased. When DNA is stretched along its length, it is elastic and the elastic energy is restored upon relaxation. The reversible nature of this stretching allows us to determine the Gibbs free energy by integration.

A useful interpolation equation for force-extension curves obtained from force experiments is the worm-like chain (WLC) for polymer elasticity. In the context of biological polymers, the model was initially described for DNA[58] but has since been successful for both polynucleotides and polypeptides.

$$F = \frac{k_B T}{P} \frac{1}{4(1-\frac{x}{L})^2} + \frac{x}{L} - \frac{1}{4} \tag{1.8}$$

Where L is the contour length, x is the distance between two points upon which the force is applied, F is the force, and P is the persistence length. The persistence length is higher for more rigid structures (a completely rigid rod has P equal to L). DNA has a persistence length of about 50nm. It is important to note that the WLC mainly captures the entropic contributions from reduced conformational freedom a stretched molecule experiences. However, as a molecule is stretched to $\triangle x$ values approaching L, enthalpic contribution becomes significant and the WLC model fails. An extension of this model is necessary for more extreme stretching conditions, where enthalpic terms have considerable contributions. Extension experiments with the PEVK region of titin showed that at physiological muscle conditions, both entropic

Table 1.2: Mechanical Properties of Selected Molecules

Molecule	$\triangle G$	F_u (pN)	$\triangle X^{\ddagger}$ (nm)	Structure at breakpoint
dsDNA	1.5-3[4]	9-20	–	DNA base pairs
P5ab hairpin	37.5±4.8	14.5±0.4	11.9	RNA base pairs
Titin I27 dm.	7.6	~100	0.59	parallel β-sheet shear
Titin I28 dm.	3.0	257±27	0.25	parallel β-sheet shear
Fibronectin[5]	-	74±20	0.38	antiparallel β-sheet shear
Spectrin	4.8±0.5	25-35[6]	1.7±0.5	α-helix bundle
Ubiquitin	6.7	203±35[7]	0.25	β-sheet shear

and enthalpic terms are relevant[53].

Table 1.2.1[3] compares the measured unfolding forces (F_u) with the corresponding mechanically induced separation $\triangle$x, the Gibbs free energy, and the structures that 'break' for each of the studies. The table summary suggests that it is not trivial to predict mechanical stability from Gibbs free energy or melting temperatures. Within a set of similarly stabilized structures, relationships are linear. Nucleic acid duplexes, for instance, increase in strength with increase in GC content and duplex length as predicted thermodynamically. Nucleic acids with tertiary structures (RNA) require a more complex analysis, but can also be described within thermodynamically predictable trends. Comparing different thermodynamically stabilized structures, no clear relationship is observed between the mechanical and thermodynamic stabilities. Global generalization to entire proteins is even more challenging because tertiary and quaternary relationships make it difficult to isolate individual structures of interest while understanding them within their local environment.

While neither Gibbs free energy nor temperature seem to effectively predict the mechanical stability from one structure to another, it is possible to predict the mechanical stability from three parameters: the distance of the transition state along a reaction coordinate, the height of the energy barrier of the transition state, and the loading rate[51, 15]. The following equation, derived from the multiple state treatment of force to induced thermodynamic and kinetic energy landscapes (Equation 1.9), provides a measure of mechanical stability given all the variables can be

[3]Table adapted from [15]

determined.

$$F_u^* = \frac{k_B T}{\triangle x_{transition}} \ln\left(\frac{r \cdot \triangle x_{transition}}{k_{unfolding} \cdot k_B T}\right) \tag{1.9}$$

Here, the loading rate is $r = dF/dt$ in pN/sec, F_u^* is the most probable unfolding force (found from the peak of a statistical distribution of forces). In general, an earlier transition state along the reaction coordinate, corresponds to a higher critical force necessary to yield the transition; transition states farther along the reaction coordinate (larger $\triangle X^{\ddagger}$) require less force induce the transition. As an example, shorter range interaction such as hydrogen bonds that maintain secondary structure have closer transition states and require more force to break than longer range interactions such as hydrophobicity that maintain tertiary structures and have longer distances to their transition states.

Unfortunately, to predict the most probable unfolding force for an novel structure, information is necessary about the loading rate within its physiological context, the rate at which the structure unfolds, and the separation necessary to unfold the structure - all variables usually determined through precise experimental conditions. Some recent work in nucleotide studies has addressed this issue[89]. We are interested in isolating some of these thermodynamically stabilized structures and incorporating them into our reporter molecules to in turn sense forces of various strengths.

1.2.2 Methods for measurement

Current technology for measuring forces is usually based on measuring deflection of a beam of light such as with atomic force microscopy (AFM) and microneedle manipulation or applying an external field to a sample such as with optical and magnetic tweezers and laminar flow. Other methods rely on tracking beads embedded in a gel of determined compliance to mathematically calculate a force measurement such as with traction force microscopy. The technology available today spans several magnitudes of sensitivity to force ($10^{-14} - 10^{-9}$ N) and thus can be used to make mechanical measurements on both the molecular and cellular scales[16] (Table 1.3[8]).

[8]Adapted from reference[16]

Table 1.3: Comparison of instruments for force measurements

Methods	F_{minmax} (N)	X_{min} (m)	Stiffness (N m^{-1})	Practical advantages
Mechanical transducers[9]				
Cantilevers	$10^{-11} - 10^{-7}$	10^{-10}	$0.001 - 100$	High spatial resolution Commercially available
Microneedles	$10^{-12} - 10^{-10}$	10^{-9}	$10^{-6} - 1$	Good operator control Soft spring constant
External field manipulators[10]				
Flow field	$10^{-13} - 10^{-9}$	10^{-8}	n.a.	Rapid buffer exchange Simplicity of design
Magnetic field	$10^{-14} - 10^{-11}$	10^{8}	n.a.	Specificity to magnets Ability to induce torque
Photon field	$10^{-13} - 10^{-10}$	10^{-9}	$10^{-10} - 10^{-3}$	Specific manipulation High force resolution

Unfortunately, much of this type of commercially available technology is expensive, highly specialized, indirect, and often invasive when applied to sensitive biological samples. We seek to develop molecular sensors to measure forces with standard microscopy techniques (via optical readout). However, to develop such molecules, we still rely on the methods above for calibration. We are particularly interested in sensing molecular forces, and can easily access this range (about 10-150pN) with an optical trap. Furthermore, to develop reporters with optical readout, it is especially appropriate to use an optical trap setup with the ability to measure combined and coincident fluorescence and force. Still, the single molecule measurement serves as an exact calibration. In order to collect information from a population of molecule, we also measured molecular response in bulk but in an isolated system before proceeding to make measurements on biological systems with variable sources of noise.

The optical trap

An optical trap delivers pN forces with nm displacement precision. This fine control is made possible by tightly focusing a laser through a high numerical aperture objective. Incident photons transfer momentum to a nearby dielectric particle. This momentum transfer can be decomposed into two components: scattering and gradient force. Scattering force acts in the photon-incident direction. Incident photons are

scattered in all directions and their net contribution to force is mostly canceled. Some photons are absorbed and impart force in the direction of their propagation; this is the direction of the scattering force. Gradient force pushes particle according to the spatial light gradient. A dipole in an inhomogeneous field is forced in the direction of the gradient. The dipoles induced by the laser into the dielectric particle interact with the inhomogeneous intensity gradient to impart gradient force upon the particle. For the gradient force to be strong enough to balance the scattering force, the the intensity gradient has to be steep. This is possible by focusing a laser through a high NA objective to a diffraction limited spot. This discussion is adapted from [64].

There are two regimes of scattering that depend on size of trapped particle: Mie scattering and Rayleigh scattering. Mie scattering applies to particles much larger than the incident wavelength and the index of refraction of the dielectric bead, in turn determines the angle of refraction of the laser light and thus the net direction of the imparted force. Higher indices of refraction bend light towards center. Rayleigh scattering applies to particles much smaller than the laser wavelength by treating them as point dipoles. In practice, the particle tends to be comparable to laser wavelength. To explain this regime, theoretical models have provided more complete theories.

The force attainable by an optical trap depends on maximum trap stiffness and is controlled by the laser power. The maximum force at the specimen plane achieved with micron-scale beads is about 1pN/10mW. Laser power typically ranges mW to about a Watt (measured in the specimen plane) and depends on a the optical configuration of the system. An important consideration is that to make measurements on biological samples, laser wavelength must be considered. Biological samples are 'transparent' to wavelengths 750-1200nm (Nd:YAG). This fact plus the multi functioning with fluorescence lead to the longer wavelength criteria for trapping lasers. For non-biological samples, the wavelength is a less significant criterion for trap stability and power.

An optical trap can be built by modifying an inverted microscope with a high numerical aperture objective, a stable laser source (with a single mode output), and

beam expanding and guiding optics. Independent of the laser power, the efficiency of the trap (power vs stiffness) is most sensitive to the choice of objective. The numerical aperture determines the ability of the objective to tightly focus the incident laser beam. The focus of the trapping beam has an axial trapping range of about 5-20 μm from the surface. The position of the beam is determined by imaging the trapping beam (or a low power detection laser) on a quadrant photodiode (QPD). The quadrants of the QPD are summed pairwise and normalized by the total signal from the four quadrants. A dichroic mirror can be incorporated on the condenser side to filter out specimen scatter and use the trapping beam to detect position directly. Axial position can be detected from the total intensity at the back focal plane of the condenser and takes advantage of the interference of light scattered off the bead and un-scattered light. A Guoy phase shift (π) is collected by the light traveling through the focus of the beam. When light is scattered by a particle near the focus, the phase of that light, acquired prior to scattering is preserved. Light that is not scattered will collect the full Guoy phase shift. The interference of the two phase shifted beams yields an axial-position dependent intensity. Position control is most precisely achieved by acousto-optic deflectors (AOD). An AOD is a a transparent crystal inside of which an optical diffraction grating is generated by the density changes associated with an acoustic traveling wave of ultrasound. AODs can control trap position (through deflection) and stiffness (through light level). A pair of AODs provides x and y control. Use of AODs leads to about 40% power loss. Position control of the specimen relative to the trap is achieved with a piezoelectric stage. The precision control is high and limited only by the rate of communication with the stage 50Hz. Precise measurement of mechanical processes requires mechanical isolation of the system, which can be achieved with an air table.

The optical trap is a Hookian spring and thus governed by $F = \alpha x$. Where α is the stiffness, and x is the displacement from the equilibrium position of the trap. The displacement of the molecule from the center of the trap can be determined for a trap whose position and stiffness have been calibrated. The position of the trap can be calibrated by scanning a stuck bead across the detection range. In other words, a

bead with known position is translated defined amounts, and the signal on the QPD is recorded in an xy (nm) position plot.

The stiffness of the trap is most commonly determined in one of three ways: frequency roll-off, equipartition, and drag. The power spectrum for the thermal fluctuations of a trapped bead in a harmonic potential fits a Lorentzian and and relates the roll-off frequency, the drag on the particle, and the the stiffness: $f_0 = \alpha(2\pi\beta)^{-1}$. The drag, β, can be determined form Stoke's law: $\beta = 6\pi\eta\alpha$ if the bead is free in solution and far from the surface. The drag calculation is more involved in the more frequent case where the bead is close to the surface. Axial stiffness can be determined from the axial power spectrum, but the drag in the axial direction is more difficult to to evaluate. The third method of stiffness calculation, equipartition, is independent of the drag term: $\frac{1}{2}k_BT = \frac{1}{2}\alpha < x^2 >$. With the equipartition method, position variance of a trapped bead is measured. The displacement variance here is also related to the position power spectrum of a calibrated detector.

1.3 Fluorescent force reporter

The DNA polymer has been well studied mechanically. DNA's well controlled length and structure render it a good candidate scaffold for a molecular sensor. The optical trap setup described above has been adapted to measure force and fluorescence. As a result, modifications to the polymer scaffold can benefit from the precision of the delivered forces. The following is a discussion of mechanical properties of a set of polymers and the requirements for adapting one such polymer as a molecular sensor.

1.3.1 Biological polymers

Mechanical studies of biological polymers (such as proteins, DNA, and RNA) have characterized chemical and mechanical aspects of folding, processivity, stability, and the energy landscapes of these processes. Some studies have also hinted at the relationship between the chemical and mechanical reaction coordinates, naming this field of study: mechanochemistry. It has even been suggested that mechanical pertur-

bations necessary to molecular investigations are more physiologically relevant than those of temperature within a live cell. However, the relevance of these investigations to our sensor molecules is a general appreciation for how different thermodynamically stable relationships yield to mechanical loads.

Force extension experiments of both double and single stranded DNA molecules varying in length and sequence have characterized DNA by applying a force along both its helical axis and perpendicular to it to measure the unzipping forces[30, 70]. Additionally, the forces required to pull the double stranded DNA along its vertical axis and to unzip it are both sequence dependent[70]. The unzipping of high percentage A-G sequences requires about 9pN $\pm$ 3pN and high percentage G-C sequences require about 20pN $\pm$ 3pN by optical trap measurements[70, 90]. Similar magnitudes were obtained in AFM experiments[24] and microneedle-based mechanical manipulation studies of sequence-force dependence within 100-500 base regions of a bacteriophage λ DNA[24]. More recent experiments on DNA hairpin molecules show the G-C content of a stem sequence, the loop length, and the stem length determine the force needed to unzip a hairpin is dependent on a stem length up to 25 nucleotides[90]. Further studies have reported effects of single base mismatches on the properties of the transition state profile[89]. Mechanical studies of RNA show similar secondary structure stabilities to those of DNA. However, RNA's ability to readily form tertiary structures in the presence of Mg^2+ accounts for some more stable RNA-based structures[54].

Mechanical studies have also given proteins a fair amount of attention, both to understand their physiological role in the mechanical environments they regulate and to gain some insight into the properties of protein folding as a whole. Three classes of proteins subject to mechanical experiments have been proteins that undergo a transition in state at β structure 'breaking point', at an α structure 'breaking point', and molecules that drive the machinery of the cell (molecular motors). Molecular motors convert ATP into mechanical energy that drives protein degradation, DNA and RNA translocation. These proteins include helicases, chaperonins, proteosomes. Many of these molecular machines have been studied[27, 18, 91, 9]. All of these apply

mechanical work upon their substrate to perform their function.

Mechanical properties of molecules with tandem repeats of structural domains, of which many are responsible for maintaining the integrity of a process or structure, have also been studied . The proteins investigated thus far have elucidated the mechanical stability of alpha and beta-based tertiary structures. Titin (sacromeric muscle contraction protein) and tenascin (cell adhesion and motility mediating protein), for instance, have tandem repeats of β-barrel domains that are responsible for the saw-tooth pattern common to the force-extension curves showing individual unfolding of each domain [82, 66]. Experimentally, when a mechanical load is applied to a protein, the protein is pulled apart from the outside (the internal core remains intact), for example, one β-sheet at a time. Spectrin (a molecule whose flexibility is important to the integrity of erythrocytes) also has tandem repeats, but their tertiary structure is based on coiled-coil interactions. Studies with titin and spectrin show that β-sheet stabilized tertiary structures (fibronectin and immunoglobuliin domains) are 5-10 times stronger than α-helix stabilized tertiary coiled-coil interactions (spectrin repeats)[57]. It is important to note that, although the individual protein domains can be repeatedly folded and unfolded[71], after several domains are unfolded, some percentage of the domains remain denatured and does not reversibly relax[39, 57]. Therefore, unlike with the RNA folding studies, the protein folding problem is more difficult to solve with mechanical experiments.

1.3.2 Molecular force sensor

The polynucleotides and polypeptides described thus far have thermodynamically stable structures that comply with the two state (structured and random) thermodynamics and kinetics outlined above. The two state sensor system provides a discrete one-bit (per reporter) signal in response to a mechanical stimulus. Current technology for reporting traction forces (commonly described by a vector field) either relies on a complex computation that requires assumptions to deduce a unique solution (tracking displacements of embedded beads) or limits cell migration to an array of flexible posts or cantilevers[52]. Molecular force sensors provide a means to report

vector fields of traction forces based on threshold forces exerted by cells. As a cell migrates along substrate or matrix immobilized sensors, a map of threshold force will be generated; the presence of a force strong enough to yield the transition between the presence and absence of thermodynamically stabilizing interactions for a particular sensor will be mapped.

A single sensor may not provide a wealth of information relative to the current methods, but several sensors spanning the force range relevant to leading-edge adhesions, cell contraction, and rear-of-the-cell release may be sufficient to capture the mechanical regimes important to cell locomotion. Our emphasis is on measuring the traction forces exerted at the focal adhesion complex connecting the intra- and extra-cellular machinery via the membrane-bound integrins. The traction forces are primarily a function of actomyosin contraction, which contracts the cell through the actin cytoskeleton and the focal adhesions. This contraction yields forces that pull at the leading edge of the cell and release the adhesions at the rear of the cell. The result is a net force in the direction of migration. Traction forces are reported in the hundreds of picoNewtons to tens of nanoNewtons range. The forces at a focal adhesion complex of a fibroblast cell have been estimated to be several nanoNewtons[73]. The proposed sensors will be immobilized within the substrate or matrix and will include a ligand to the integrin (an RGD peptide sequence). Therefore, the sensor design requires the net sensitivity to be on the hundreds of picoNewtons to several nanoNewton range. However, the focal adhesion complexes are many-molecule congregations (of integrins and ligands, for example) and a single sensor does not need to be of nanoNewton sensitivity to map the threshold forces that capture processes key to cell locomotion.

In fact, since the force necessary to yield a transition between two states is related to the loading rate, r (Equation 1.9), to determine the suitable range of force sensors, it is important to consider the 'loading rate' that a motile cell may apply to a sensor. Cells move on the order of one cell body per hour (30μm/60min). Focal adhesions range in size up to several micrometers in diameter. The stresses (force/area) reported for cell motility from bead tracking calculations are $11\text{pN}/\mu\text{m}^2$

- 19nN/μm^2. Thus, motile cells apply loading rates of roughly 3pN/sec-160nN/sec. The mechanical measurements summarized in Table 1.2.1 were carried out with an atomic force microscope at stretch rates of 600nm/sec. Given a typical cantilever stiffness of 10pN/nm, the experiments in Table 1.2.1 range in loading rate 3pN/sec - 6nN/sec. These measured transition forces are often roughly linearly dependent on pulling speed. In this accord, we propose that sensors for tens of picoNewtons and hundreds of picoNewtons should address the magnitudes relevant to traction forces.

In the last decade, many experiments and methods have been developed to understand the forces involved in cell motility. Until recently however, the focus has been on understanding forces in two dimensions and many of the methods described are limited to two dimensional analysis of traction forces. Cells in three dimensions have a different (spindle-like) morphology, and the composition of their focal adhesion complexes is different than in two dimensions. The molecular force sensors described in this report will extend well to 3-D studies as well.

Modular design

To address the modular requirement of the design, the sensing, reporting, and functionality parts of the sensor need to be independent. For a DNA hairpin, the parts are as follows: the stem of the hairpin serves as the force sensing module, the flanking arms of the hairpin serve as docking areas for the reporter module, and the five and three prime terminal ends of the arms are activated for functionality. The loop of the hairpin allows the measurement to be carried out multiple times.

The hairpin step makes up the sensing module. The complementary base pairing within the stem stabilizes the oligunucleotide's secondary structure. Addition of energy be it thermal, mechanical, or chemical, can, under the right conditions, disrupt the secondary structure. The resulting melted,unzipped, or denatured molecule, adopts a single stranded configuration. We are interested in the hairpin's application as a force sensor and will rely on the mechanical unzipping events to transition between the open and closed hairpin structures. The conformation then determines the presence/absence of a mechanical load. The thermal and chemical contributions are

controlled to isolate the mechanical unzipping.

The reporting module consists of a pair of fluorophores with spectral overlap such that the higher energy fluorophore relaxes and gives off energy in the excitation range of the lower energy fluorophore, making FRET possible. This pair of fluorophores is confined to the base of the hairpin allowing them to be within their Förster radius (for Cy3 and Cy5, for instance, this distance is 5.3nm). The fluorophores are modifications to synthesized oligonucleotides that are complementary to the flanking arms of the hairpin. One fluorophore is a five prime modification and the other a three prime modification, when the complementary strands are annealed to form an entirely duplex structure, the fluorophores are confined and energy transfer becomes a reported measure of the conformational state of the molecule. The open conformation adds twelve nanometers to the distance between the fluorophores and the energy transfer relationship is lost.

The functionality module consists of two parts. It is the most dynamic from experiment to experiment and is located at the five and three prime termini of the oligonucleotide sequence. The functionality allows the molecule to either be anchored to a species of interest or to present receptors for species to bind to. There are several functionalities that can be added during oligonucleotide synthesis and make the attachment chemistry possible. The synthesized modifications are, antidigoxigenin, biotin, and a primary amine. The primary amine functional group allows me to build the necessary functionalities for each experiment. In general, I will always refer to the anchoring functionality that has chemistry complementary to a cover slip surface and a functionality that allows me to grab the molecule at the opposite end.

Experimental Considerations

To make a measurement repeatable and capable of reporting both application and removal of load, we turned to a hairpin design. Advantage is that by controlling the loop and stem length and sequence, the oligonucleotide forms readily in solution. Discreet vs Continuous. The advantage of having a continuous readout of an applied force, is that most often the applied force is continuous and when it is not, no information is

lost by having the ability to capture the application continuously. It is however much more difficult to quantify when relying on FRET because the fluorescence intensity relationship here is already so sensitive. The disadvantage of the discreet reporter is that information may be lost during the application of the load (because it is not reported). The discrete reporter only gives information about whether or not the load is applied and not the magnitude of the load.To report the magnitude, multiple discreet reporters are necessary. However, the signal of a discreet reporter is clear even in the noise of the system being measured.

There are two main modes of interaction between dyes at length-scales of less than 12nm. One dominates the 0-2nm distance range and is often called contact quenching. Contact quenching is an electronic coupling between molecules that maintains an attraction between them and keeps them within a preferred radius of one another. This relationship increases the strength of the interaction between the pair participating in contact quenching [59]. At separations of more that 2nm but less than 12nm (depending on pair of dyes), long-range dipole-dipole electronic coupling can give rise to FRET if the pair of molecules has sufficient spectral overlap.

To ensure our design satisfies the FRET regime, several nucleotides at the base of stem are left unpaired. Three thymidine residues are included flanking the GC rich stem to simultaneously discourage further secondary structure and to provide sufficient separation between the donor and acceptor pair to ensure FRET instead of contact quenching. FRET can be verified by comparing absorption spectra of the donor in the absence and presence (within 10nm) of the acceptor. In contact quenching mode, the absorption spectra differ, while in FRET mode, same overall shape is retained [32].

An important consideration in designing FRET assays with cyanine dyes is the quantum yield is considered in determining the Förster radius. The combination of the dye's linkage to the DNA and the ways it can interaction with the DNA structure yield sometimes strong differences in quantum yield and in turn the radius at which 50% of the energy is transferred[60]. This difference can be as large as several Angstroms between ss and dsDNA and would lead to inaccuracies if used as a molecular ruler.

In our case, the measurement resolution is binary and the transfer efficiency is not critical to the result.

Chapter 2

Single molecule sensor calibration

This section discusses the design and assembly of a molecular force sensor. The molecule is based on a DNA hairpin structure and takes advantage of the DNA's well characterized, chemical, physical, and mechanical properties. The design is modular and consists of sensing, reporting, and functional attachment modules. The attachment functionality allows the molecule to be anchored at its ends. For the two-dimensional case, the molecule is immobilized on a surface at one end and is capable of bearing a load at the other end. The mechanical load is transduced through the hairpin stem. Above a critical force, the duplex melts and yields a single stranded molecule. This conformational change is captured by a pair of fluorophores whose physical separation (from the conformational change) can be detected as a spectral change captured as the emission wavelength intensity ratio. We calibrated this prototype molecule to determine the critical force, 18pN, and confirm the corresponding loss of energy transfer in a single molecule experiment. In more complex environments, this calibrated sensor will be used to report discrete, threshold forces of 18pN. This section is adapted from [77].

Single-molecule techniques have been responsible for substantial advances in the field of biophysics. Among these approaches, single-molecule fluorescence resonant energy transfer (FRET) spectroscopy provides an experimental view of the structural properties of individual molecules, whereas optical-tweezers force microscopy allows direct manipulation of the reaction coordinate of a single molecule. However, the

simultaneous application of these techniques is complicated by optical-trap-induced photobleaching, which substantially reduces fluorophore longevity to unacceptably short timescales. Herein, we apply a general solution to this problem to calibrate the force-fluorescence relationship for a novel force sensor based on a DNA hairpin, in the first successful combination of optical trapping and FRET.

By alternately exposing the sample molecule to the optical-trapping and fluorescence-excitation lasers, we demonstrate the ability to reversibly manipulate a single molecule while simultaneously monitoring its structural configuration. This integrated measurement provides high-resolution mechanical control over molecular conformation with fluorescence-based structural reporting. The application of this technique for single-molecule exploration will lead to new experiments that employ combined optical trapping and single-molecule fluorescence for the simultaneous and active manipulation and monitoring of molecular structure in real time.

Single-molecule force microscopy and fluorescence spectroscopy reveal individual molecular properties that are clouded by the inherent averaging of ensemble methods. However, the individual approaches of these techniques often fail to uncover the interplay between applied mechanical forces and structural changes. A single measurement of a force-sensing molecule connects these two perspectives by directly manipulating a molecular reaction coordinate while simultaneously detecting localized structural effects.

Among the biophysical techniques capable of probing single-molecule properties, optical-tweezers force microscopy operates at piconewton force levels that are optimal for the detection of nanometer-scale conformational transitions. Likewise, single-molecule FRET spectroscopy provides complementary information about dynamic structural properties, including environment, orientation, and proximity, with comparable spatial resolution[29]. Previous efforts to combine these two techniques for a single, coincident measurement have been complicated by accelerated photobleaching rates induced by the high-intensity optical trap. Because of this effect, which is especially pronounced in common single-molecule FRET donor labels such as the dyes Cy3 and Alexa 555 [84], previous advances towards combining these techniques

have spatially separated the fluorescent markers from the optical trap [36] or have employed uniquely robust chromophores [46].

We recently described a broadly applicable solution to this problem by alternately modulating the fluorescence-excitation and optical-trapping beams, which dramatically reduced this phenomenon without compromising trap integrity [12]. Herein, we show that such an optical modulation can be adapted to extend the emission times of FRET-paired labels without otherwise affecting their photophysical properties. To demonstrate this technique, we describe the first combination of optical-tweezers force microscopy with the single-molecule FRET detection of a novel force-sensing molecule into a single, integrated method capable of actively controlling molecular structure while simultaneously monitoring the conformational state of a single DNA hairpin molecule.

2.1 Experimental Design

The mechanics of DNA hairpins have been studied at the single-molecule level and, thus, offer a benchmark for examining optical tweezers and single-molecule FRET in a combined arrangement. These structures, which are commonly used as a model secondary structure in nucleotides, are readily adapted for the mechanical exploration of conformational dynamics, as they undergo a length and sequence-dependent, reversible unzipping transition [54, 90]. Alternate constructs have been adapted for force-sensing applications, as well[30]. The range of force detection available to a DNA based sensor is thus bound by the sequence and length practical within the experimental constraints. Typically, AT rich sequences require about 9pN $\pm$ 3pN forces to unzip and G-C rich sequences unzip at 20pN $\pm$ 3pN, as determined by optical trap measurements [71, 90] and AFM experiments [24].

We have employed a DNA-based hairpin structure as a prototype molecular force sensor at the high range of unzipping force for DNA, about 20pN. As a sensor for molecular scale forces (10^1 – 10^2 picoNewtons) this 20pN range is on the low end, providing good sensitivity for a prototype molecule. Chemically, DNA provides an

excellent scaffold for building a variety of structures[74, 4], making it ideal for sensor applications where multiple functionalities are typically necessary. Taking advantage of these chemical and mechanical properties, we developed a molecule that can be integrated between two species of interest to sense and report changes in force between the two species.

We impose several requirements on the hairpin reporter. A molecular sensor must have the capability to sense force, to report the applied force, and provide functionality to integrate within the system of interest. A modular design, ensures that these three capabilities can be varied independently. A further consideration is reproducibility of the measurement. Ideally, a single sensor can report multiple cycles of load and release. Lastly, we aim to address molecular scale forces on the order of picoNewtons. Mechanical measurements of single molecules confirm the range of forces required to disrupt higher order molecular structures is about 10-150pN. The design takes advantage of higher order structures to develop the sensing module of the molecule. In the weaker range, DNA secondary structure, base pairing interactions provide a convenient and well tested paradigm.

To address the modular requirement, the sensing, reporting, and functionality parts of the sensor must be independent. For a DNA hairpin, the parts are as follows: the stem of the hairpin serves as the force sensing module, the flanking arms of the hairpin serve as docking areas for the reporter module, and the five and three prime terminal ends of the arms are activated for functionality. The loop of the hairpin allows the measurement to be carried out multiple times.

The hairpin stem makes up the sensing module. The complementary base pairing within the stem stabilizes the oligonucleotide's secondary structure. Addition of energy be it thermal, mechanical, or chemical, can, under the right conditions, disrupt the secondary structure. The resulting melted, unzipped, or denatured molecule, adopts a single stranded configuration. We are interested in the hairpin's application as a force sensor and will rely on the mechanical unzipping events to transition between the open and closed hairpin structures. The conformation then determines the presence/absence of a mechanical load. The thermal and chemical contributions are

controlled to isolate the mechanical unzipping.

The reporting module consists of a pair of fluorophores with spectral overlap such that the higher excitation energy fluorophore relaxes by energy transfer in the excitation range of the lower energy fluorophore, making FRET possible. This pair of fluorophores is confined to the base of the hairpin allowing them to be within their Förster radius (for Cy3 and Cy5, for instance, this distance is 5.3nm). Several unpaired bases are incorporated at the mouth of the hairpin to achieve the separation of 5.3nm. Without the extra bases, the fluorophores anneal to a smaller distance where short range effects, such as contact quenching, can falsely diminish the signal and increase the measured force of unzipping. The fluorophores are modifications to synthesized oligonucleotides that are complementary to the flanking arms of the hairpin. One fluorophore is a five prime modification and the other a three prime modification. As a result, when the complementary strands are annealed to form an entirely duplex structure, the fluorophores are confined and energy transfer becomes a reported measure of the conformational state of the molecule. The open conformation adds twelve nanometers to the distance between the fluorophores and the energy transfer relationship is lost.

The functionality module consists of two parts. It is located at the five and three prime termini of the oligonucleotide sequence. The functionality allows the molecule to either be anchored to a grounding point or to present ligands that can be bound. There are several functionalities that can be added during oligonucleotide synthesis and make the attachment chemistry possible. The synthesized modifications we use include, digoxigenin, biotin, and a primary amine. For the calibration experiment, a digoxigenin was incorporated at the 5' end and a sticky end was formed on the 3' end allowing sticky end ligation to a 1007base handle and thus attachment to a bead. The experimental setup is detailed below.

2.2 Experiments

A modification to the optical trap design described in Chapter 1, makes it possible to measure force and fluorescence simultaneously. By frequency modulating the trapping laser with the excitation laser to decrease the time of sample exposure to the strong trapping laser thereby increasing the life of the probe, while not compromising the stiffness of the trap. Under this implementation, the trap can deliver up to about 100pN loads and a Cy3 fluorophore can be monitored for about 80 seconds before it bleaches. With this significant improvement to fluorescence integrity, we made measurements on the DNA hairpin molecule.

The instrumentation was carefully aligned to ensure coincident illumination of the sample plane by optical-trapping (1064 nm; Coherent, Santa Clara, CA (USA)), position-detection (975 nm; Corning Lasertron, Bedford, MA (USA)), and fluorescence-excitation (532 nm; World Star Tech, Toronto, ON (Canada)) lasers. To confirm the integrity of the two functional attachment points and separate fluorophore labels, the FRET activity on individual slides was verified through wide-field imaging on an intensified camera, translation of a single chromaphore to a predefined pinhole region, and acquisition on two separate avalanche photodiodes (Perkin Elmer Optoelectronics, Fremont, CA (USA)). After slide verification, tethered beads were prepositioned in a 0.204-pN nm-1 optical trap using a custom automated centering routine (Labview, National Instruments Corporation, Austin, TX (USA)), and individual hairpins were loaded to estimate the conformational transition force. The fluorescence excitation, set to 532 nm and 500 W, was then uncovered, and the individual hairpins were loaded at 250 nm s-1 back and forth through several unzipping transitions. During this movement, the bead-position signals were filtered through an in-line anti-aliasing filter at 200 Hz (Krohn Hite, Brockton, MA (USA)) and then acquired at 20 Hz (Labview). The donor and acceptor fluorescence signals, which were also sampled at 20 Hz, were spatially isolated through a 200-m pinhole, spectrally separated by a 628-nm dichroic mirror (Chroma Technologies, Rockingham, VT (USA)), and focused through 5-cm focal-length lenses onto separate avalanche photodiodes.

2.2.1 Single molecule assay

We intend to measure the force required to induce a conformational change in the hairpin and register that change with fluorescence. To make this measurement, we immobilize the hairpin at one end to the cover slip via a digoxigenin-antibody linkage. At the other end, we attach a polystyrene bead displaced by a 1kb duplex tether. The tether displaces the rather large bead from the molecule and facilitates the distinction between hairpin-bound beads and non-specifically attached candidates. The bead itself provides a handle for applying a controlled force at the opposite end of the molecule, along the coordinate determined by the point of attachment. At the critical force, the DNA hairpin unzips and a 12nm increase in distance between the FRET pair, reverses the intensity relationship between the donor and acceptor.

Single molecule experiments are carried out in flow chambers. The chambers make it possible to use small sample volumes and evenly deliver and wash molecules to the surface. The flow chamber consists of a chemically etched cover slip and slide attached by double sided adhesive. The separation provided by the adhesive yields a flow chamber with a 20-50μl volume. To the chamber, we deliver anti-digoxigenin antibodies and allow the antibodies to non-specifically adhere to the surface of the cover slip. The remainder of the cover slip is blocked with casiene. Phosphate buffer, pH 7.4, with 0.1% Tween (to discourage non-specific interactions) is used in all the wash steps and flow chambers are incubated in a humidity chamber for all the reaction steps.

The hairpin molecule is prepared by ligating the DNA hairpin to a 1kb tether and attaching to a polystyrene bead. The digoxigenin functionality is included during DNA synthesis, but the attachment to the bead requires an additional step. We included a sticky end at the 3' end of the sequence to be ligated to a 1kb duplex handle. The handle is generated as a PCR product from a fimbrin construct, purified, and sticky end ligated to the 3' end of the hairpin. The PCR primers for the 1kb duplex individually include an abasic site and a biotin, as shown in Table 2.2. The abasic site produces the sticky end on one end of the duplex and the biotin primer contributes

a biotin moiety to the other side of the duplex. After ligation to the hairpin, a long tether with a biotin at one terminus, can be attached to a streptavidin polystyrene bead. The complete molecule can be immobilized on the cover slip surface by an antibody linkage and attached to a polystyrene bead through a biotin-streptavidin linkage.

The complete assay consists of the surface-treated flow chamber and the bead with hairpin molecule (Figure 2-1). The streptavidin beads are thoroughly washed and then incubated with the hairpin complexes, in solution, prior to introduction to the flow chamber. The stoichiometry at this step controls the density of surface molecules and must be titrated to achieve single molecule concentrations. High concentrations are problematic both for single molecule fluorescence imaging, and ensuring that each bead is only attached to the surface by one hairpin molecule (although the latter can be isolated more easily). The bead-associated hairpins are introduced to the flow chamber in the final incubation step and unbound molecules are removed in a final wash. The final wash buffer contains glucose oxidase to improve the longevity of the fluorophores. Wobbling beads tethered to the surface (Figure 2-4) roughly validate single molecule assay assembly.

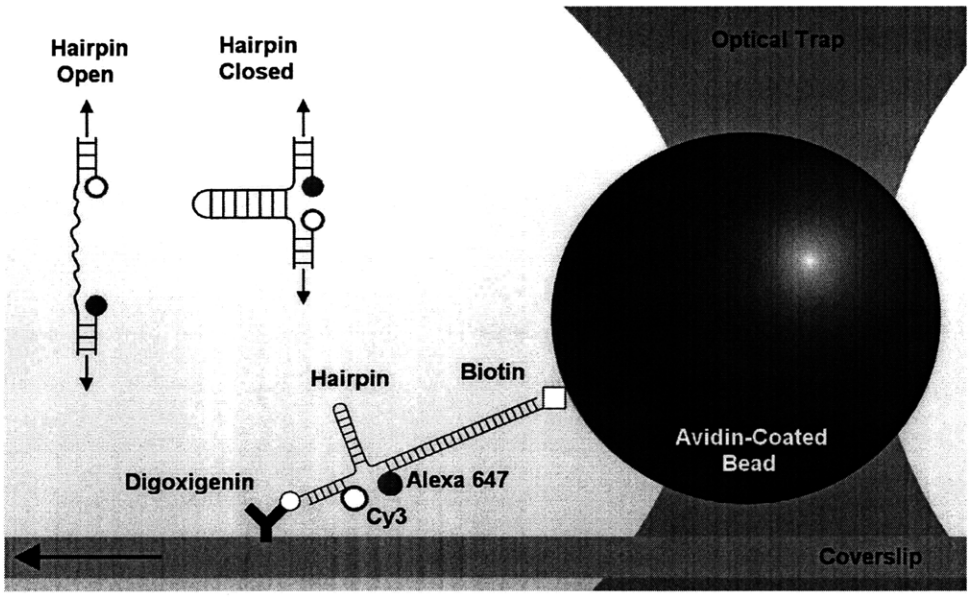

Figure 2-1: Single molecule assay design for force-fluorescence measurement.

A digoxigenin-labeled segment of single-stranded DNA with a 44-base self-complementary

Table 2.1: Oligonucleotides for Single Molecule Measurements

Name	Sequence 5'to3'
Dig.HP.100	Dig - GAT GAT GGT AGA TGA TGT ATT GTT GTT TCG CCG CGG GCC GGC GCG CGG TTT TCC GCG CGC CGG CCC GCG GCG TTT GTG GAG CTG AGA TGA GAT GGT ACT G
Cy3.25	Cy3 - CAA CAA TAC ATC ATC TAC CAT CAT C
30.AF647	GGA TCC AGT ACC ATC TCA TCT CAG CTC CAC - AF647

Table 2.2: Primers for 1KB Tethers

Name	Sequence 5'to3'
primer1	Biotin- CAA ATC ATC TGT TTC ATT GAA ACC TGA CAT G
primer2	GAT CC - Abasic - A TGG ATG AGA TGG CTA CCA CTC AGA TTT CC

internal sequence (Dig.HP.100; Integrated DNA Technologies, Coralville, IA (USA); detailed in reference [90] and shown in Table 2.1) was annealed at its ends to oligonucleotides labeled with Cy3 (Cy3.25;Integrated DNA Technologies) and Alexa 647 (30.AF647; Integrated DNA Technologies). This complex was then phosphorylated at its 5 end with polynucleotide kinase (New England Biolabs, Ipswich, MA (USA)) and ligated with T4 ligase (New England Biolabs) to a biotinylated 1007-base-pair segment of double-stranded DNA (PABX4T-fimbrin; primer 1, primer 2; Integrated DNA Technologies). Low concentrations of hairpin complexes were incubated with 750-nm avidin-coated polystyrene beads (Bangs Laboratories, Fishers, IN (USA)) and immobilized on an antidigoxigenin (Roche Applied Science, Indianapolis, IN (USA))-coated glass coverslip (Corning Life Sciences, Inc., Acton, MA (USA); Figure 1). Other assay conditions and force-fluorescence instrumentation were as previously described [12].

2.2.2 Force-fluorescence measurement

The polystyrene beads are a good indicator of the number of molecules tethered to the surface, but non-specific surface interaction of DNA molecules not tethered to the beads cannot be visualized in bright field. We must confirm that we are at single molecule concentrations to ensure the fluorescence collected through a pinhole is a

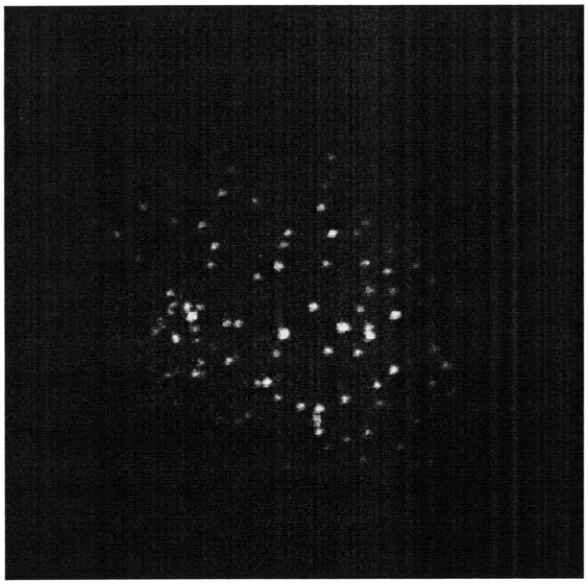

Figure 2-2: Single molecules are imaged upon an intensified CCD camera.

product of only one molecule. We ensure this by imaging the cover slip surface on an intensified CCD camera. A dark background with distinct bright spots determines the appropriate concentration relative to the starting materials. An example is shown in Figure 2-2. At the determined dilution, we can move one of the imaged fluorescent spots to the pinhole and monitor the fluorescence intensity on an avalanche photodiode. We can confirm that the fluorescence indeed comes from single molecules by recording a bleaching event. A single molecule bleaches in one discreet step as shown in Figure 2-3.

Candidate beads are selected based on the criteria above. Once the bead is trapped it appears static within the stiffness constraints of the trap, whose waist is raised from the cover slip surface. In this configuration the force application geometry is well defined. To apply a force to the hairpin molecule, the stage is translated relative to the trap. With a known, calibrated, trap stiffness, the recorded displacement of the stage can be related to a force. As a force is applied, the tether becomes taught. When the applied force reaches a critical value, the hairpin stem melts, and the overall molecule gains 12nm of slack. This 12nm gain in length is registered as a hitch in the mechanical trace as the bead displacement briefly changes relative to the trap. The reverse trajectory can be applied to close the hairpin. A hairpin that is maintained at

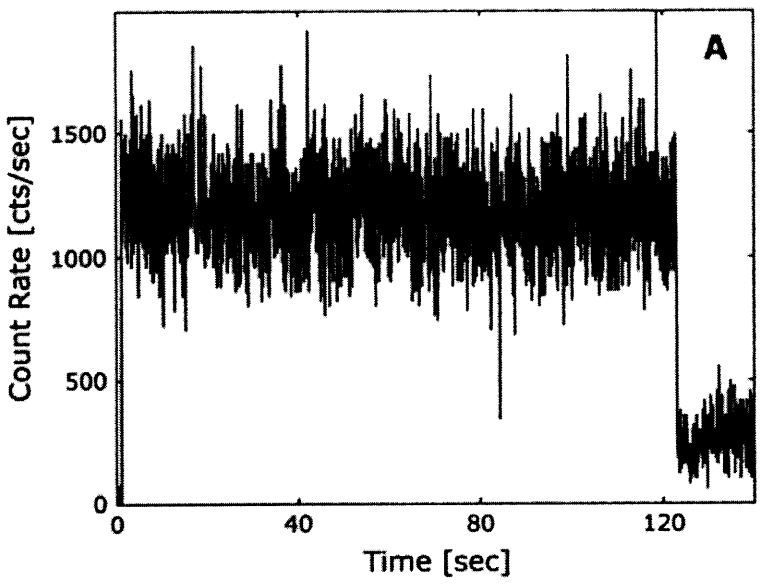

Figure 2-3: A single bleach event is seen as a step in the intensity plot measured with an avalanche photodiode. (Courtesy of R. Brau).

the critical force spends half the time in the open state and half the time in the closed state. Figure 2-5 shows an example of a molecule transitioning repeatedly between the conformations. The hairpin molecule experiences this critical force at 18pN.

Having confirmed the fluorescence and mechanical properties of the molecule, we measured them simultaneously. In this measurement we are monitoring the fluorescence of two fluorophores in two separate avalanche photodiodes, while using one excitation wavelength (535nm) to excite the donor Cy3 fluorophore. In the initial, closed hairpin, state only fluorescence from the acceptor (AF647) is observed. If an AF647 fluorophore photobleaches, the discrete bleaching step is accompanied by a step increase in donor (Cy3) fluorescence. The same process can be measured for a molecule under a load. The 18pN mechanical transition is accompanied by an anti-correlated step in the fluorescence traces. Figure 2-6 shows multiple cycles of the hairpin opening and closing in the fluorescence and mechanical traces.

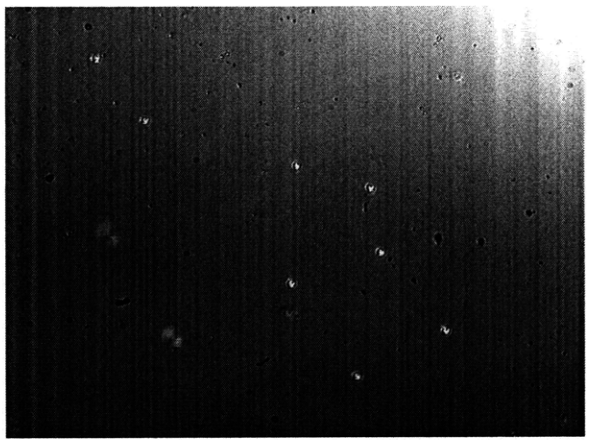

Figure 2-4: Successful surface attachment is confirmed by observing beads wobbling on the cover slip surface. Stuck beads do not experience Brownian motion and do not wobble. Beads not attached to the DNA, diffuse away from the cover slip.

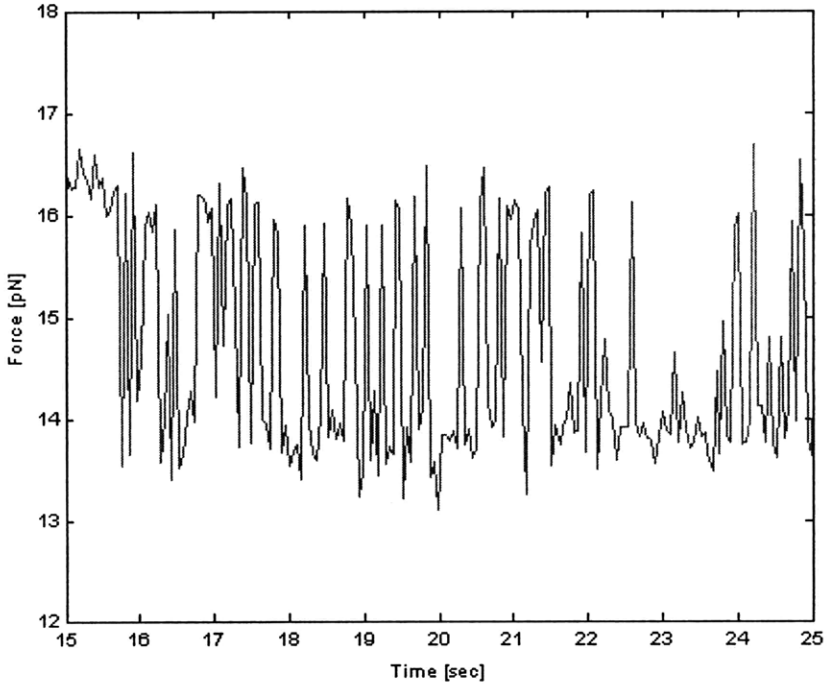

Figure 2-5: The hairpin yields at 18pN and we observe a hitch in the trace corresponding to an increase in length of 12nm. The hairpin can also be trapped at the critical force to show that it spends about 50% of the time in the open conformation and closed conformations.

2.3 Discussion

The structure used in this work, which contains a 20-base-pair hairpin stem, is flanked by non-complementary sequences annealed to oligonucleotides functionalized with the

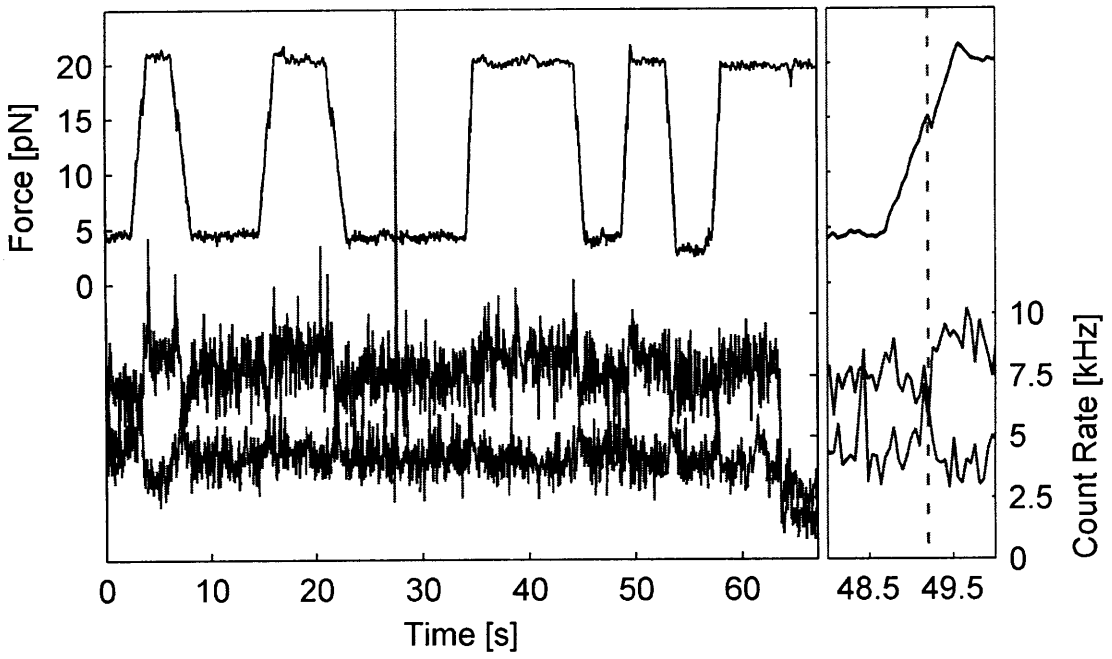

Figure 2-6: A simultaneous trace of the fluorescence and extension show that our sensor undergoes a FRET transition when the hairpin changes conformation between open and closed states.

fluorophores Cy3 and Alexa 647 (Figure 2-1). Complexes exhibiting single-molecule FRET emission were mechanically loaded with the optical trap, effectively reducing the energetic barrier to hairpin opening. This unzipping transition, which occurs at a force of approximately 18 pN, comparable to other similar measurements [90], was reflected by the displacement of the bead toward the center of the trap.

The conformational transition was accompanied by a simultaneous reduction in FRET efficiency caused by the increased physical separation of the Cy3 donor and the Alexa 647 acceptor, which indicated the precise location of the structural change caused by the translation of the mechanical load between the low-force (ca. 6 pN) and high-force (ca. 24 pN) states (Figure 2). The DNA complexes were moved through several transitions in a process corresponding to the reversible opening and closing of the hairpin segment, which demonstrated both the high degree of mechanical control and the simultaneous reporting by FRET emission. Furthermore, in the representative trace, single-step photobleaching of the donor after approximately 65 s verified the single-molecule measurement. Figure 2-6 summarizes the result.

This combination of optical-tweezers force microscopy and single-molecule FRET detection represents a significant advance for measuring the effects of structural changes on molecular function in a single molecule. By mechanically altering the conformational energy landscape, we actively induced a structural rearrangement pinpointed by strategically placed fluorescence labels. With minor modifications to existing assays, this approach can be extended beyond this model system to provide important new insight into the localized effects of mechanical force in biomolecular systems. For example, this combined technique can be adapted to monitor the intermolecular processes involved in the formation of a mechanically loaded protein complex [17], the effects of mechanical deformation on single-enzyme catalysis [20], or the intramolecular movements involved in biological-motor motility [10, 8].

In addition, the presence of quantized single-molecule fluorescence signals can provide unambiguous verification of the size and location of a mechanical event, a critical tool for the design of often complex single-molecule assays. The new perspective that arises from this ability to physically deform single molecules while simultaneously measuring structural changes will allow the design of novel force-sensing molecules and will permit a new class of experiments for probing the interrelationship between molecular structure and biochemical function.

Chapter 3

Force sensor for cell adhesion

The objective of this work is to adapt the hairpin sensor molecule, calibrated in the previous chapter, to a cell assay and use it to map the distribution of forces associated with cell adhesion. To adapt the reporter molecule for a cell assay, we incorporated a cell adhesion peptide at one terminus. Cells specifically adhered to sensor coated surfaces but did not register a strong change in FRET. We instead observed a differential decrease in fluorescence contributed by the cells to the donor and acceptor channels. This differential quenching of donor and acceptor obscures the calculated FRET ratio.

The calibrated molecular sensor was applied to cell adhesion measurements. Cell migration is a mechanical process that results from forces generated by a cell adherent to the surrounding extracellular matrix. Integrin receptors integrate the mechanical and signaling cues and transmit them to generate a mechanical and biochemical response [37]. Initially, the cell establishes small areas of contact with the extracellular matrix (ECM) by integrin receptors binding to ligands in the matrix. These focal contacts enlarge into focal adhesions by integrin accumulation and attachment to the actin cytoskeleton [47]. The adhesions support membrane protrusion by actin polymerization and translocation of the cell body by contraction of the internal actomyosin machinery. Together with de-adhesion, these steps combine to produce a net movement. The mechanics associated with this movement have been measured for two dimensions. However, three dimensional force measurements currently rely

Table 3.1: Cell Traction Forces

Method	Force Measured[1]
Traction force microscopy	11 pN/μm^2 - 19 nN/μm^2 (cell migration forces)[63]
Micropatterned substrate	nN/μm^2 scale[6]
Elastomer pillar deformation	0.5n N/μm^2 (center), 1 nN/μm^2 (edge)[23]
	5-20 nN (whole cell traction forces)[76]
Cantilever deflection	0.2-4 nN/μm^2[26]
Silicon wrinkling substrates	10-20 nN (whole cell traction forces)[31]
Centrifugal force stalling	2.59 nN (wt myosin)[25]
	0.9 nN (myosin mutants)

on indirect and computationally cumbersome approaches and molecular sensors may offer a way to simplify the experimental transition into three dimensions.

To understand how cells migrate, we need precise and accurate methods for measuring cell-based forces at the molecular level. The ideal criteria are: molecular resolution, high dynamic range, high sensitivity, fast time resolution, and computational simplicity. The current force-measurement technologies are often technically or computationally challenging. They can be grouped into two categories: measurements of deviations from a pre-calibrated material and direct measurements using an optical trap or atomic force microscopy. The former methods are passive approaches that measure force from movements of markers embedded into a flexible substrate [63], distortions to a patterned substrate [6], bending of elastomer pillars [23, 76], deflecting a cantilever [26], wrinkling of the substratum [14, 31], or migration against a centrifugal force [25]. These displacements are calibrated by applying a controlled magnitude of external force to the two-dimensional substrate. From the strain reported by the markers or surfaces in response to cell motility, the calculated cellular forces are in the range of nNs/μm^2 as summarized in Table 3.1. Unfortunately, these measurements are technically challenging and often require specialized equipment. The methods offering experimental simplicity, are computationally complex. More generally, these techniques offer cell-level measurements that are limited in their spatial resolution to identify the molecular origin of force.

An alternative force-measurement approach is to identify the matrix ligand-cell adhesion receptor interactions at the molecular level. The classic model is the fibronectin

Table 3.2: Integrin Rupture Forces

Method	Force Measured[2]
AFM	15-109 pN for loading rates 1-305 nN/s[50]
AFM	35 pN average loading rate 59 nN/s (overall 32-97 pN)[42]
Optical trap	13-28 pN at loading rates of 5-100 pN/s[78]

RGD-integrin binding site [67]. The force sufficient to rupture RGD-integrin binding have been measured by AFM [50, 42]and optical trapping [78] experiments to be 25 pN [50], 32 pN [42], and 13-28 pN [78]. Although these physical methods are low throughput and sometimes complex, they are direct and informative. The molecular measurements are summarized in Table 3.2.

FRET imaging is a promising alternative to physical approaches and has been shown to image the traction force applied by cells to a matrix [43]. In this example, the authors, covalently integrated fluorescent (donor and acceptor-labeled) adhesion peptides into a substrate matrix. Cells introduced to the matrices, rearranged the matrix upon forming new adhesions. Much like the cantilever, pillar, and bead methods outlined in Table 3.1, here the authors pre-calibrated the mechanical properties of the substrate. As a result, changes in FRET efficiency were directly associated with a cell's ability to apply a force. The resulting traction maps showed that receptors rearranged and clustered as the cell applied compressive forces to the matrix. Another FRET-based approach for measuring the strength of ligand-receptor interactions labeled ligands in the gel and receptors on the cell surface with acceptor and donor molecule, respectively[44]. These results demonstrate that FRET-based imaging methods are capable of measuring the cell-level traction forces applied through focal adhesions and focal contacts.

Because the cellular (Table 3.1) and molecular (Table 3.2) forces are in the pN-nN range, mechanical measurements of cell migration forces must have dynamic range across the same force scale. Our design uses the unfolding of stable macromolecular structure as a means to sense force. Well-studied models of stable structures are the DNA duplex and the Fn and Ig domains of fibronectin. For a prototype sensor, we focused on the mechanical properties of DNA, because of the simplicity of its higher

order structure (only secondary) and perhaps more importantly the high integrity of the re-folding pathway. The mechanical properties of DNA have been studied in single molecule optical trap experiments, atomic force microscopy, and micro-needle configurations. Complementary DNA strands unzip when forces are applied to both strands on the same end of the duplex. Experiments show a sequence and length dependent 9-20 pN range of force required to pull apart two complementary strands of DNA. The unzipping forces are larger for duplexes with a GC-bias or higher complementarity [70, 90, 89, 24]. In addition to simple linear DNA structures, DNA duplexes can assume a hairpin secondary structure. We have measured an unzipping force on a DNA hairpin of 18 pN [77]. In contrast to double-stranded DNA, single-stranded RNA readily forms hairpin and three-helix junctions in the presence of Mg^{2+} and the higher order intramolecular interactions account for the additional stability of RNA-based single-stranded structures [54]. The P5ab hairpin is destabilized by 14.5 pN, while in the presence and absence of Mg^{2+}, forces of 11.4 pN and 19 pN, respectively, are required to destabilize the P5abc three-helix junction.

The direction in which stress is applied to the double stranded DNA results in different denaturation forces. When force is applied collinearly to strands on the opposite end of the duplex, at a critical force, the DNA strands shear apart. Typically, larger forces are required to shear a length of DNA. For 10-20 base duplexes AFM experiments measure a 20-60 pN shear force [75]. Similarly, a shearing force (37 pN) versus unzipping force (10 pN) was measured for a 15-base duplex by fluorescence[46]. These studies have established that the stability of double stranded oligonucleotides is in the same force range as the intermolecular forces of a matrix ligand-integrin receptor bond.

While a thorough mechanical understanding of nucleic acids is important to the force sensing capabilities of the molecular reporter, it is also important to have fine control over the fluorescence reporting capability of the sensor. Single molecule experiments with fluorescent-dye conjugated oligonucleotides have addressed many key design considerations essential to fluorescence studies. Various designs and configurations of fluorescent oligonucleotides have been addressed in kinetic studies of RNA

catalysis and folding [92], cation dependent RNA folding [41], and branch migration of a holiday junction [61]. In particular, these single molecule arrangements have shown that single fluorophore [28], quencher pairs [46], dye FRET pairs [77, 92], quantum dot FRET pairs [33] and triple FRET configurations [34] can be applied in single molecule fluorescence studies.

A purpose-built molecular-scale force sensor has not been developed. As described in the previous section, FRET microscopy has shown the ability to detect cell traction forces through labeled peptides in the matrix but the force is inferred from the change in FRET efficiency [43]. However, one group has demonstrated FRET to report an elastic application of force along the axis of a single stranded DNA [30]. The authors calibrated a percent FRET efficiency with applied force. When the single stranded DNA was hybridized to a complementary sequence constrained in a circular conformation, the reporter strand yielded a FRET change. Another group addressed DNA-based sensors as a means of improving specificity on protein biochip assays [2]. A DNA molecule is presented on a glass chip surface and is brought into annealing proximity with a complementary molecule on a PDMS surface. The resulting annealed structure is a pair of DNA duplexes with a fluorescent dye between them. Imaging the glass surface allows the authors to determine which duplex configuration ruptures first (imaging whether the PDMS retains the fluorescent moiety or if the fluorescence is transferred to the glass chip). The authors calibrated the system and used a DNA-antibody construct with a fluorescent dye between them attached on the PDMS surface and various antigens on the glass chip. The two surfaces are brought into contact to determine interaction specificity. Both of these approaches demonstrate the feasibility of DNA-based sensors.

3.1 Experimental design

The following experiments focus on modifying the two functionality modules of the sensor design: one end of the molecule is immobilized on the cover slip and the other end interacts with the cell. The surface immobilization requires a stronger, covalent

surface attachment chemistry. The cell adhesion ligand presenting end used a peptide conjugated and unconjugated sensor to determine specificity of cell-array interactions. After verifying the product at each step in solution, we proceeded to assemble the molecule on the cover slip surface. The oligonucleotides used for cell-adhesion assay are shown in Table 3.3.

Preserving the reporting and sensor components, we modified the functionality modules of the calibration molecule. At one end, the molecule is anchored at the cover slip surface (preserving the calibration geometry). At the opposite end, an adhesion peptide biases specific interaction between the cell and the hairpin molecule such that a cell-applied force is transduced by the duplex and the molecule unzips. These multiple points of modification take full advantage of DNA as a scaffold for the sensor allowing the complete molecule to be assembled in parts. The 3' and 5' modifications are carried out on separate oligonucleotides because the complete molecule is too long for commercial synthesis and to isolate each chemistry to the point of interest. We assemble the molecule in solution to validate each modification point. With verified chemistry and modifications, assembly directly on the cover slip yields cleaner product with well defined contributions to the signal. Cells are introduced to the surfaces coated with hairpin sensor. Specific attachment between cell and sensor should yield a change in conformation. Our objective was to report distributions of applied forces as a function of Cy5/Cy3 intensity ratios. The assay is shown in Figure 3-1.

The functionality module in the calibration experiments was relevant to the restrictions imposed by an optical trap setup. The sensor was anchored to the cover slip via a digoxigenin-antidigoxigenin linkage. This linkage breaks at about 40pN. While this level of attachment integrity is sufficient for the single molecule experiments, because the transition we are measuring is at 18pN, it is not appropriate for cell experiments because of the higher forces. The biotin-streptavidin pair provided the simplest transition because it is stronger than the digoxigenin-antidigoxigenin linkage and was no longer reserved for bead attachment. Nonetheless, this attachment did not stand up to the flow experiments as imaged by a conventional CCD

Table 3.3: Oligonucleotides for Adhesion Force Sensing

Name	Sequence 5' to 3'
NH2.64	NH2(C6) - GAT GAT GGT AGA TGA TGT ATT GTT GTT TCG CCG CGG GCC GGC GCG CGG TTT TCC GCG CGC CGG C
P.30.NH2	Phos - CCG CGG CGT TTG TGG AGC TGA GAT GAG ATG - NH2
Cy3.25	Cy3 - CAA CAA TAC ATC ATC TAC CAT CAT C
19.AF647	CAT CTC ATC TCA GCT CCA C - AF647

camera. A covalent attachment strategy was employed instead; an amine terminated oligonucleotide was attached to an aldehyde cover slip.

While DNA can be synthesized with a variety of modification and obtained commercially, from a yield perspective, it is not practical to synthesize a 94mer sequence with both 5' and 3' modifications. The hairpin portion of the molecule is therefore assembled from two parts. Each part is individually chemically modified to address the particular application. The two oligonucleotides are then ligated together to complete the 94mer hairpin. The 3' end of the hairpin sequence receives the peptide. The 5' end carries the amine which allows surface immobilization.

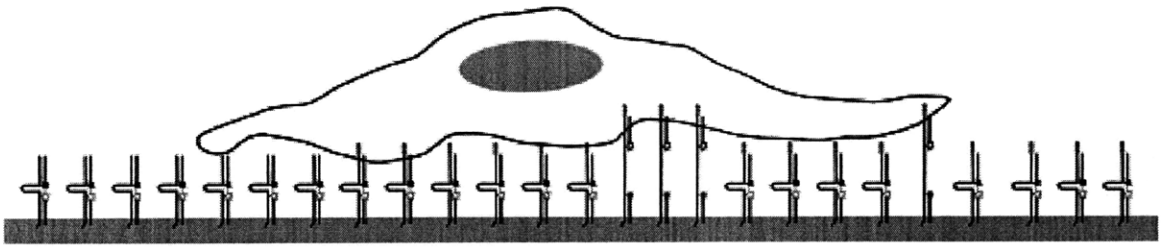

Figure 3-1: Sensor-coated surface for cell adhesion assay. Reporter molecule is immobilized on a cover slip surface presenting an adhesion peptide at the opposite terminus.

3.2 Validation

As a scaffold, DNA provides many opportunities for modification and the techniques to monitor each modification step are readily available. We introduce modifications at four points of the hairpin reporter molecule. All modification points are introduced during oligonucleotide synthesis. Two are the fluorophore pair of reporters and two provide chemical functionality for further modification. In solution, we validated the

chemistry at each step with electrophoresis separation. Assembly on a cover slip surface was monitored by fluorescence. Lastly, cell-sensor interactions were validated on a sensor array.

3.2.1 Validation in solution

Three of the molecular assembly steps can be verified in solution. Oligonucleotide conjugation to RGD peptide and the ligation of the 5' and 3' oligonucleotides are verified by electrophoresis. Steady state fluorimetry yields structural verification of the hairpin and the annealing of the fluorescent oligonucleotides. The 5' functionality is included in the commercial synthesis. The 5' functionality is further addressed in Section 3.2.2.

In the single molecule experiments, the 3' functionality was originally a simple sticky end terminus which was ligated to a 1kb duplex. For this set of experiments, we require interaction with a cell. Cell-mediated force transduction requires that cells interact with the sensor molecules. We addressed this requirement by incorporating a the adhesion peptide, GRGDSPC, at the 3' end of the oligonucleotide. The peptide oligonucleotide conjugation protocol is adapted from [83, 87]. The RGD peptide is conjugated to the 3' 30mer oligonucleotide with a 5' phosphate and a 3' primary amine. The phosphate allows us to easily ligate this oligonucleotide to the 5' modified 64mer. The 3' primary amine is conjugated to a thiol in the the peptide GRGDSPC, which is incorporated only for conjugation purposes. The remaining amino acids flanking are native to the fibronectin amino acid sequence and increase the peptide's biochemical activity. Cells preferentially attach to surfaces patterned with the RGD peptide (Figure 3-2).

To conjugate the peptide and oligonucleotide, the heterofunctional cross-linker, sulfo-MBS, was used to covalently attach thiols to amines. The 30mer presenting the amine, is transferred to 0.1M $NaHCO_3$ buffer (MicroBioSpin P-30 Tris Chromotography columns; BioRad). The concentration was measured via absorbance at A_{260} (ND-1000 Spectrophotometer; NanoDrop). To 300 picomoles of the phosphorylated 30mer, 1mg sulfo-MBS (Pierce) is added and incubated at room temperature for 30

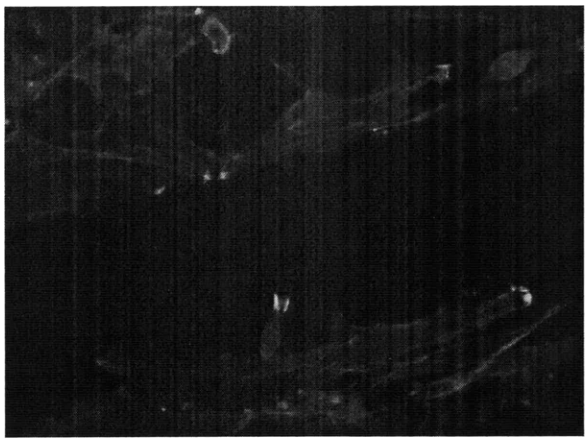

Figure 3-2: The cell adhesion peptide GRGDSPC biases cell-surface interaction. Here, the peptide was covalently attached to the surface via the same thiol as outlined for the oligonucleotide conjugation reaction. The biasing activity is retained, and cells attach to peptide-coated regions.

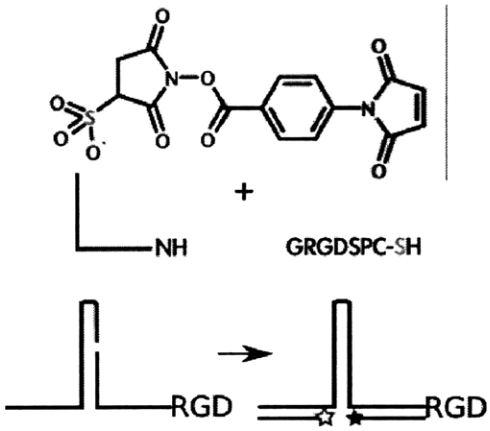

Figure 3-3: Molecular assembly and modification scheme for cell assay requires adhesion ligand for specific cell-mediated force transduction. The long DNA scaffold is assembled in several independent steps, which are the same for solution and cover slip assembly. Cross-linker, sulfo-MBS is used to conjugate oligonucleotide to peptide in a two step reaction. The oligonucleotides are then ligated to form the final length of the hairpin and complementary fluorescent oligonucleotides are annealed. Ligation and peptide conjugation are confirmed with PAGE. Complete molecular assembly is confirmed with steady state fluorescence.

minutes. At this step the electrophilic primary amine attacks the ester and forms a covalent bond to the DNA oligonucleotide. Activated oligonucleotide is exchanged into phosphate buffer pH 6.6, which also removes excess sulfo-MBS, and peptide is added. The cysteine incorporated into the peptide sequence presents a thiol func-

tionality. Fifty micrograms peptide are added to the reaction mixture with one third final volume of acetonitrile. The reaction proceeds at room temperature for eight hours. The acetonitrile is evaporated under vacuum before proceeding. The electrophilic maleimide portion of sulfo-MBS forms a covalent attachment to the thiol on the cysteine within the peptide. The resulting molecule is a peptide-oligonucleotide conjugate.

The conjugated peptide-oligonucleotide produces a doublet in electrophoresis. The peptide-oligonucleotide conjugate (POC) reaction is monitored by PAGE after the entire 94mer was assembled. The additional DNA character added after the ligation step allows us to observe cleaner bands. The 30mer conjugate otherwise runs less predictably and bands are not clearly distinguishable. The PAGE gel shown compares two ligation reactions. One is a typical ligation of a 30mer and 64mer and their 94mer ligation product. The second reaction shows the ligation product of a 64mer and a POC 30mer. The product band for the unmodified 30mer is a singlet and the peptide-conjugated 30mer yields a doublet. The small separation in bands is due to the small size difference between 94mer and a 94mer plus peptide, and the small positive charge contribution of the peptide in the pH 8 TBE. PAGE conditions were as follows: 6%, 22W, 40 minutes Figure 3-4 shows the result.

To assemble the molecule, the 5' and 3' ends are ligated, and fluorescence reports the final structure. The phosphorylated 30mer is ligated to a 64mer oligonucleotide with a 5' primary amine modification. The ligation is carried out with the 30mer in 2.5-fold stoichiometric excess. Extent of ligation is monitored by 94mer product band using PAGE and ethidium staining. Once the 94mer is confirmed, annealing the fluorescent oligonucleotides to their complements on the flanking arms completes the molecular assembly. The secondary structure was verified by bulk fluorescence. The emission spectra of randomly oriented fluorescent oligonucleotides were compared with the emission spectra of fluorescent oligonucleotides annealed to their complements on the flanking arms. The annealed structures confine the fluorophores within their Förster radius. The bulk fluorescence data shows that exciting the donor fluorophore when the fluorophores are randomly oriented yields a mostly donor emission

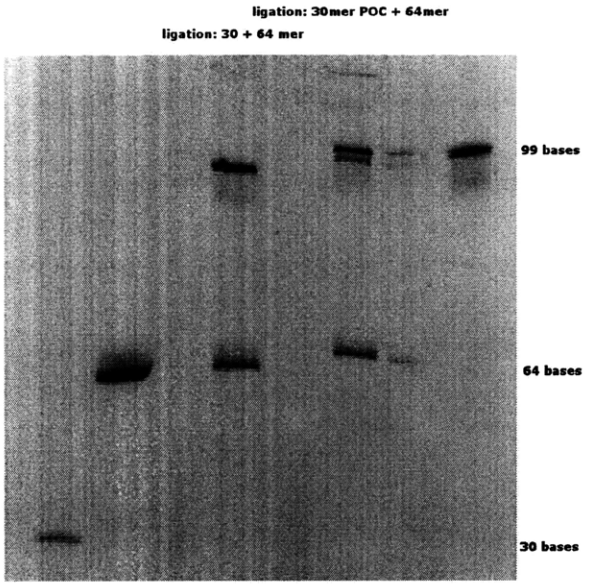

Figure 3-4: Validation of 3' RGD attachment by PAGE. Left to right: 30mer · 64mer · ligation: 30mer and 64mer · ligation: 30.RGD + 64mer. The doublet, in the last column, is a product of RGD conjugation to the oligonucleotides and is thus absent in the unmodified ligation reaction. The reaction is about 65% efficient.

spectrum. However, exciting the assembled molecule at the donor wavelength gives rise to a more defined peak at the acceptor wavelength (Figure 3-5).

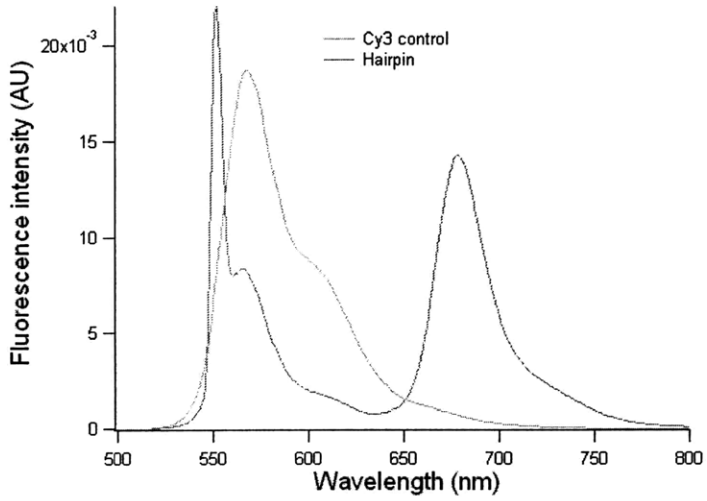

Figure 3-5: FRET peak confirms molecular assembly. Fluorescent oligonucleotides annealed to the hairpin show FRET and confirm final structure.

This experiment was not carried out in reverse. While it would be informative to

measure the conformational transition as a function of FRET and characterize the population profile as a function of unfolding, the design is intended for mechanical unfolding pathways. A thermal unfolding first yields the lower Tm flanking arms to melt. As a result, the reporters are no longer associated with the hairpin portion of the molecule, and do not capture the melting of the duplex stem. A chemical pathway of denaturation would encounter the same result.

3.2.2 Validation at interface

Initially, to preserve the attachment chemistry from the single molecule experiments, the reporter's 5' attachment was a biotin streptavidin linkage. Poor integrity to successive washing steps necessitated a covalent attachment to the surface. With a stronger attachment, we were able to assemble the reporter molecule directly on the cover slip surface and confirm each assembly step with fluorescence. Better integrity to preparation conditions and intensity quantification at each step facilitated transition to cell experiments.

Another advantage of covalent attachment and improved array integrity is the option to build the molecule on the cover slip. We assemble the molecule from two fragments of oligonucleotide that are ligated together to yield the complete hairpin sequence. One oligonucleotide is synthesized with the primary amine at its end for cover slip immobilization. The other end is conjugated to RGD peptide to provide cells with an adhesion ligand at the opposite terminus. This configuration defines the axis of force transduction restricting the transition between open and closed states to the unzipping mode (instead of shearing). The assembly on the cover slip begins by printing an amine terminated oligonucleotide on the glass surface.

5' Validation

In addition to better signal integrity, changing the 5' functionality from biotin to an amine allows more DNA molecules to pack per unit area further improving signal intensity. Drawing on techniques developed for imaging DNA microarrays, we im-

proved the surface sensor signal significantly and were able to image sensor-activated cover slips with a CCD camera (Figure 3-6). With the new scheme, we can wash out contaminants after each reaction step by controlling the detergent and salt concentrations. Both the amine and the biotin are added during oligonucleotide synthesis, therefore this change does not contribute to experimental complexity.

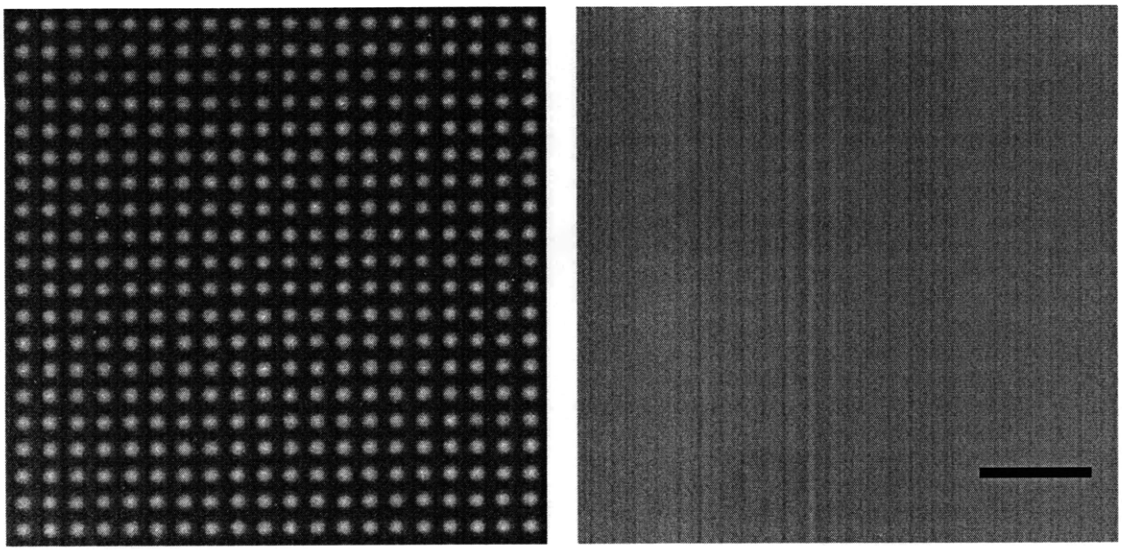

Figure 3-6: Printed oligonucleotide array confirms 5' attachment chemistry and surface evenness. The hairpin was immobilized via a primary amine on an aldehyde treated cover slip surface. Oligonucleotide-free areas are not reactive and show dark background. Printed oligonucleotides are hybridized to their fluorescent complements and yield a bright intensity with good signal to noise. Each spot in the array is 8μm. Non-arrayed surface (right) shows high uniform intensity. Scale bar is 10μm.

The 5' primary amine is added during the oligonucleotide synthesis (64mer) and reacted with an aldehyde-presenting cover slip. Aldehyde surfaces were prepared slightly differently depending on whether cells were plated in subsequent steps. Sterilized glass cover slips were aminosilinated with two percent 3-aminopropyltriethoxysilane (Sigma) in ethanol for ten minutes. Four five-minute ethanol washes follow. Aminated cover slips are then cured in a 90°C oven for thirty minutes, cooled to room temperature, and treated with 2.5% glutaraldehyde in PBS for one hour. Aldehyde surfaces are washed with distilled water and dried. The highly reactive aldehydes can react with primary amines on the DNA. Oligonucleotides with primary amines are added to the aldehyde surfaces in a 5μM solution with 1x SSC and 10% glycerol.

Cover slips with DNA are incubated in a humidity chamber over night. Dehydration favors the formation of a reversible Schiff base. The Schiff base between the DNA and the surface is reduced with a sodium borohydride solution (2.5mg $NaBH_4$) for fifteen minutes. This step also reduces the remaining active aldehydes to alcohols preventing cross reactions in future steps. The covalent attachment can be verified by hybridization to fluorescent oligonucleotide and shows good signal to noise. Arrays prepared with this chemistry have much stronger signal after subsequent washing steps than the biotin-streptavidin arrays.

To visualize the surface chemistry, the surface-immobilized oligonucleotides are annealed to fluorescent complementary strands. The printed oligonucleotide is hybridized to its fluorescently labeled complements by incubating under a cover slip for thirty minutes in a humidity chamber at room temperature. The cover slips are again soaked for ten minutes each first in .1% SDS and 1x SSC solution and then .1x SSC to remove excess unbound and non-specifically bound oligo. Cover slips can be imaged directly in the secondary solution. The ligation was also monitored by fluorescence. The choice of fluorophore is important here because the improved packing of DNA molecules in the covalent strategy, brings the fluorescent oligos closer together. Some dyes experience contact quenching which increases with dye concentration and can be as strong as quenching by a quencher molecule. The cyanine dyes, used in the outlined experiments, do not exhibit this concentration dependent behavior [60]. This consideration also ensures that differences in Cy3 intensity should be attributable to the proximity of Cy5 acceptor.

Molecular assembly

Initially, the complete sensor was assembled prior to printing and the resulting reaction mixture was printed on the cover slip. The sensors were then either singly or dually hybridized to their fluorescent complements. Fluorescence intensities from individual fluorophores were detected in their respective channels. These measured intensities are a function of all surface-bound molecules, and may be contaminated by autofluorescence from amine-presenting by-products. The cover slip ligation was

not as efficient as that in the test tube, but yielded sufficient signal in the donor and acceptor channels.

Fluorescence imaging was used to confirm each step of the molecular assembly on the cover slip surface. The fluorescent oligonucleotides with the reporter FRET pair were hybridized to the surface-immobilized oligonucleotides to monitor, attachment, ligation and fret efficiency. Attachment efficiency is determined by the fluorescence intensity of the hybridized fluorescent oligonucleotide. The surface-attachment is the first step and, as a result, the efficiency of this step affects the yield of the final sensor molecule. We set this intensity as a reference signal for evaluating the efficiency of all assembly steps that follow. Thus, this signal provides the control for subsequent steps.

The ligation was also monitored by fluorescence. The 30mer and 64mer have independent dye complements; 30mer can be monitored by AF647 (in some examples AF488) fluorescence intensity, 64mer is monitored by Cy3 (in some examples Rhodamine) fluorescence intensity. Single color controls show that the conditions we used yield orthogonal hybridization of fluorescent oligos. The 30mer and the 64mer, printed individually, are spectrally separate and do not contribute to the other's fluorescence channel. The most significant channel cross talk is between the Cy5 and FRET (Cy3 excitation filter/Cy5 emission filter) channels. On the other hand, areas of successful 30mer and 64mer ligation show both colors. The ligation efficiency can be determined by comparing the signal from ligated oligonucleotide to the reference signal of the same oligonucleotide printed directly on the surface. It is easy to spatially confine oligonucleotides and thus compare the ligation and control on the same coverslip undergoing the same treatment.

The hairpin sensor molecule was assembled directly on the cover slip using the same conditions as in solution. The aminated 64mer is first printed on the aldehyde cover slip and incubated in a humidity chamber over night. The remainder of the reactive aldehydes are reduced with a sodium borohydride solution as detailed above. The 30mer is then added to the coverslip and the sample is heated to 62°C to melt out secondary structure and cooled to allow the oligos to anneal. A ligation mixture

of ATP, 10x T4 Ligase buffer, and T4 ligase are added and the reaction proceeds at room temperature for 1 hour. The sample is incubated 62°C for ten minutes to inactivate the ligase. Primary was buffer is added and the sample is again heated to 62°C for ten minutes. The wash is aspirated immediately upon removing from oven to wash away annealed but unligated constructs. Secondary wash buffer, with lower salt concentration and no detergent follows. The complete 94mer hairpin is hybridized to the complementary fluorophores for thirty minutes in a humidity chamber, at room temperature, under a coverslip. Unbound fluorescent oligos are removed with a primary 1X SSC wash containing 0.1% Tween and then a secondary 0.1X SSC wash without Tween. This description applies to cell experiments. The resulting molecule is a hairpin with a 4 nucleotide loop, a 20 base stem, and a FRET pair within 5nm distance. As a result, FRET also serves as a measure of conformation.

For clarity, intensity profiles across an image are shown to relay the quantitative relationship between background and signal. Figure 3-7 shows independent oligonucleotides printed on the cover slip surface. The intensities determine the extent of channel crosstalk and serve as references for subsequent assembly steps. For instance, a ratio of intensities between the surface printed and ligated oligonucleotides relays the ligation efficiency (relative to surface attachment efficiency).By monitoring the acceptor, we isolate the ligation efficiency measurement from the potentially obscuring energy transfer pathway which also alters perceived fluorescence intensity.

The ligation is not 100% efficient and the intensity of the ligated oligonucleotide will be lower than the one printed directly. The ligation efficiency directly affects the measured energy transfer efficiency and must be considered. For the energy transfer estimate, the printed donor intensity is compared to the donor intensity of the ligated sample. Successful assembly yields comparable acceptor and FRET channel intensities and increased ligation efficiency yielding decreased donor intensity. The intensity of Cy3 and higher detector sensitivity in the red part of the spectrum yields high donor intensities. Energy transfer is reported as the change in ratio between donor and acceptor. Figure 3-9 shows an example of a ligation reaction carried out on a cover slip surface. For comparison Figure 3-8, shows the edge of a printed fluorescent

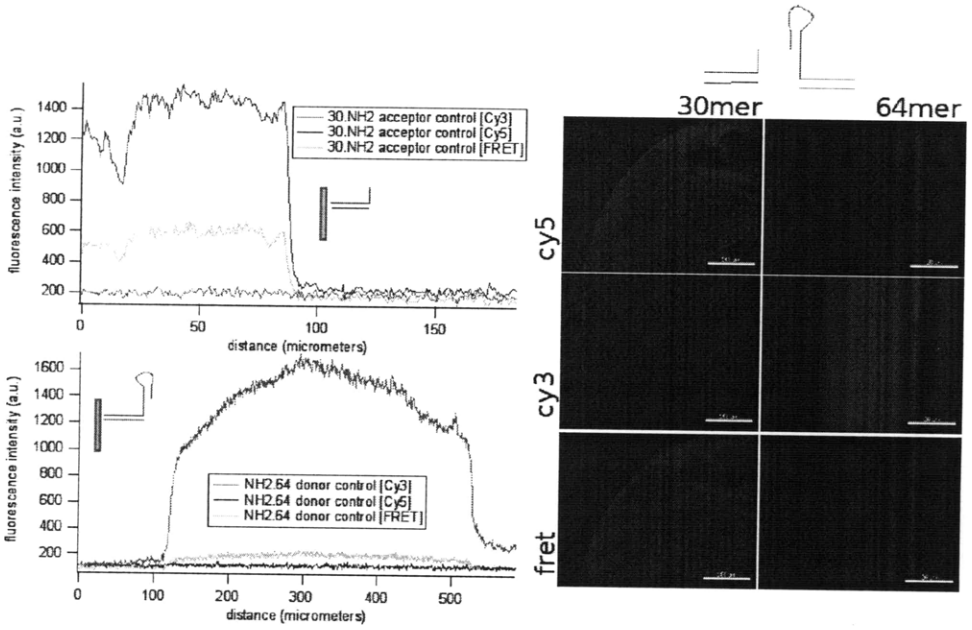

Figure 3-7: One color controls show surface attachment of the oligonucleotides, strong independent signal, and the extent of bleed-through into each of the channels.

feature that was ligated in solution. The test tube ligation carries contaminants that contribute to the high background fluorescence. The cover slip ligation shows lower intensity, but also lower background.

3.2.3 Validation of cell-sensor interaction

As was previously mentioned, initial cell-sensor experiments relied on a biotin-streptavidin attachment of reporter to coverslip. However, this attachment method lacked integrity to successive wash steps and more importantly, cellular conditions. We registered the specific interaction between the cell and the sensor using the biotin-streptavidin linkage. Here, cells aligned with arrays of printed sensor molecule on otherwise cell-excluding surfaces. However, the fluorescent signal was very low and precluded a FRET measurement in this assay. Our covalent strategy was used in further experiments. Figure 3-11, shows cell alignment with array features.

Printing on streptavidin surfaces offered an added advantage that cells were not adherent to the non-arrayed areas (Figure 3-10). In the covalent scheme, after printing the DNA onto the cover slip, the remaining aldehydes are reduced to alcohols. Cells

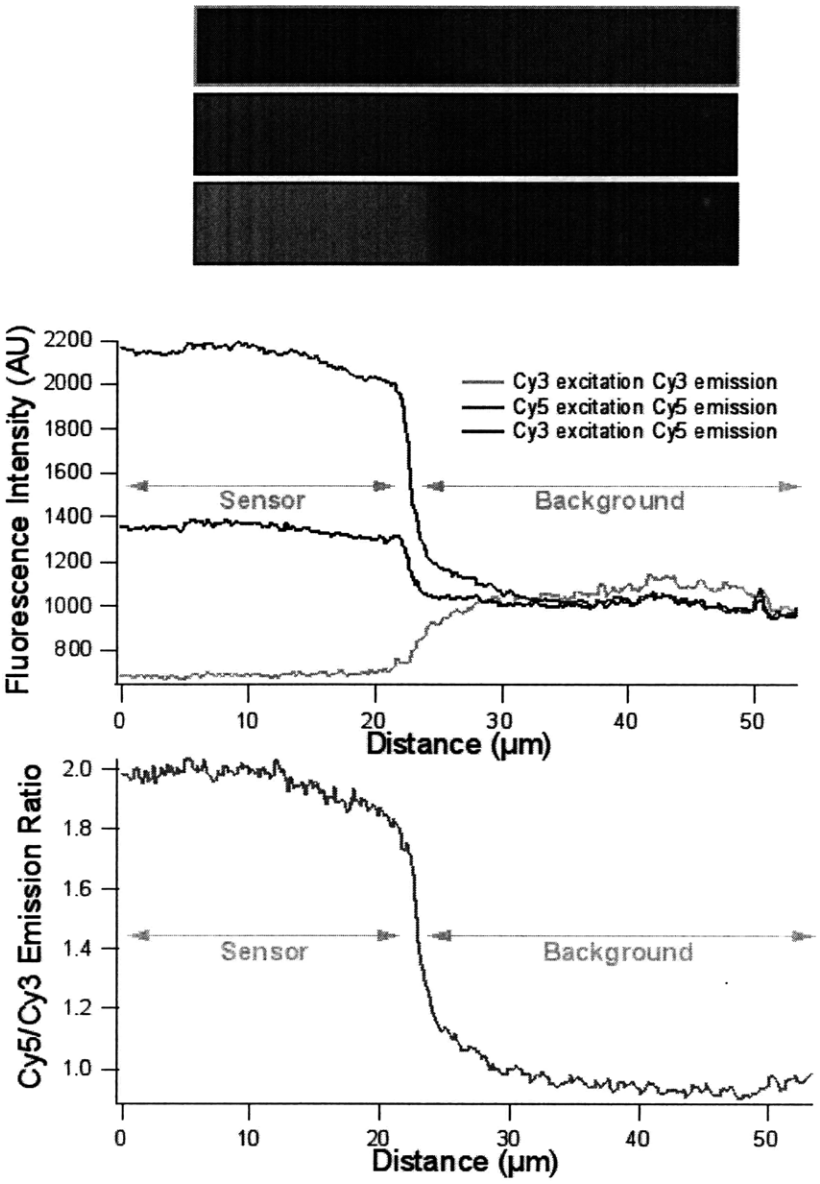

Figure 3-8: Sensor molecules assembled in solution show high FRET values in regions of sensor and low FRET values in regions without sensor. In this test tube ligate example, impurities in the sample contribute to high background signal in all the channels

are not excluded from these surfaces. As a result, specific alignment along the printed arrays is not observed for the covalent scheme. An advantage here is that the sensing is passive; adhesions can be registered when cells coincide with arrays. Specificity can still be controlled by the presence or absence of a biasing element, an RGD peptide. A significant difference was not observed, as spaces between sensor spots are favorable to

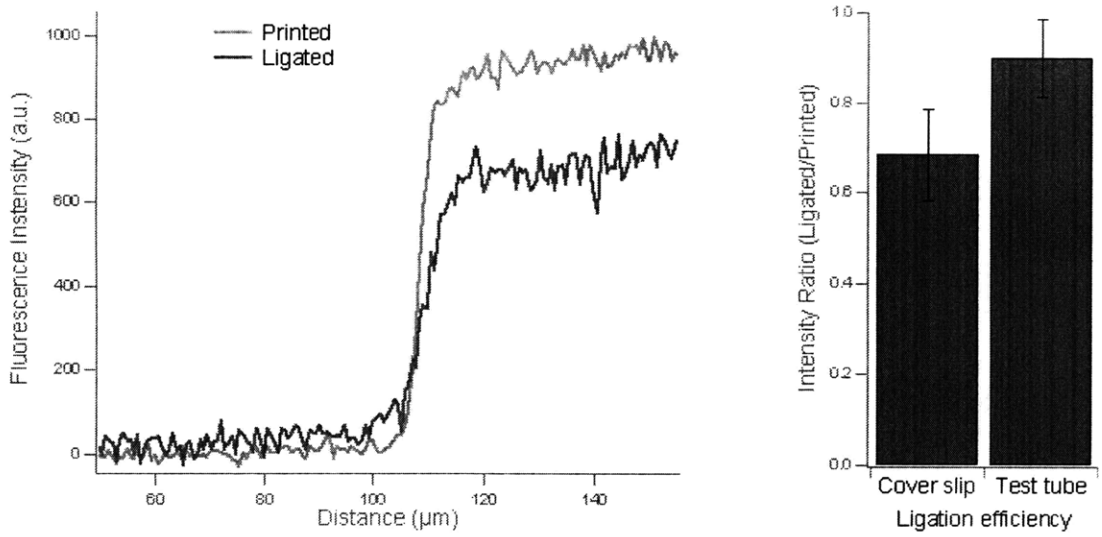

Figure 3-9: The cover slip ligation scheme and method for measuring ligation efficiency on the cover slip.

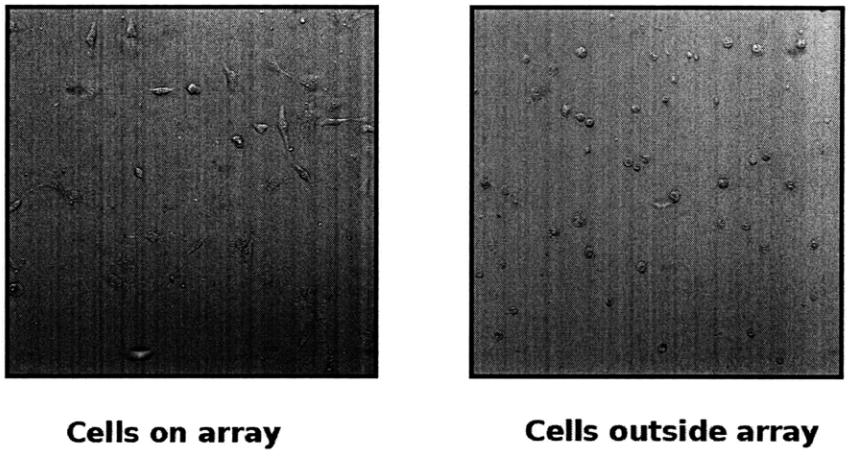

Figure 3-10: Cells are exclusively viable within sensor-coated regions. Cells on uncoated regions do not spread.

cell adhesion. Exclusion of sensor array surfaces with BSA resulted in poorly adherent cells. In conclusion, printing adhesive molecule on an otherwise non-adhesive surface is a more effective way to asses specificity than passivating adhesive surfaces with blocking protein which may obscure the biochemical activity of the RGD peptide presented by the hairpin.

The covalent strategy for immobilizing the sensor molecule yields higher fluorescent signal which generally correlates with larger numbers of fluorescent molecules on

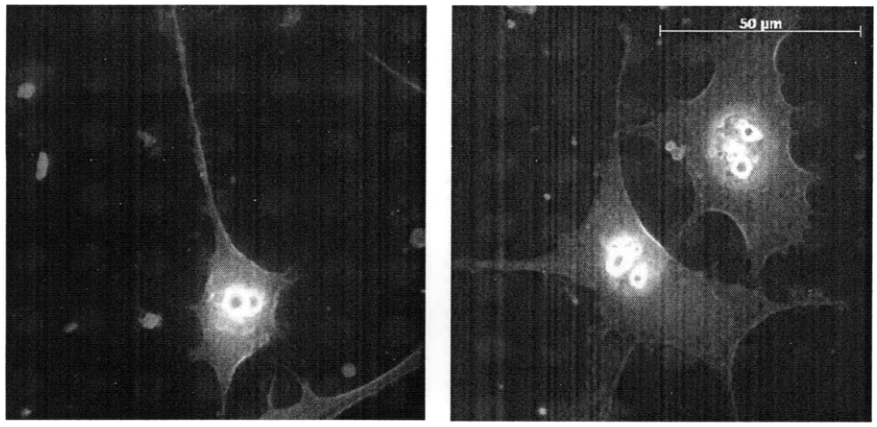

Figure 3-11: Cells align with array features. Sensor molecule (solution assembly) was printed in an array leaving the intermittent area cell-exclusive.

the surface. In the array examples, a single 4μm spot has a volume of about 3.5 femtoliters. At μM spotting concentrations, and without considering maximum spatial packing of molecules, the number of molecules per printed spot is on the order of 10^3. In one adhesion-sized spot (about 2μm), cells will engage with only 10^2 molecules at any one time. It is ideal to match the number of molecules available to bind and the number of molecules a cell needs to make an attachment because the match results in a larger fractional signal change upon cell engagement. A minimum concentration of fluorophores, and thus molecules, is required for detecting with a CCD camera. Dilutions of the printed sample show that the signal becomes significantly dimmer, requiring significantly longer exposure times at 10^2 molecules per printed spot. Given that ligation efficiency is not 100%, the dilution results suggest that even at low coupling efficiencies, there are enough peptide-presenting molecule available for cells to make adhesions.

3.3 Cell adhesion reporter

For cell adhesion experiments, we modified the functionality modules of the molecule. The functionality modules for the calibration experiments are not relevant for the cell adhesion experiments. The new functional modules provide a covalent linkage between the sensor and the surface on one terminus and an adhesion peptide at the

opposite terminus, included to encourage cell-sensor interaction. We coat the surface with the hairpin molecule by assembling the complete construct on the cover slip surface (a ligation step and a hybridization step) as was discussed in the previous section. The efficiency of each step is confirmed by imaging fluorescence in the appropriate channel. Delivered to each coverslip is a millimeter sized drop of control oligonucleotide and the oligonucleotide used to build the hairpin molecule. Cells are introduced to the cover slips, incubated until they are well adhered, and are imaged in the Cy3, Cy5, and FRET channels. The FRET channel is the signal collected from Cy3 excitation and Cy5 emission. FRET is reported as a change in the ratio of acceptor emission intensities when the sample is excited at the donor and the acceptor wavelengths.

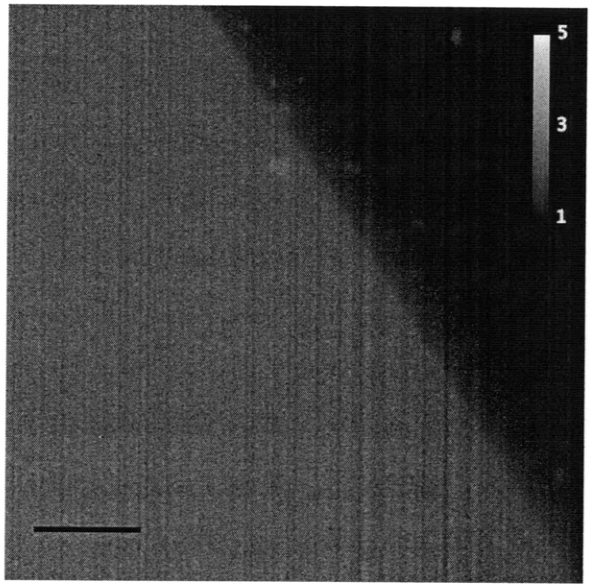

Figure 3-12: FRET ratio for cover slip-assembled sensors shows good signal. Ratio is evaluated by subtracting contributions from background and crosstalk between channels (determined from single color controls) and dividing the acceptor image by the donor image (at donor excitation).

Cells are plated on the sensor-coated cover slip surface to report cell adhesion as changes in Cy5/Cy3 ratio. We first evaluated the contribution of cells to each of the fluorescent controls individually to account for non-specific changes in fluorescence. Both controls showed cell-contributed intensity changes. Intensity changes appear as dark areas that co-localize with the adherent cell body. The brighter Cy3 control

was more significantly affected by cell adhesion with changes up to 30%. AF647 channel is dimmer and less sensitive to cell presence, with intensity changes upto 15%. Furthermore, the quenching is not always uniform underneath the shape of the cell (Figure 3-13). (Figure 3-14 adresses the difference in cell contribution to the donor and acceptor channels for a sensor surface presenting the two colors individually.

Both test tube-assembled and cover-slip assembled sensor molecules show good FRET signal (Figure 3-8 and 3-12). The ligation efficiency is lower for coverslip assembly. As a result, the donor channel intensity is significant compared with the completely quenched donor for test tube ligated samples shown in Figure 3-8. Both assembly schemes show a large change in the Cy5/Cy3 ratio compared with background (non-specific contribution to FRET). Changes in Cy5/Cy3 ratio should report specific interactions between the cell and surface. However, upon introducing cells, changes in FRET were not specific to the localization of the cell.

Similar results were recorded for another FRET pair, AF488 and Rhodamine. For this pair, stronger changes in intensity were also observed for the red fluorophore, Rhodamine. AF488, the donor in this case, had much lower sensitivity to cell presence. We expected that a decrease in fluorescence intensity will be measured only in the donor and FRET channels depending on whether a cell is engaged (FRET decrease) with a particular area or not (donor decrease). The differential quenching was an unexpected result. The weak threshold sensor should experience high levels of activation under cell loads. This high level of activation, combined with a reasonably close match of available sensor molecules to required sensor molecules for a cell to adhere, suggested the FRET signal may be more significant than the differential intensity changes contributed by cells to each of the channels.

3.3.1 FRET specificity to RGD

We hypothesized that specific cell-induced/sensor-transduced forces would register as low FRET (high donor) signal localized to adhesion areas within the cell. As discussed earlier, when cells migrating, they form new adhesions at the leading edge and release adhesions at the lagging edge. This dynamic process should be relayed

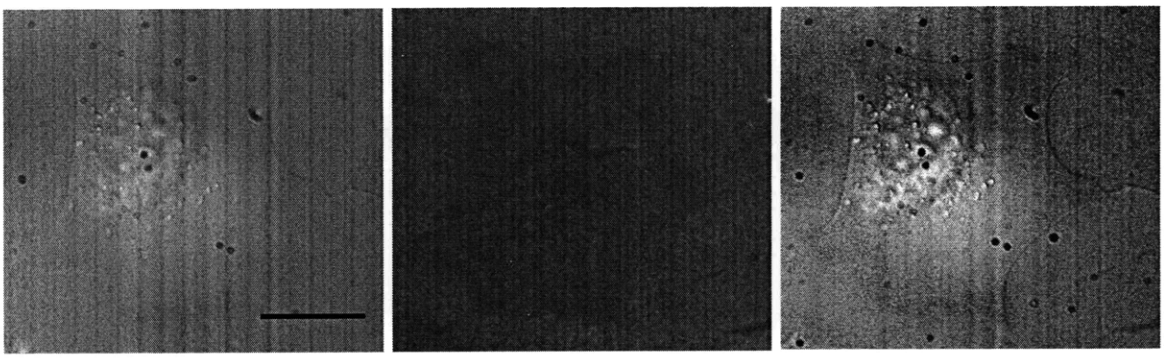

Figure 3-13: Cell presence decreases fluorescence intensity in the donor channel. Assembled hairpin molecules hybridized individually to donor-labeled oligonucleotide show the the cell's contribution to fluorescence intensity for a single-color hybridization.

in the fluorescence images mapping adhesion activity as a FRET/Cy3 ratio. The hairpin loop allows the high FRET conformation to recover once cell disengages from a particular area. We can thus capture the evolution of the distribution map of a threshold molecular force applied by cells.

The intensity in the donor channel and fret channel should be anti-correlated. The donor fluorescence should initially be low and increase upon cell binding. Accordingly, the FRET channel should initially have high intensity and FRET intensity should decrease upon cell adhesion to RGD peptide. Meanwhile, the acceptor channel fluorescence should remain constant and serve as a control. Ligation and FRET efficiency affect the strength of donor signal in the absence of cells and we observe this as increased background signal attributed to high initial donor fluorescence. The change in donor and FRET channels must be large enough to detect in the background of sensor molecule.

However, instead of fluorescence changes localizing to punctate adhesions, we observed cell-shaped regions localizing to cells. The darkest of these regions do not recover fluorescence after cells detach. Because the sensor design accounts for internal reversibility, this result suggested an external, cell-induced process. Additionally, it was not likely that the dark regions were a result of FRET because they appeared in all of the channels and anti-correlation was not observed. As a result, all attempts at calculating FRET have yielded images where areas of decreased FRET do not

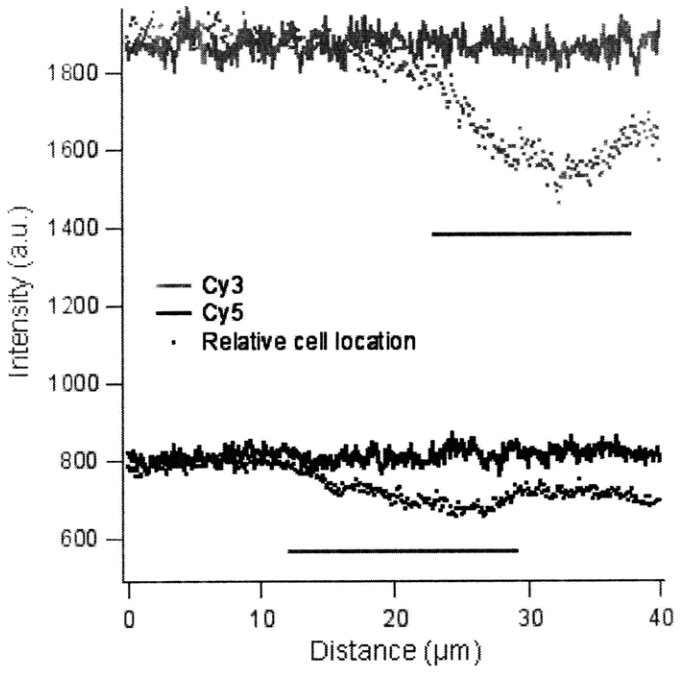

Figure 3-14: Cell presence decreases fluorescence intensity for both donor and acceptor channels in one dye controls. Assembled hairpin molecules hybridized to individual donor and acceptor oligonucleotides show the difference in intensity change in the individual channels. Note that the intensity is not 100% immediately to the right of the cell region in the acceptor profile. Extended incubation periods yield unevennes in surface intensities. These irreversible contributions are discussed in Section 4.2.2.

localize to areas of adhesion within cells. We suspected that the darkest regions can be caused by cell internalizing the sensor, scratching the sensor off the surface, and chemically degrading the sensor. These possibilities are discussed in Chapter 4.

The fluorescence decrease is strongest in the donor channel. The FRET ratio was initially evaluated as Cy5/Cy3 at 535(30)nm excitation. Background intensity and crosstalk between channels is initially subtracted. Cy3-Cy5 crosstalk is low. The most significant crosstalk is between the FRET and the Cy5 channel. Because the donor is most strongly affected by the cell, we valuated FRET by other means. Using the acceptor fluorescence as a control should account for differences in intensity contributed by cells. We calculated a FRET from the ration of acceptor emissions (at 710(60)) when excited at the donor/acceptor wavelength. Here, Cy5 fluorescence is independent of the donor and serves as a reference. This method is better controlled but still did not return differences in FRET localizing to the cell. The difference in

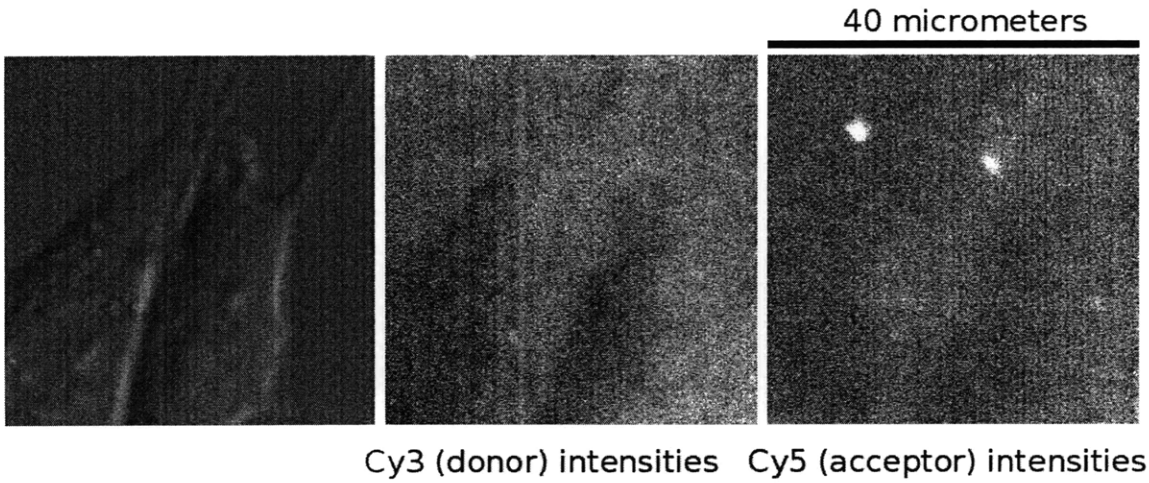

Figure 3-15: Dual color controls show relative cell-effects of donor and acceptor channels. Assembled hairpin molecules hybridized to both donor and acceptor oligonucleotides show relative cell-effects of donor and acceptor channels.

intensity contribution to the two channels may be at the root, and was considered next. Figure 3-15 shows an example of the donor and acceptor channels of complete sensor molecules assembled on the surface and plated with cells.

Since the donor and acceptor channels are differentially affected by cell presence, we sought to correct for differences and calculate a a ratio image after taking into account the difference in cell contribution to each channel. The cell-mediated quenching is usually either very uniform throughout the body of the cell or localized more to the outer edges. In many cases, the intensity decreases were similar for both the donor and acceptor channels, but the extent of decrease differed. We normalized the donor and acceptor images to correct for the differential effect of the cell upon different channels and determine a ratio based only on the mechanical transition and not the environmental contribution of the cell. Ratios of normalized images returned changes in FRET (acceptor-controlled) that localized to the cell bodies. These changes were significant, but were opposite from the hypothesized specific changes induced by a mechanical transition. In other words, we expected a decrease in the regions occupied by cells for the acceptor-controlled ratio images, but instead observed an increase in the ratio image localizing to the cell.

To address the specificity of this change we removed the 3' RGD peptide. We ini-

tially incorporated the RGD peptide at the cell-presenting end of the hairpin molecule to bias cell-sensor interaction and provide a handle for specific mechanically-induced conformational changes. Thus to evaluate the specificity of our observed result, we removed the peptide. Because cells still require adhesion molecules to spread on the surface, we incubated sensor dishes with supplemental fibronectin (1mg/ml; Invitrogen 33010) over night in DMEM (Invitrogen 21063). For the peptide-free sensors we evaluated FRET ratios as described above for the peptide-presenting sensors. We observed the same series of results.

Image analysis is based on the intensities collected at each pixel. For instance, to determine the ligation and FRET efficiencies, intensity plots across a sensor coated region were analyzed. The ligation efficiency is determined by comparing the intensities of an oligonucleotide printed directly on the surface with an oligonucleotide that is ligated. FRET efficiency is requires consideration of evaluated ligation efficiency. FRET values are determined by taking a ratio of acceptor intensities at the donor and acceptor excitation wavelengths. FRET efficiency can also be calculated as a ratio of donor intensity in the presence and absence of acceptor. Both methods were tested. All images are initially background subtracted. Emission crosstalk is then corrected. The corrected FRET can then compared against either of the above controls in a ratio. However, the resulting FRET values are not distributed as expected. Often higher FRET values are localized to the cell area and low FRET values the regions outside the cell. This suggests that true FRET changes do not occur by the designed route.

We confirmed that evaluated FRET does not occur by the expected route by omitting the RGD adhesion peptide at the 3' terminus of the hairpin. Comparing the FRET images from these experiments, with the RGD-containing experiments, yielded similar results. The observed dark regions may be contributing too strongly to the individual fluorescence channels to evaluate a significant FRET ratio image result.

3.3.2 Discussion

As previously mentioned, the quenching effect is not specific to the cyanine FRET pair and larger differences were detected for the brighter red dyes. To alleviate this quenching effect in our FRET assay, we also tried a quencher system. In this case, a FRET ratio can still be evaluated by comparing the donor intensity in the quenched region against the donor intensity of a quencher-free region. This measurement also did not return high ratios localizing to cell adhesion. Given our results with the other fluorophores, it is reasonable that the open hairpin conformation leading to the fluorescence 'on' state (un-quenching) returns diminished signal as a result of quenching by cells. Depending on the strength of the initial signal and the extent of quenching by cells, the unquenched fluorescence may be difficult to resolve.

Experimental factors that may obscure the FRET signal include contaminants, detector sensitivity, and interaction stoichiometry. The coverslip assembly method removes most sources of contamination which may otherwise falsely contribute to the signal. As a result, the most significant signal contamination comes from inefficiency of each reaction step in the molecular assembly. Fortunately, the contributions from these contaminants are characterized at each step and easy to isolate. To address the signal to noise, we consider the fraction of molecules capable of acting as reporters (completely assembled), within the constraint of the fraction of molecules a cell requires for specific, integrin-mediated attachment.

The percentage of molecules capable of contributing to signal depends on the efficiency of the ligation reaction (typically around 80%) and conjugation of the peptide to the oligonucleotide scaffold (typically about 65%). The efficiency of the reaction is not considered because all intensities are referenced to it. This reaction efficiency is also the highest. As a result, oligonucleotides in earlier assembly steps (in this case the donor) have stronger contributions to the signal. Fluorescent oligonucleotides are added in excess and unbound oligonucleotide is removed. Well within the conditions favoring annealing, for the following estimate, the fluorescent oligonucleotide is assumed to be completely annealed to its complement. This assumption is fur-

ther validated by referencing all measurements to the same conditions in the control. Considering the efficiency of ligation and peptide conjugation, three populations of molecules predominantly contribute to the fluorescence signal: unligated 64mer (Cy3 signal; 20%), ligated hairpin with no peptide (Cy5 and FRET signal; 30%), and complete ligated hairpin sensor with peptide (Cy5 and FRET signal; 50%). In other words, 50% of the total molecular population can report anti-correlated changes in FRET and donor intensities. However, the remainder 50% of the molecules do not all contribute to the same channel.

The three populations of molecules described above affect signal in each channel differently. The unligated 64mer contributes 100% of the Cy3 signal, because all of the ligated molecules constrain the FRET pair within their Förster radius and no Cy3 emission is observed in this case. We have confirmed this statement by ligating molecules in a test tube and then immobilizing them on a cover slip surface. Here, the ligation efficiency is closer to one hundred percent, and the Cy3 channel has no fluorescence. Thus, the unligated molecule comprises all of the Cy3 signal and has no contributions to the Cy5 and FRET. The remaining 80% of the molecules are ligated; they contribute 100% of the FRET and Cy5 channels. As mentioned above, about 65% of the total FRET (and Cy5) signal belongs to molecules that can specifically report conformational changes. Thus, 50% of the molecules on the coverslip can theoretically report changes of 2:3 ($\text{FRET}_{\triangle}$:$\text{FRET}_{reference}$) in response to cell adhesion. The resulting signal change is expected to be about 10% ($\triangle$(FRET/Cy5)). We should be able to resolve this change with a CCD camera.

While 10% is a detectable change in signal, it is important to consider the fraction of molecules cells require in order to adhere to a surface. From above, 50% of the total *molecules* produce 65% of the FRET *signal* capable of reporting adhesion forces. A cell requires 10^3 molecules per μm^2 to attach to a surface (reported for an integrin close packing model). Since our sensor surfaces present a comparable number of molecules, mechanically induced transitions should be possible to resolve with fluorescence[43]. However, because we are looking for a maximum FRET ratio change of ten percent the fluorescence quenching contributed by the cell becomes more significant.

Measuring a ten percent change in FRET ratio necessitates signal localization. The model for integrin-mediated cell adhesion suggests that adhesions are localized micrometer sized areas of integrin clusters. In the case of integrin clustering, the receptors (integrins) and ligands (RGD- sensor molecules) are at high effective concentrations within the localized clusters. Assuming a system where the number of adhesion and ligand molecules is conserved, less tightly localized adhesions, where integrin clusters are not as pronounced, have lower effective concentrations. The point of effective concentrations is significant because if one micrometer-diameter integrin cluster is spread over a four micrometer-diameter cluster, the effective concentration drops eight-fold and the 10% change now corresponds to a little more than a 1% change. As a result, in the absence of integrin localization, the cell-mediated quenching would completely outcompete the FRET change.

To effectively concentrate the adhesion molecules and take advantage of the maximum contrast, we experimented with another cell line, IC21macrophages, known to have more pronounced punctate adhesions, called podosomes. Podosomes are easy to visualize and their coincidence with changes in FRET can further support a specific response. Unfortunately, the IC21 cells turned out to be much more aggressive to the sensor coated surfaces than the 3T3 line used up to that point. The macrophages left dark trails where they attached, and these areas remained dark after cells disengaged suggesting an irreversible inactivation of fluorescent sensor. Low effective concentrations of activated sensor molecules together with differential cell-mediated quenching are sufficient to obscure a FRET measurement.

Fluorescence quenching of Cy3 in DNA and of gel-embedded dyes by cells has been mentioned in[56] and [43], respectively. However, in the latter case, a gel was labeled with fluorescent dyes, and the decreased intensity was attributed to cell remodeling of the gel. A surface coated with fluorescent dye molecule does not exhibit intensity changes when cells adhere to the surface. We suspect that this decreased intensity is a direct product of the high initial intensity. FRET systems with initially 'off' configurations are insensitive to this effect because the probability of FRET-producing proximity keeps the intensity low. Molecular beacons, on the other hand, are most

frequently used in bulk solution experiments that consequently report an average across spatial contributions to intensity. In our system, the fluorophores are external to the cell and are not protected within a gel. This direct exposure to the cell-milieu and the relatively high contribution from localized, cell-mediated quenching, together obscure the FRET measurement. Attempts to eliminate or isolate the quenching in a quantifiable manner both experimentally and digitally led us to consider the possibility that the cell-mediated quenching can be adapted as a reporter of cell-surface interaction.

Chapter 4

Reporter surfaces for sensing cell-substrate proximity

Upon functionalizing cover slip surfaces with fluorescent DNA molecules, we observed that when cells are introduced to these surfaces, the surface fluorescence decreases in cell-occupied areas. Surface sensing is a powerful technique. Therefore, the cell-mediated quenching is important to consider in assay design to either eliminate or take advantage of this result. For instance, this cell-mediated quenching precludes surface FRET from being measured when the donor and acceptor dyes are on the same molecule. In this chapter, we discussed potential sources of the sensitivity to determine guidelines for controlling the effect. We also propose one way to take advantage of this quenching as a means of measuring cell-surface proximity. Comparing our Cy3 results with reflection microscopy, a technique used to image a cell's proximity to the surface, we suggest that the Cy3-DNA complex reports the intimacy of the cell-surface interaction which displays a relatively binary response within a thickness of 15nm.

4.1 Experimental design

Multiple imaging techniques have been adapted to address the distance between the cell and the surface. Among them are interference reflection microscopy (IRM), to-

tal internal reflection fluorescence (TIRF) microscopy, fluorescence resonance energy transfer (FRET), surface plasmon resonance (SPR), and electron microscopy[21]. A similarity between these methods is that they limit the measurement to a thin section adjacent to the surface of illumination and with varying degrees of sensitivity return information about the cell-surface distance as a function of signal intensity. The cell-surface separations, as determined by these methods, are generally 5-100nm and can be classified in three regimes of contact. Theoretically modeled energy minima for cell-surface separations have yielded consistent results and note three energy minima for cell-surface separation distances[3]. The first two regimes of contact are adhesive contacts. The third regime results from the bounds placed by the nearby adhesion contacts. As a result, the closest (focal) contacts at the lamellar region of the cell, constrained by a van der Waals attraction-repulsion balance, are 5-10nm from the surface. The surface-membrane separations of specific adhesions to ligands are constrained by the protruding extracellular proteins that specifically meet the ligand and yield 20-40nm separations. The remaining non-adhesive separations can be as large as 100nm.

Taking these measurement considerations into account, our experimental design is also sensitive within a thin section adjacent to the surface. However, the advantage of a molecular sensing system is the ability to extend the measurement to thin sections further from the surface, in contrast to many methods where surface confinement is instrumentally constrained. This flexibility is specific to both quenching and FRET. We use a quenching-based technique and introduce cells to highly fluorescent surfaces. A quenching based measurement is less restricted than FRET because one quencher molecule does not have to be identified and we can measure the overall effect contributed by introducing a cell. The following describes our all-fluorescence assay (Figure 4-1). for reporting the intimacy of the cell-surface interaction.

In this cell assay, we took advantage of the modular design, described in previous chapters, to yield independent, attachment, reporting, and biasing capabilities. The reporter complex consists of the Cy3 and DNA. The DNA backbone also provides an ideal scaffold for further modifications to the molecule. At the 5' end of the DNA

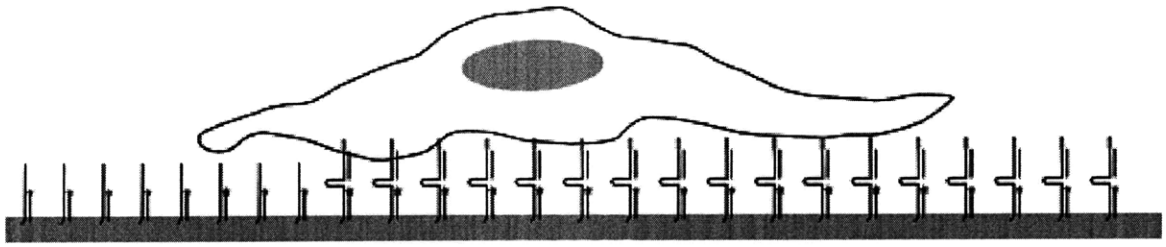

Figure 4-1: Duplex DNA with Cy3 modification with and without a biasing RGD adhesion peptide. When cell is near the surface, fluorescence is quenched.

scaffold, a primary amine serves as the attachment point to a glutaraldehyde coated cover slip. At the 3' end, the presence or absence of an adhesion peptide can bias cell sensor interaction. The Cy3 is at the 5' end of a complementary oligonucleotide and is introduced via an annealing step to form the final duplex. The validation steps to confirm peptide and surface attachment chemistries are discussed in the previous chapter, sections3.2.1 and 3.2.2.

Surface intensity reports the interaction of cells and fluorescent surfaces. The initial fluorescence intensity is high, uniform, and provides a strong reference signal. We observed that plating cells on a surface coated with fluorescent DNA oligonucleotide, yields lowered fluorescence intensities in areas coincident with the cells. The extent of this quenching is measured as a ratio to the reference background signal. As a cell makes more intimate contacts to its substrate, the surrounding media is excluded and the sensor's micro-environment approaches that induced solely by the cell. We test the hypothesis that this sensor system reports cell-surface proximity.

One technique developed to evaluate the cell surface proximity is reflection microscopy. Reflection microscopy yields an image of the topography of the contact-side of the cell. The reflection microscopy method was first developed by Vasicek and Van den Tempel, but introduced to cell biology by Curtis. The optical configuration for reflection requires the same components as differential interference contrast (DIC), with the difference that in reflection mode, the illuminating light traverses the objective side twice. The reflection configuration can thus be achieved by modifying the fluorescence light path with a half mirror in place of a dichroic mirror. A mercury lamp provides the light source filtered by 545/30 band pass filter and the reflected light is

attenuated by a 535/30 filter in front of the CCD camera. The field diaphragm and iris aperture are adjusted for minimal extraneous illumination and maximal contrast.

The reflectivity of the glass determines the imaged intensity of light. The reflectivity, R, is the ratio between incident, I_0, and reflected, I_r, beam and is entirely a function of the index of refraction, n: $R = \frac{I_r}{I_0} = (\frac{n_1-n_2}{n_1+n_2})^2$. The highest reflectivity is at the glass surface due to the high index of refraction of glass. As a result, the background of reflection images appears light. The reflectivity decreases when the glass is in contact with the cell membrane (high index of refraction 1.4) and less so when in contact with medium (lower index of refraction 1.34). The intermediate intensities result from multiple reflections that vary with the thickness of the medium layer between the glass and the surface and thus the cell-surface separation. In theory, the intensities provide a direct map of the proximity of the cell to the glass surface.

The reflection image is a result of differences in the distance light traveled before reflection and the differences in index of refraction between reflecting surfaces. The dependence on thickness and index of refraction is reminiscent of the transmitted light pathway where phase shifts result from retardation by the sample based on these same two principles. Unlike transmitted light, the reflected beams can interfere with each other to produce an image with lighter and darker regions representing separation distance from the surface. This separation distance is the thickness, d, of the medium between the cell and surface. The difference in optical path, $\triangle$, traversed by the beam reflected from the interface and refracted into the sample before reflection at the second interface, is given by the cosine law: $\triangle = 2n_{medium}d\cos\theta$.

The optical path difference will yield a dark fringe when the difference is an integral number of the wavelength and a light fringe at half integral values of the incident wavelengths. At high illuminating numerical apertures, the illumination cone incident upon the sample covers a wide range of angles. As a result, the interference image becomes a continuum of fringes that almost completely cancel each other. The remaining interference image shows only converged zero-order intensities. These zero-order intensities span about 150nm (depending on the incident wavelength/2), with a continuous transition of dark to light. A sample reflection image is shown in Figure 4-

2. Although there is some controversy on the topic of quantifying reflection images, semi-quantitative reflection images can be obtained with control over illuminating numerical aperture and incident wavelength.

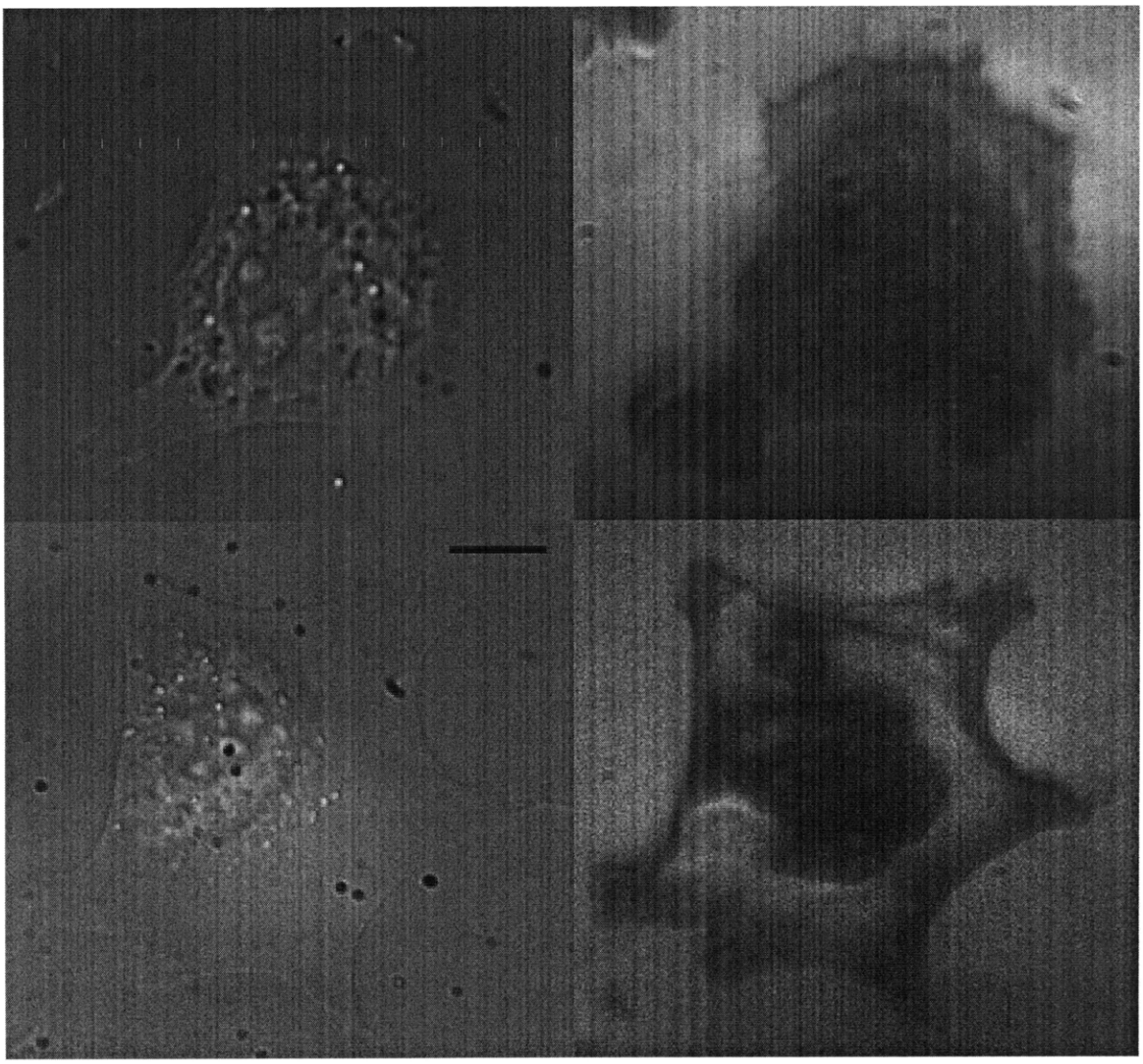

Figure 4-2: Reflection images show cell-surface separation. The reflectivity of the glass determines the background intensity. Smaller separations appear darker and can be seen in regions where cells make more intimate contacts to the surface.

The reflection images show regions of lower intensities against a light background with smaller cell-substrate separations. Dark regions outline the ruffles near the periphery of the cell. Polarized cells, with lamellar extensions at the leading edge, also show a narrow band of increased separation prior to the ruffled lamella. This observation is consistent with migrating cells searching the space at the leading edge

by protruding lamellar extensions prior to making strong contacts. To compare the range of intensities from the reflection and fluorescence images, we configured the Zeiss Axiovert inverted microscope to sequentially collect DIC, fluorescence emission, and reflection images.

Table 4.1: Oligonucleotides for Reporting Cell-Substrate Proximity

Name	Tm (°C)	Sequence 5' to 3'
Cy3.25	51.7	Cy3 - CAA CAA TAC ATC ATC TAC CAT CAT C
25.Cy3	51.7	CAA CAA TAC ATC ATC TAC CAT CAT C - Cy3
NH2.64	71.6	NH2(C6) - GAT GAT GGT AGA TGA TGT ATT GTT GTT TC G CCG CGG GCC GGC GCG CGG TTT TCC GCG CGC CGG

We applied our fluorescent assay to quantify three cell-mediated pathways that yield decreases in fluorescence intensity. Our primary interest is in quenching due to the cell-sensor interaction. To isolate the intensity change due to quenching and eliminate false positives, we evaluated the intensity contribution of two competing pathways: sensor inactivation by the cell and fluorescent oligonucleotide incorporation into the cell. Cy3 quenching resulting from cell-imposed microenvironment resembles reflection microscopy images. This relationship suggests that the molecular sensor is a reporter of cell-surface proximity.

4.2 Quenching characterization

Fluorescence quenching results when multiple processes compete for route to relaxation back to ground state. By design, the most desirable of these processes is fluorescence emission. We showed that introducing cells to fluorescent surfaces leads to reduced fluorescence intensities localizing to the body of the cell. Quenching is typically reported as a percent representing the ratio between sample and reference intensities. Since, the cellular environment is complex, and the quenching ratio averages across multiple processes that lead to intensity decrease, in this section we evaluated contribution from several competing sources of intensity decrease to isolate

quenching specifically due to cell environment imposed upon the fluorescent surface. Other contributions to quenching may arise from permanent intensity decreases such as chemical inactivation of sensor or physical incorporation of fluorescent oligonucleotide.

Quenching due to cell-mediated interaction that is recoverable may be used as a reporter of cell-surface proximity. Cell images are collected over long timescales. Consequently, the fast, short-lived interactions have an average contribution to signal intensity. Other, non cell-specific contributions to quenching are normalized to the reference signal. The longest-lived contributions are due to specific interactions between a fluorophore and quencher or specific interactions between molecules that in turn bring the fluorophore and quencher into proximity. We considered the effect of cell adhesion specificity to the fluorescent surface to localize areas of more intimate cell-surface contact. As a result, we found that non-specific attachment leads to intensity changes that strongly compete with the quenching measurement.

Table 4.2: Intensity decrease contributions

Source	Quantity[1]
Spatial (total)	0%-70%
Chemical	–%
Physical[2]	–%
Temporal (per 15 min)	
Bleaching (cell-free)	2%
Bleaching (cell-coincident)	1.4%
Incorporation	0.9%

4.2.1 Spatial contributions

Adding cells to the fluorescent surfaces yields areas of decreased fluorescence localized to the adhered cell bodies, as imaged by Cy3 fluorescence and transmitted light. These lower intensity regions are highly correlated to cell incidence, but the two do not co-localize entirely under some conditions. In some cases, the cell-trail coincidence varies with incubation time and binding specificity. In fact, the ratio of cell-to-trail

area has been observed to be as high as 130%. This deviation from one-to-one correlation results from competing temporal contributions to intensity decrease such as fluorescent oligonucleotide uptake by the cell (Section 4.2.2). This important observation brings attention to processes other than quenching that decrease fluorescence as well. To isolate cell-mediated quenching, we quantified contributions from other processes that decrease fluorescence but are not a direct consequence of cell-mediated quenching. Two significant considerations were degradation and incorporation by the cell. Sections 4.2.1 and 4.2.2, respectively, discuss experimental modifications to reduce contributions from these factors.

A set of intensity values associated with quenching phenomena emerges when the distribution of intensities is normalized. The background intensity in the cell-free area serves as a reference intensity for evaluating extent of quenching. The lower boundary on intensity is given by fluorophore-free portions of the cover slip, which define the background level of fluorescence. These two boundaries define the dynamic range of intensity information. We find that intensity decreases due to specific cell-adhesion mediated quenching are around 15-40%, non-specific cell-adhesion and non-quenching mediated processes yield much larger changes that span a broad range. Figure 4-3 shows an example of an intensity plot through the cell body on a fluorescent surface. In this figure, the cell attaches specifically and quenches surface fluorescence by about 40%.

The fluorescence decrease is uniform and spans a narrow distribution of intensities. We sampled small areas ($25\mu m^2$ squares) and generated intensity histograms to asses whether strongest quenching localizes to the leading edge of the cell, where close contacts are most frequent the cell is in closer proximity to the surface. Comparing intensities in the leading edge of the cell, the cell body, and the lagging edge we found that the lowest intensities localize to the leading edge, while the least quenching is observed for the lagging edge. Stronger quenching, we expect, is indicative of more intimate surface contact. For the assay conditions described above, the intensity differences between the leading and lagging edge are small (several percent). The cell body shows intermediate values of quenching, also within the several percent range,

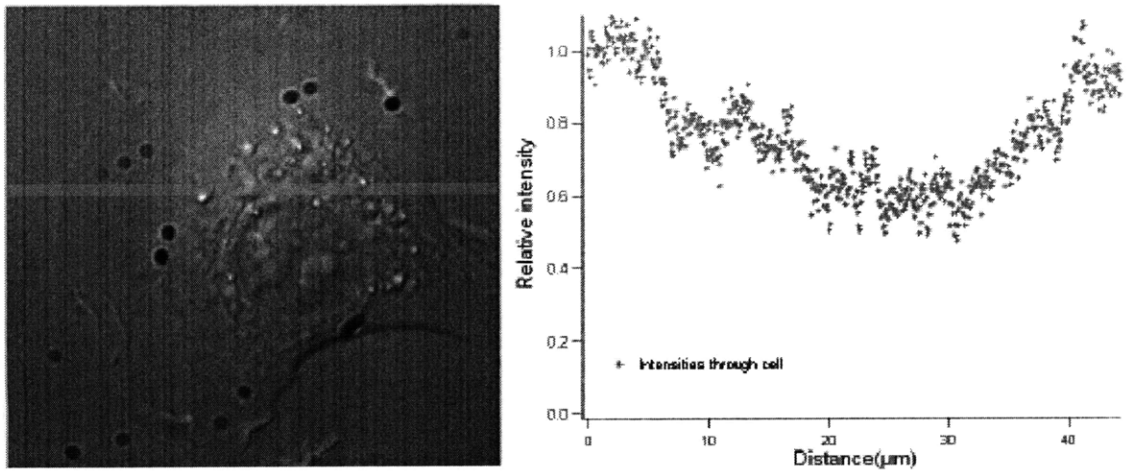

Figure 4-3: Cells quench surface fluorescence. Cell-adhesion to the fluorescent surfaces quenches fluorescence underneath the cell. Left image indicates the pixels represented in the profile plot on the right. Right graph plots the intensity values vs distance for the corresponding Cy3 image.

and the Cy3 response to cell appears mostly binary. We measured larger intensity variation for other surfaces (Section 4.2.3).

Physical and Chemical

Potential contributions to the intensity include physical and chemical processes that are not factors in the absence of cells. Examples of physical processes introduced by cells include removal of fluorescent oligonucleotide and cell-sensor interactions that decrease the fluorescence intensity. Oligonucleotides that are removed from the surface, but are not incorporated into the cell are free to re-anneal to the sensor complex. The equilibrium of duplex state is regulated by the temperature and ionic concentration; at 37°C and $1{\cdot}10^{-1}$M NaCl concentration, duplex state is more favorable. As a result, any removed oligonucleotide confined within the extracellular space between the cell and the substrate experiences favorable conditions to reanneal. However, on the cell imaging time scale (image/10-15minutes), contributions from this potential pathway are averaged into the overall quenching signal.

Another mode of decreased intensity may result from cellular-degradation of the sensor molecule. Two possible modes of this degradation are chemical and physical

degradation. Chemical degradation would yield an unrecoverable loss of fluorescence, due to fluorophore oxidation, for instance. Physical degradation can result from the cell removing the fluorescent dye mechanically. Mechanical Degradation is discussed in more detail in Section 4.2.2.

The difference between these two phenomena can be captured in the ability to recover fluorescence intensity through a chase experiment. Both modes of inactivation are irreversible, for time-scales of interest. We distinguish between the two modes by adding fresh fluorescent oligonucleotide and repeating the hybridization step to asses the fluorescence recovery. For the physical inactivation pathway, adding fresh fluorescent oligonucleotide, recovers fluorescence. Alternatively, chemical inactivation of sensor requires removal of inactive fluorophore, prior to hybridization of fluorescent oligonucleotide to recover fluorescence. These chase experiments distinguish between chemical and physical pathways to sensor-inactivation. Both modes of sensor inactivation yield a decrease in fluorescence intensity, which competes with the environmental quenching.

Physical inactivation is more likely for 3T3 fibroblasts. In the case of 3T3 cells, cells and trails are not one hundred percent coincident. We observe trails in areas that do no co-localize with cells in the bright-field image. Areas where a cell adheres, however, are usually accompanied by trails underneath the cell. The extent of quenching underneath the cell and within the trails varies. When a healthy cell migrates away from a particular area, most of the fluorescence intensity recovers. Cell-detachment followed by cell-death, leaves dark trails behind after detachment. These trails leave a record of the space traversed by the cell prior to detachment. The fluorescence within the trails can be recovered by chasing in fresh fluorescent oligonucleotide. In essence, the chase step resets the surface memory for where the cell has been.

For more aggressive, IC21 macrophages, chemical inactivation is the more likely pathway. IC21 cells also recover fluorescence during migration-induced detachment from the sensor surface. Detachment preceding cell-death however, yields irreversible fluorescence decrease. This fluorescence is not readily recovered by a chase experiment (Figure 4-4), suggesting a chemical pathway of inactivation. Furthermore, melting

away bound oligonucleotide and introducing fresh fluorescent oligonucleotide in its place, does not recover the fluorescence either. It is possible that these cells inactivate the fluorescent oligonucleotide through a physical pathway and inactivate the scaffold through a chemical one.

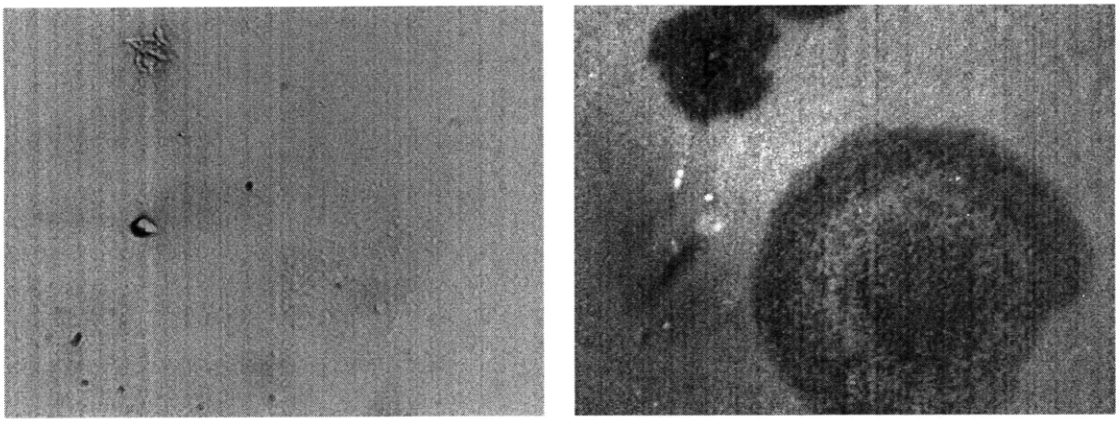

Figure 4-4: Chemical inactivation of sensor leads to irreversible intensity loss. IC21 macrophage cells plated on fluorescent surfaces incorporate fluorophore more aggressively. Removing cells and adding fresh fluorescent oligonucleotide does not return even fluorescent surfaces. Cell shaped regions remain in the Cy3 channel (right). Some cell debris indicating initial location of the macrophage can be seen in the transmitted image (left).

The morphologies of the dark regions differ for IC21 macrophages and 3T3 fibroblasts. 3T3 trails are more suggestive of the cell shape with distinct trails following cellular projections. IC21 trails are somewhat globular and loosely follow cell morphology as imaged in the bright-field. It is important to note that cellular debris yields similar fluorescence quenching to that underneath the cell. This observation is in line with the hypothesis that quenching a direct product of cell proximity. The proximity of the membrane to the surface is reported in both cases of cellular debris and cell adhesion. In the case of debris, the quenching is more pronounced and flat. It is thus easy to distinguish from a live cell quenching profile.

4.2.2 Temporal contributions

The cell-surface relationship evolves with time as a cell initially adheres to the surface and then as it migrates along the surface. We addressed temporal contributions

to quenching to account for any unevenness in surface intensity due to extended exposures to cells. The Cy3 is attached to the scaffold via a complementary oligonucleotide. This attachment is not covalent and allows us to measure the contribution of the relatively complex cellular milieu to the simple Cy3-based sensor. This design yields access to quantifying a cell's ability to remove the fluorescent oligonucleotide by internalizing it or chemically degrading it. To rule out chemical degradation of the sensor complex as a competing pathway leading to quenched regions, we confirm that the fluorescence can be fully recovered after removing cells and rehybridizing to fluorescent oligonucleotide.

In some instances the uptake of the dye is high yielding an overall increase in fluorescence co-localizing to the cell. This fluorescence increase is in the plane of the cell, not the plane of the otherwise fluorescent surface. Imaging in time shows that darker regions mostly recover after cells migrate away. The relative difference in recovery by hybridization (rescue back to background values) and after cell migration, can be attributed to uptake of fluorescent oligonucleotide. We accessed the rate of uptake by comparing expected intensity value to measured intensity.

The removal can follow multiple pathways, to yield one of two results. The fluorescent oligonucleotide can subsequently end up external or internal to the cell. It would be difficult to resolve fluorescent oligonucleotides, which are removed and externally deposited because they remain free to re-anneal/reassemble on the scaffold once the external force is removed. We therefore measured the result of fluorescent oligonucleotide uptake into the cell. In theory, we should be able to monitor the uptake into the cell by imaging in the plane of the cell. In practice however, confining the fluorescence to the plane of the surface yields much greater signal than fluorophores distributed axially within the cell. Furthermore, fluorescence within the cell can only be detected after long incubation periods and large incorporation of fluorescent oligonucleotide.

We therefore monitor the effect the cell has on the hybridized fluorescent oligonucleotide, by measuring the changes in surface fluorescence instead of the fluorescence internal to the cell. To show the effect of cell-sensor interaction, we measure the

fractional recovery of intensities as a function of multiple cell overlaps with a region of interest (ROI), via a time lapse. The interval between images is 15 minutes; this defines the time resolution. The incorporation per 15 minute-period of coincidence is about 1%.

To measure fluorescence recovery, we address two types of areas: those that coincide with the cell and those that don't. Fluorescence intensity populations in these two areas are distinct, and one can follow cell disengagement from an area by monitoring a bimodal (cell-coincident) to unimodal (cell-free) shift of the distribution of intensities. If the cell does incorporate the fluorescent oligonucleotide, the surface fluorescence looses evenness in intensity with time. This is unfavorable because we would like to measure the changes in cell-surface intimacy as a function of fluorescence decrease. The recovery of the fluorescence after the cell disengages from an ROI gives a measure of cell incorporation. This defines a threshold for incorporation-based 'noise' and allows us to isolate the quenching due to cell-sensor proximity.

Bleaching

The sensor system begins in an 'on' state and thus changes are referenced against the background fluorescence intensity. Deviations from the initial fluorescence are reported as ratios and capture any bulk and cell-independent phenomena affecting intensity, such as bleaching.

Background fluorescence in a cell-free area and the fluorescence in a cell-occupied area decrease linearly with time as fluorophores bleach. The two distinct environments bleach at different rates. This observation supports a static quenching pathway, and is further discussed in Section 4.3. It is important to consider the differential rates of quenching allowed by different environments to isolate fluorescence decrease due to bleaching from fluorescence decrease due to internalization. The independent bleaching rate of the fluorescent oligonucleotide is determined by measuring the average fluorescence intensities in a cell-free area of $25\mu m^2$. Likewise, the rate of bleaching for an ROI that is engaged with a cell is an average over $25\mu m^2$ under the cell nucleus. Both areas have an almost linear decrease in fluorescence over the course of 18 time

points, where each time point is an interval of 15 minutes.

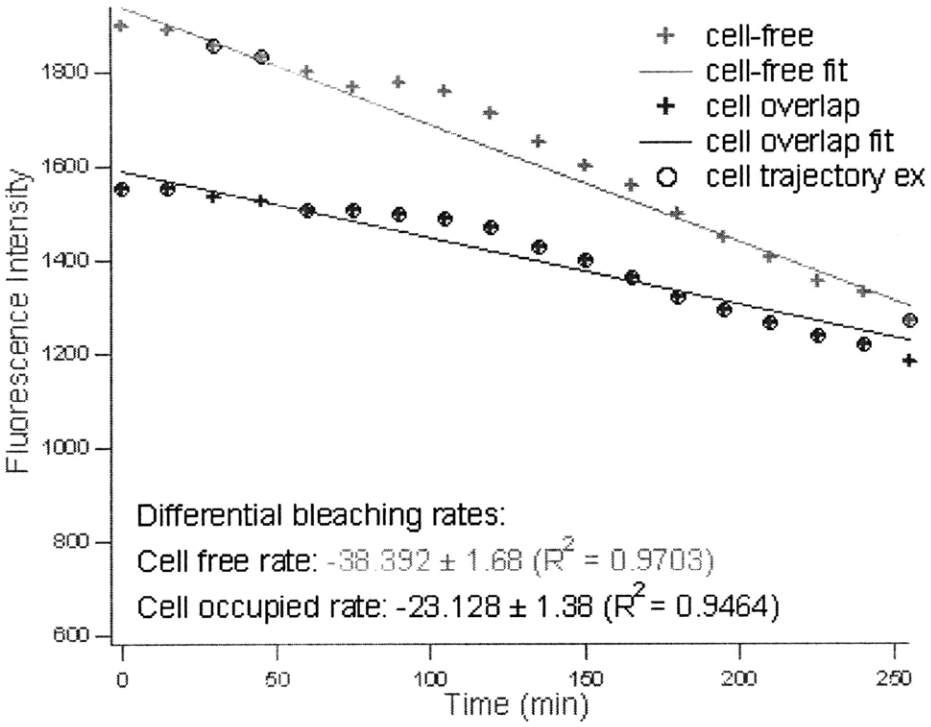

Figure 4-5: Bleaching rates vary with environment. The control plots show intensities of representative cell-free and cell-coincident areas at 15 min intervals. The exposure per interval is about 800ms. The bleaching rate is faster for cell unoccupied areas, 2%. The cell-occupied rate, 1.4%, is a function of bleaching and incorporation. S.E. ¡1 fluorescence a.u.

The bleaching rate of the cell occupied area is slower than that of the cell-free area. The cell-free bleaching rate is -38.392±1.68 a.u./frame and the cell-occupied bleaching (and incorporation) rate is -23.128±1.38 a.u./frame. The difference in bleaching rate supports the difference in chemical environment experienced by the dye. For instance, intersystem crossing mediated bleaching of the dye by oxygen molecules in solution, may be less likely in regions where the dye is shielded by the cell. Alternatively, quenching due to formation of a non-fluorescent complex between the cell and a fraction of the sensor molecules may protect the complex-engaged molecules from bleaching, while non-complexed molecules bleach at the regular rate. These rates are determined by fitting the time evolution of intensities in the two regions as shown in Figure 4-5. A frame represents 15 minutes and defines our temporal resolution. The

slower bleaching rate of the cell-occupied area is likely a convolution of bleaching and the rate of fluorescent oligonucleotide incorporation as will be discussed further in Section 4.2.2. Intensities in fluorophore-free regions record variations in illumination that might occur during the time span of the experiment.

We correct for the differential bleaching rates by taking the two distinct environments into account. For one cell trajectory, with a particular sequence of overlaps and disengagements with an ROI, we can calculate the fluorescence decrease due to bleaching given the two environmentally-dependent bleaching rates.

$$I_{bleach}(Frame) = -(k_{cell-free} * Frames + k_{under-cell} * Frames) \tag{4.1}$$

We thus correct each measurement in the cell trajectory for bleaching using the two control curves in a binary fashion. Still, the bleaching rate for the cell-occupied area is likely a product of both bleaching and incorporation. I discuss this point further in Section 4.2.2.

After removing bleaching effects, the remaining time-dependent features in the trajectory reflect incorporation. To quantify the rate of Cy3-oligonucleotide incorporation, we consider two pathways. The measured intensities that are corrected for bleaching carry memory of the cell trajectory through the incorporation of dye. In other words, deviations from the expected bleach-corrected background intensity are proportional to the incorporation because the bleach-corrected background has no memory of the cell trajectory due to incorporation of dye. The bleach corrected background (expected intensity) is generated by subtracting the same pattern of differential bleaching rates as for the trajectory. Because we evaluate the expected curve on a point by point basis, instrumental artifacts are conserved in both curves and removed when the curves are compared.

The intensity sampled areas are small relative to the cell, but large enough that partial overlap occurs in some frames. The partial overlap, as monitored in the bright-field image, is binned in a binary fashion to either on or off. However, the shadowed regions and cells are not always entirely coincident. Consequently, the cell might

co-localize with the ROI in the bright-field but the interaction may or may not be intimate enough to quench the fluorophore. This feature reflects the axial range of reporter sensitivity conversely to the lateral contributions discussed so far. Reporter sensitivity is further discussed in Section 4.3.

Incorporation

There are two time-dependent contributions to intensity. One is photobleaching and the other is deactivation by the cell. Chemical and physical deactivation were described in the previous section. This section focuses on incorporation-based deactivation, cell internalizing the fluorescent oligonucleotide. To access the internalization rate, sequential images were collected at 15 minute time intervals. We found the contributions of successive exposures to the bleaching rate. Correcting for the loss in intensity due to bleaching yields the loss of intensity due to internalization of fluorescent oligonucleotide.

The problem with the time-dependent contributions, is that they yield intensity unevenness across the surface. Because fluorescence intensity is the readout signal, these time dependent effects contribute artifacts to the measurement. The contribution from bleaching is not a significant factor for single time point data. Time lapse data are affected because some areas are coincident with cells and thus protected from this bleaching, yielding unevenness of the initial surface. Without a complete history of cell trajectory, it is difficult to extract the source of the unevenness: differential bleaching rates for cell-occupied and cell-free areas, incorporation by the cell, or both. For single time point images, only the rate of incorporation affects the evenness of the surface. To measure the internalization as a function of time a cell spends engaged with an ROI, all time dependent factors must be considered.

The recovery of fluorescence after a cell disengages from an ROI, serves as a measure of cell-mediated fluorescent oligonucleotide incorporation. The recovery decreases with the amount of time a cell spends in contact with an area, as monitored by the number of frames. The incorporation of the dye does not seem to be toxic to the cells because cells look healthy after long incubation periods, which correlate to more

incorporation. Furthermore, the recovery rate would help deconvolve internalization and cell-coincident bleaching. The instantaneous recovery is the measure of intensity change due to quenching (the remainder of the intensity going to incorporation). Unfortunately, the time resolution necessary here, would likely bleach the fluorophore and kill the cell too quickly to make the measurement.

The problem arises from the fact that the removal of dye from the surface, contributes to surface fluorescence unevenness. This unevenness is difficult to asses from a static image with no memory of where the cell was previously. We are therefore limited to determining the maximal internalization at a given point occupied by a cell by using the incubation time prior to imaging to calculate a noise parameter and threshold changes in quenching above this noise parameter.

The percent recovery is reported the ratios between the expected average intensity and the measured value. In other words, after a cell disengages from an ROI, any fluorescence lost (after accounting for bleaching) is attributed to incorporation by the cell. The percent recovery is determined from a projection of the fluorescence intensity based on differential bleaching rates. The same pattern of bleaching corrections is used to determine the expected fluorescence when there is no incorporation, and to correct the measured intensities for bleaching. As a result, we make a comparison between a curve with no memory for cell trajectory (one that does not loose fluorescence due to incorporation of dye) and a curve with memory for the cell trajectory (the one we measure from experiment). The memory contains information about incorporation.

The measured intensities are normalized to the initial value of the cell-free intensities and corrected for bleaching using 4.1. The same bleaching corrections is applied to the memory-free background intensity to evaluate an expected intensity value and percent recovery as follows:

$$I_{exp} = I_{cell-free} - I_{bleach} \tag{4.2}$$

$$Recovery = \frac{I_{measured}}{I_{exp}} \tag{4.3}$$

The percent not recovered is the amount internalized by the cell. The recovery de-

creases with the time a cell spends engaged with the fluorophores within an ROI. For one trajectory, we evaluated the recovery as a function of engagement time. The cell-free end points of one cell trajectory (see trajectory 1 in Figure 4-5) yield an incorporation rate of 0.9% fluorescence intensity incorporation per 15 minutes. Assuming close packing of sensor molecules, this roughly correlates to 90 molecules/μm^2.

We used this same trajectory to establish the incorporation relationship. The trajectory requirements are two points where a cell is not engaged with an ROI, to serve as endpoints for an otherwise cell-engaged time trajectory. We show one such data set that estimates incorporation rate for a cell that was engaged with a particular area for 0, 30, 195, and 225 minutes. Evaluating the endpoint difference for each time interval, the measurement yields an incorporation rate of 0.951% per 15minute time point with our temporal resolution. This rate in combination with the incubation time prior to imaging sets the threshold noise.

Incorporation of fluorophore creates unevenness in fluorescence intensity, thus, to compare different ROI trajectories, we normalize them. The initial cell-free endpoint is normalized to the averaged intensity value in the cell-free control plot at the corresponding time point. This step erases previous memory of the fluorescent surface and sets the initial point to a value that is unaffected by cells while preserving the relative relationships of the subsequent time points. The normalization is propagated to the final cell-free end point and the resulting fluorescence changes remain a function of bleaching and incorporation rates. From the same initial normalized cell-free endpoint, an expected intensity is evaluated for the final cell-free endpoint. The expected trajectory is only a function of the bleaching rate. Comparing these two values thus gives an estimate of intensity loss due to internalization.

The cell-engaged sensor complexes are subjected to slower bleaching rates than exposed complexes. The rate of bleaching here is likely a product of both cell internalization and bleaching. To calculate recovery, we used the combined rate as an estimate for bleaching. As a result, the equation underestimates the extent of internalization. With the current system, it is difficult to isolate the two effects. To address the underestimation, we subtracted the rate of fluorescence loss due to in-

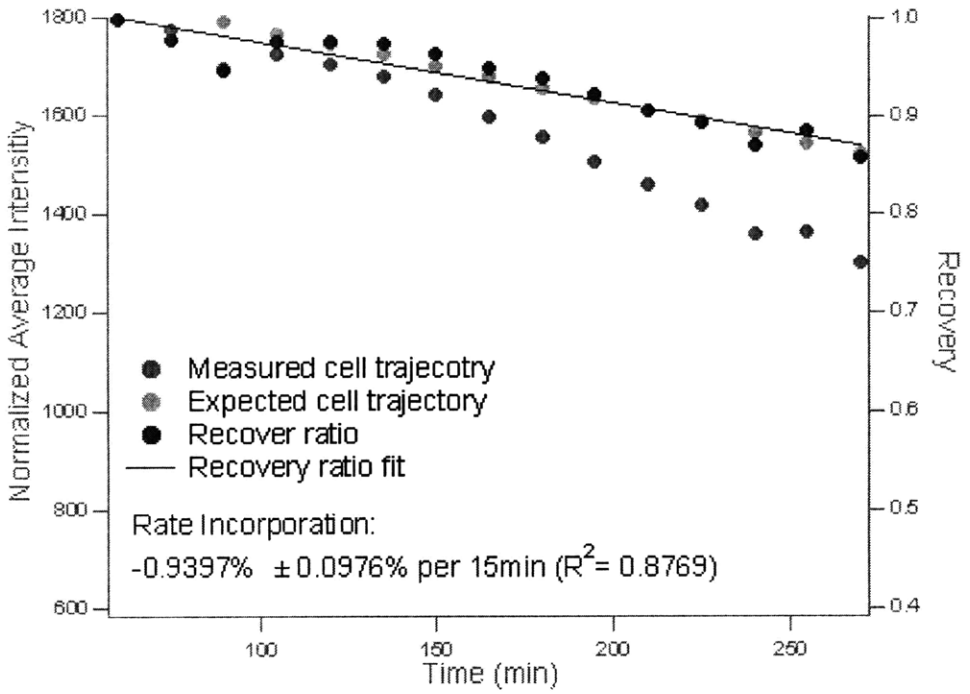

Figure 4-6: The incorporation rate is about 1% per 15 minutes. The incorporation rate is determined from two cell-free end points of an otherwise cell-ROI coincident trajectory. Initial values are normalized to the cell-free background at the corresponding time point in the control plots. The bleaching rate determined for the cell-occupied area is used to evaluate the expected cell trajectory. The Measured value is compared against the expected value at the two end points to determine the rate of fluorescence intensity decrease due to incorporation by the cell. The determined rate is subtracted from the initial bleaching rate, and a new bleaching rate is computed. This process is iterated four times before the rate of incorporation converges to four decimal places.

corporation calculated from the combined bleaching and incorporation rate. The loss is fairly small and four iterations yield convergence to four decimal places. The cell-mediated incorporation of dye molecule is therefore $0.9397 \pm 0.0976\%$ as determined from a fit to the cell-free end points of a cell trajectory shown in Figure 4-6.

We have observed both fluorophores inside the cell (proximal to the nucleus) and the decreased recovery of the trails on the surface. The incorporation of fluorescent oligonucleotides by the cell decreases the evenness of the surface. With the ability to quantify this effect, and keeping incubation time between plating and imaging short, we can set a threshold for determining real signal due to quenching. The next section addresses the difference in registered quenching signal in the presence and absence of

a biasing peptide terminal to the sensor. The incorporation rate discussed here, was evaluated only for peptide-presenting surfaces due to limited viability on peptide-free surfaces fro extended periods of time.

4.2.3 Specificity contribution

The specificity of the cell-surface interaction affects the morphology of fluorescence quenching at the cell-surface interface. We looked at interaction specificity by comparing cells on RGD-presenting surfaces with cells on RGD-free surfaces. Up to this point, we have biased the cell-surface interaction by incorporating an adhesion ligand at one end of the scaffold to encourage interaction between the cell and the surface. We removed the bias to look at the differences in adhesion maps between specific and non-specific sensor binding. We compare the maps based on metrics of intensity distributions reporting the fractional fluorescence decrease of Cy3 compared to cell-free regions. On peptide-free surfaces, cells tend to be weakly bound and less viable. The differences in quenching morphologies as imaged in the fluorescence channels are show in Figure 4-7.

Cells require adhesion moieties on the surface to adhere and spread. Hairpin sensor-coated surfaces that do not present the RGD peptide require supplement to study non-specific adhesion to the hairpin sensor. We provided this supplement via non-specific surface adsorption of RGD peptide, fibronectin, and FBS, individually. For surfaces without RGD peptide at the hairpin terminus and without one of the supplements, very few cells are able to spread on the sensor surface. Cells with poor surface attachment tend to remove the fluorescent oligonucleotide leaving two types of trails: quenched and unrecoverable. The intensities arising from the two are sufficiently distinct to distinguish between them. Candidate cells were chosen, to measure the difference between specific and non-specific adhesion to the sensor surfaces, to compare only the recoverable fluorescence quenching.

The fluorescence images for the two surfaces specificities capture the different modes of cell-surface interactions under these two conditions. different morphologies. Generally, cells that are spread on surfaces presenting specific adhesion ligand

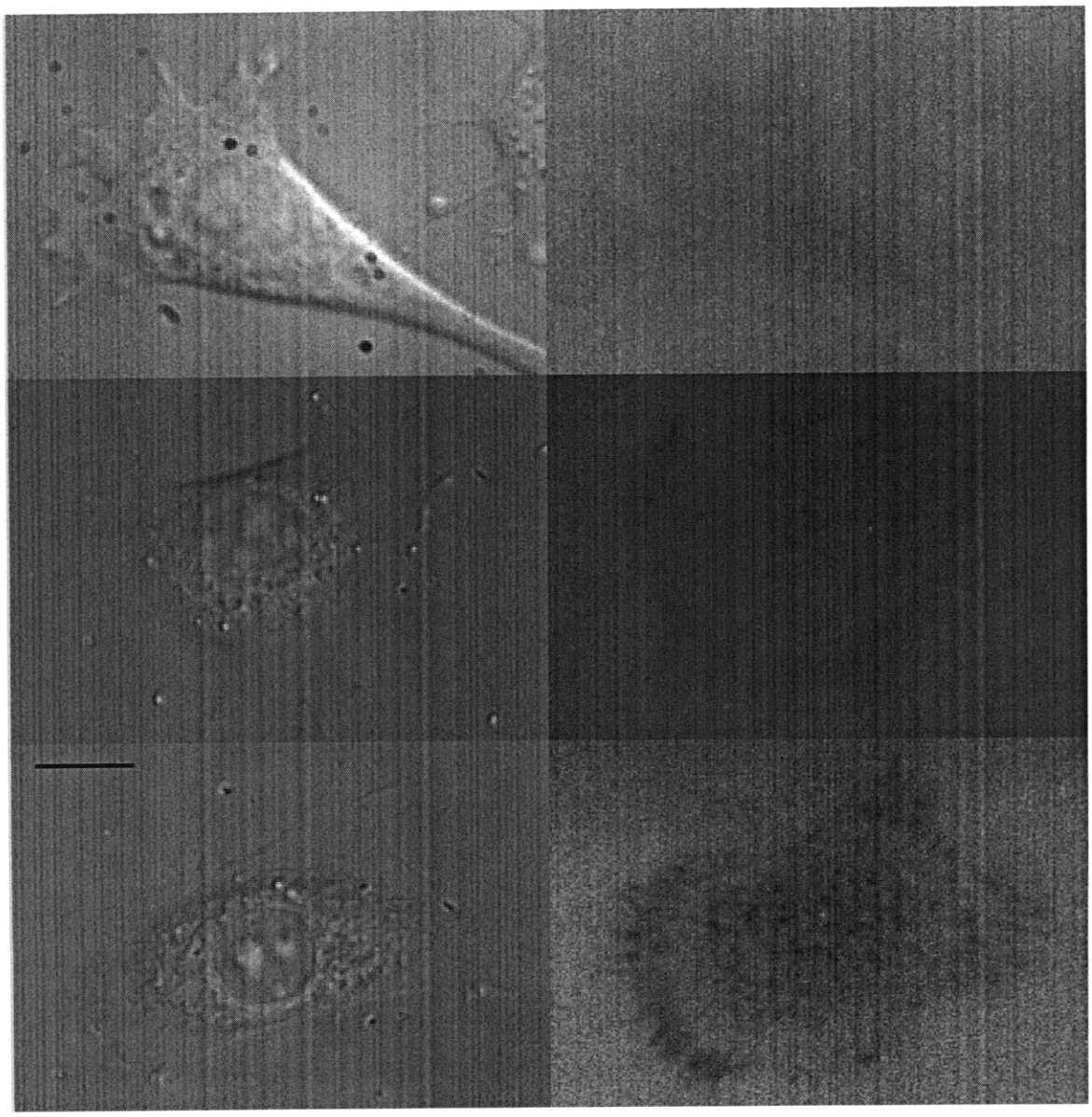

Figure 4-7: Biased and unbiased molecules show two different modes of adhesion for the RGD-free and RGD-containing surfaces. Top two images show a cell on a biased, RGD containing, surface characterized by small and uniform decreases in fluorescence. Bottom four images show morphologies reported by unbiased, RGD-free, surfaces. These quenching profiles tend to show darker radial streaks at the cell periphery. Scale bar represents 10μm.

form more uniform trails that largely correspond to the cell shape as imaged with bright-field. Cells plated on non-specific surfaces also attach, although more weakly, with more intimate contact preferentially localizing to the cell body and again to a concentrated ring near the leading edge. These two contact phenotypes, reported as

quenching variations in the surface fluorescence, readily identify the two populations of cells. The two populations are shown in Figure 4-8.

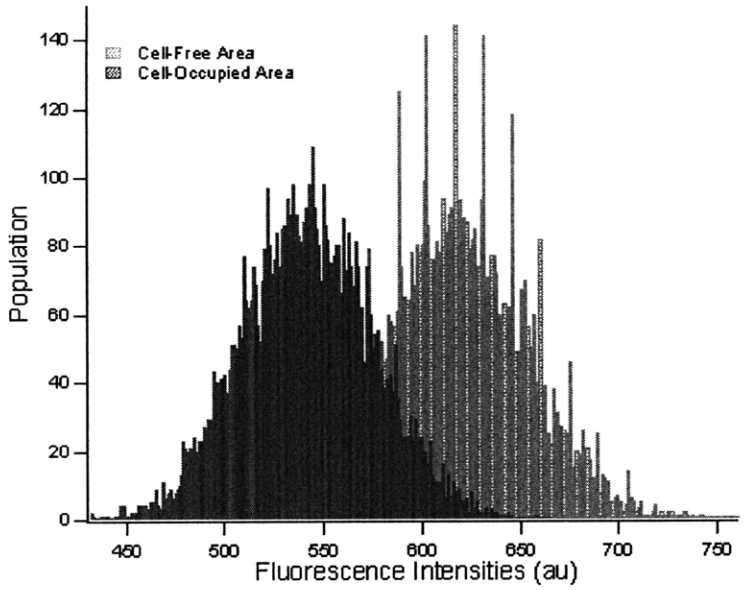

Figure 4-8: Cell occupied areas show a peak intensity shift compared with reference background yielding two distinct populations.

Small fractional fluorescence decreases and narrow intensity distributions characterize biased (peptide-presenting) cell-surface interaction. Intensity histograms for the four regions (cell-free, lagging edge, cell body, and leading edge) cover a narrow range, about 12%. The fractional fluorescence decreases are also relatively small, with the largest localizing to the leading edge. The fractional quenching relative to the cell-free areas are 0%, 4.7%, and 11.9% for the lagging edge, cell body, and the leading edge, respectively. The trails underneath these cells are uniform and less intense.

Non-specific adhesion surfaces show more variation, which is captured by the wider spread of histograms representing the four regions of interest and larger fractional decreases in fluorescence. We find that the fluorescence decreases as much as 73.4%, while the cell body and the lagging edge quench the fluorophore 47.3% and 21.6%, respectively. Of note, is that the highest quenching occurs about 5μm from the edge of the cell, following the same arc as the edge. This result is similar to actin stained cells that show a drop in actin concentration near the leading edge. These results are shown in Figure 4-9 and summarized in Table 4.3.

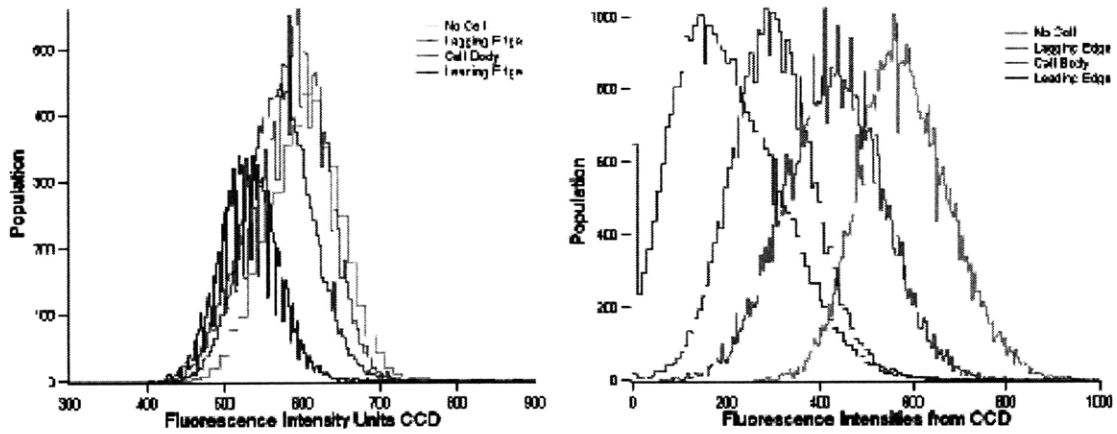

Figure 4-9: Specificity of the cell-surface interaction affects the distribution and intensity of adhesion-induced quenching. Cell on non-specific surfaces have more localized quenching, with strongest decreases at the leading edge, 73%. Cells on specific surfaces have more uniform trails with darkest regions, 12% decrease, also localizing to the leading edge.

Table 4.3: RGD Biasing Summary of Percent Quenching

Biasing	Leading edge	Cell body	Lagging edge
RGD+	11.9%	4.7%	0%
RGD-	73.4%	47.3%	21.6%

Biased and unbiased surfaces influence mode of cell attachment. Cells on biased surfaces experience a uniform and dense field of ligands. On these surfaces, cells maximize their contact with the surface through interaction with peptide molecules that are uniformly distributed underneath the cell. The intensity maps for these surfaces show fairly uniform quenching underneath the cell. On non-specific surfaces, cells adhere via a different mode. Non-specific cell-surface interactions may lack the minimal energy separation associated with membrane protruding receptor protein clusters meeting their ligands[3] and are thus more likely electrostatic in nature [85]. The van der Waals repulsion minimum yields the smallest surface separations of 5-10nm. We measure this regime of maximal quenching at the leading edge of the cell for biased surfaces and the cell perimeter for non-polarized cells on non-specific surfaces.

The strength of non-integrin cell-surface attachment is defined by the chemistry of

the surface. The surface chemistry affects non-specific cell adhesion the same way it affects non-specific protein adsorption. Proteins adsorption likeliness is related to the likelihood of the surface to release the surface-bound waters. Water can be bound to surface groups by hydrophobic interactions (structured water) and hydrophilic interactions (hydrogen bonding). Hydrophilic interactions can be guided by hydrogen bonding to neutral polar groups (-OH and -C-O-C-) or polarized by ionic groups (–COO- and -NH3+). The difference in entropic gain associated with release of structured water molecules for hydrophobic and hydrophilic surfaces drives hydrophobic surfaces to adsorb proteins most strongly and hydrophilic surfaces to exclude proteins most strongly. Negatively charged surfactants also successfully exclude cells because the interaction with the negatively charged carboxylic acid groups on proteins and cell is unfavorable. We attribute poor adhesion to RGD-free, unbiased, surfaces to this unfavorable interaction.

Two strongly guiding properties for cell adhesion are the functional chemistry of the surface and the presence of ligand for specific cell attachment. In particular, cells have a preference for binding charged, hydrophilic surfaces[7, 40, 5]. Cellular response to charge is so strong that positive surfaces with and without specific RGD ligand, do not show a significant difference in adhesion strength. Furthermore, BSA blocking of positively charged surfaces reduces the strength of adhesion, but retains the same baseline adhesion whether RGD peptide is present or absent[49]. The concentration of ligand, however, is correlated to increased adhesion strength as was evaluated on artificial extracellular matrices with incorporated RGD ligands[55]. TIRF studies of cell-surface separation show the specificity of surface adhesion is accompanied by topographical differences along the cell-surface interface[13].

We observe that cells do not attach well to surfaces with no adhesion ligand. The time to attachment (post-plating) is longer and cells are not viable as long during imaging. Incubating the sensor dishes overnight with FBS enriched (up to 40%) media or with fibronectin (up to 50μg/ml) did not significantly impact the time to adhesion, but fibronectin slightly extended viability during imaging. Enhanced background adhesion did not improve cell-sensor interaction. This is significant because

for cells that do not attach well, the incorporation mechanism competes with the environmental quenching we measure. While the two modes of fluorescence decrease are easy to distinguish, cell viability is poorer on these surfaces. We observe fluorescence in the plane of the cell after cells detach.

Including RGD at the oligonucleotide terminus significantly decreases adhesion time and improves cell viability. The decreased adhesion time is important because signal loss due to incorporation of dye is linear in time. Shorter incubation times prior to imaging mean less competition to quenching from the incorporation pathway and larger dynamic range of information within the quenched regions, due to less severe thresholding cutoffs to account for baseline incorporation as a function of incubation time. The effective concentration of the adhesion peptide linked to DNA is lower than we presented in the FBS and fibronectin experiments because the yield of peptide-DNA conjugation is about 60%, this is still more than sufficient for cell adhesion to a surface, but the specific attachment to the surface via the DNA scaffold is a significant improvement for cell viability.

4.2.4 Discussion

Cell adhesion to surfaces is sensitive to a wide range of chemical and topographical surface properties, and the degree of surface preference is relayed in cell ability to adhere and spread. Cells can bind to surfaces non-specifically and specifically. Specific interactions occur through integrin mediated ligand binding, while non-specific cell-surface interactions require agreeable surface chemistry. Cell adhesion to ligand-free surfaces is sensitive to surface rigidity [28, 38], charge, and hydrophobicity [1, 86, 7] with a preference for hydrophilic, charged surfaces. The effect of charge on cell adhesion is strong, and for two surfaces with and without RGD adhesion peptide, adhesion strength does not differ significantly. Cell-surface separation topography is sensitive to the specificity of cell adhesion to a surface [81, 13].

In addition to incorporation by cells, fluorescence decrease due to bleaching, quenching, and inactivation can be isolated. Incorporation is a function of time a cell spends engaged with a particular area on the surface. Bleaching is a function of

the total exposure time of a region of interest and the extent to which fluorescence is protected by the environment. Sensor inactivation is a binary and irreversible process within the cell experiment but in some cases can be recovered once cells are removed. Having identified the contributions from competing processes, we can measure cell-induced changes as a function of Cy3 quenching.

Our observations with fluorescent surfaces are suggestive of cell-surface separations reported by other techniques. We see largest quenching at the leading edge and observe a region of strongest contact displaced a few micrometers from the very edge of the cell as is consistent with reflection microscopy images showing lamellar extensions that have not yet adhered to the surface. One discrepancy is that the next largest quenching is within the cell body and nuclear regions for both biased and unbiased surfaces. We believe that this discrepancy may be a result of larger incorporation at the area of first contact with the surface. A cell that has just adhered and has remained fairly stationary would exhibit lower fluorescence intensities in this area.

It is feasible to have a covalent linkage between the fluorophore and the scaffold to eliminate the incorporation into the cell. Still, the current system could benefit from the study of a process where cell-surface intimacy and delivery into the cell are both relevant. Other groups have taken advantage of this phenomenon to deliver genetic information into cells. In fact, two fluorophores, one bound covalently to the scaffold and one only through complementary hydrogen bonding, could be used to isolate the two events and measure both phenomena simultaneously.

In this section we showed how DNA can be used as a scaffold for building a molecular sensor. We applied this DNA-Cy3 to reporting the interaction between a cell and a surface in two different conditions: biased and unbiased adhesion. The fluorescent surface maps distinct modes of interaction for the two adhesion specificities.

4.3 Cy3-dsDNA proximity reporter

A cell makes contacts with the surface at adhesion sites. The distribution, coverage, and strength of these adhesions is governed by various surface properties including

ligand concentration, rigidity of the surface, and specificity of the interaction between the adhesion molecule and ligand. A migratory cell is polarized and has a different adhesion relationship at the front of the cell where new adhesions are made, and the rear of the cell, where old adhesions are released. The adhesive junction connecting the cell and surface has benefitted from much investigation. With the availability of easy-to-implement techniques, the extracellular space between junctions may benefit from a deeper understanding as well.

The topography of the contact side of a cell can be fairly dynamic and is important to the cell's integration of cues from the environment[22]. A thorough characterization of the topographical cell-substrate junction can define chemical, physical, and mechanical criteria for controlling a cell's net fate along these coordinates. Insight into this control, is especially beneficial to designing biomaterials. As a result, a number of techniques have addressed the extracellular space between cell and surface to find that cell-surface separation is in the 5-100nm range for closest contacts to largest separations [21].

Interference reflection microscopy (IRM) was one of the first methods to address the separations at the contact-side of the cell and soon several fluorescence techniques were adapted to measure cell-surface separation. These techniques include total internal reflection (TIRF) microscopy and FRET. The optical configuration of IRM and TIRF limits the measurement to the surface, while molecular reporters can extend three dimensionally. We present here an alternative, all-fluorescent, molecular method for detecting the proximity of the cell and the surface. This assay reports cell-sensor interaction as a function of decreased fluorescence. We evaluate this method against IRM.

4.3.1 Reporter sensitivity

Cyanine dyes are frequently preferred probes because of their relatively high quantum yield and relatively low sensitivity to environmental changes such as pH, polarity, and ionic concentration. Cyanine dyes consist of two heterocyclic rings that are joined by a conjugated carbon chain that makes it possible to tune the spectrum in the red to

far red spectral range (yielding the cyanine dyes Cy2, Cy3, and Cy5). In the excited state, cyanines undergo photoisomerization, a cis-trans isomerization about the carbons linking the two rings. This isomerization process has lower activation energy for shorter linker chains. Thus, for Cy3 (Figure 4-10), isomerization significantly competes for relaxation back to ground state and directly affects the measured quantum yield. Table 4.4 summarizes the properties of Cy3.

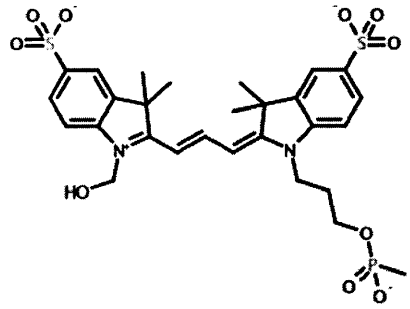

Figure 4-10: Cy3 molecule and attachment to a phosphate terminal to the DNA oligonucleotide.

Table 4.4: Cy3 properties

Excitation maximum	550nm
Emission maximum	570nm
Quantum yield[72]	
Free dye	0.04
ssDNA	0.37
dsDNA	0.16
Lifetime	180ps
Strongest solvent sensitivity	viscosity
Quenching by opposing nucleotides[59][34]	
Guanosine	46%
Thymidine	97%
Adenosine	47%
Cytidine	45%

To this extent, environments that stabilize the cis structure improve the quantum yield. For a rigid Cy3 molecule, this improves the quantum yield more than two-fold at room temperature. At higher temperatures, Cy3 isomerization competes for dominant relaxation pathway while the rigid Cy3 is mostly unaffected, yielding an even greater

improvement in quantum yield[72]. An alternative improvement to quantum yield results from increasing the rigidity of the environment. This can be achieved with lower temperatures and higher viscosities and does not require chemical modification to the dye structure. In fact, viscosity influences Cy3 quantum yield most strongly, thus constraining the dominant relaxation pathway from the excited state[88].

Along the same reasoning, bulky substituents increase the viscous drag and thus the quantum yield of Cy3. For instance, Cy3 conjugated to ssDNA increases the activation energy for photoisomerization from 19kJ/mol for Cy3 to 33kJ/mol[72]. One can imagine that within a duplex, the activation energy would be higher still, yet this is not the case, suggesting a difference in specific conformational interactions between Cy3-ssDNA and Cy3-dsDNA. The transition between the two environments can be monitored via quantum yield of Cy3.

In addition to different conformational constraints imposed by ssDNA vs dsDNA, dsDNA can introduce small differences in chemical micro-environments as a function of the nucleotide sequence. For many dyes the effect of opposing nucleotides decreases their measured fluorescence intensity, with the strongest decrease owing to Guanosine (the strongest electron donor). Cy3 intensity increases, however, for all four opposing nucleotides, with a complementary Thymidine yielding the highest intensity enhancement of 97% [59].

An interesting situation arises when molecules are not free to reorientate in solution and are instead confined to a surface. While the cis-trans isomerization can still effectively compete for relaxation pathway, the confinement changes the energetics of the resulting system and may change the photophysical properties characterized in solution. As an example, the effect of highly hydrophobic environments is difficult to test in solution where a hydrophilic molecules is not likely to remain soluble because it is free to aggregate with other similar molecules. A Cy3-ssDNA oligonucleotide hybridized to its complement in solution and at the surface of a glass slide shows the same sensitivity to registering nucleotide mismatches[60]. Still, the literature suggests that the environmental sensitivity of Cy3 is enhanced within the context of DNA so the Cy3-DNA systems has promise as a molecular sensor. In this report, we

have activated surfaces with these complexes to register the relationship between the contact-side of a cell and the surface.

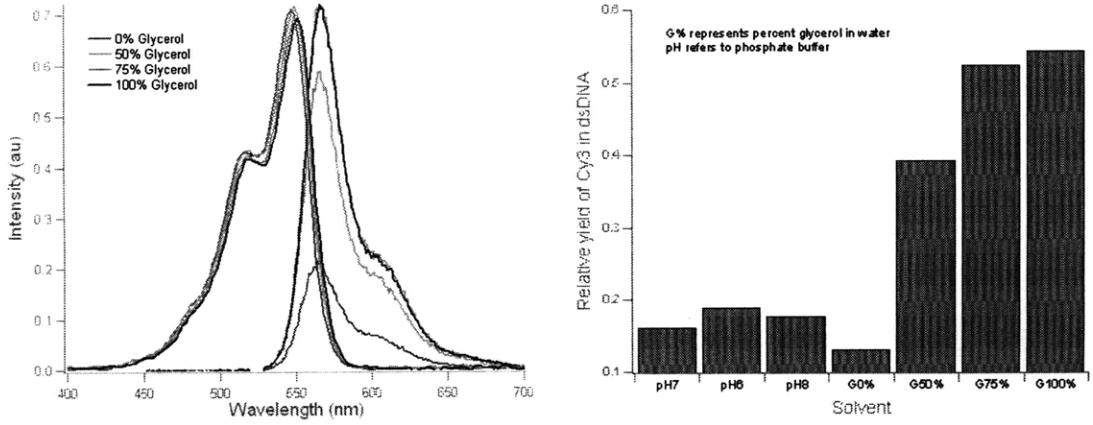

Figure 4-11: Cy3 quantum yield is strongly affected by viscosity. Cy3 emission intensity increases with higher concentrations of glycerol. Cells contribute an intensity decrease, thus environmental rigidity is not the mechanism by which cells affect Cy3 intensity.

We addressed one aspect of the reporter complex' sensitivity at the interface with steady state fluorimetry. One possible model for fluorescence changes induced by cells is that cells confine the reporter molecules within a more rigid environment. Environmental rigidity can be effectively controlled in solution by adjusting the concentration of sucrose or glycerol. In glycerol, we observe a concentration dependent increase in fluorescence quantum yield for the Cy3-dsDNA complex (Figure 4-11). This is consistent with literature reports, but does not explain the fluorescence decrease introduced by cells. We therefore conclude that the quenching is not a product of cells introducing a more rigid environment upon the sensor.

In addition to higher viscosity solutions leading to increased fluorescence, the transition from dsDNA to ssDNA should enhance fluorescence[72]. In fact, relative to Cy3-dsDNA, the most significant **decrease** in fluorescence quantum yield is reported for free Cy3 with unhindered cis-trans photoisomerization, free Cy3 in solution. A more minor dependence is reported for polarity but this relationship is attributed to the solvatochromic shift. Microscopy experiments can be particularly sensitive to such effects if the bandpass filter is not matched to the peak of the fluorescence

excitation or emission peak and this principle can be exploited to enhance sensitivity.

Multiple reports show Cy3 insensitivity to pH and to Cy3-DNA insensitivity to ionic concentration. We considered another model based on the cell's ability to disrupts duplex structure. This duplex structure destabilization may occur via multiple routes and is further discussed in Section 4.3.2. It is difficult to impose a similar process on Cy3-dsDNA complexes free in solution, with only minor perturbation to the native duplex in an energetically unfavorable way, when the molecule is free to reorientate in solution. In a simplified attempt we use urea and ionic concentration to perturb the molecule. We avoid temperature-based denaturation here for several reasons. The most significant reason is that temperature has the same string effect on quantum yield as viscosity, and would make it difficult to isolate the effect of duplex destabilization from the photoisomerization of Cy3.

Quantum yield was evaluated according to[45]:

$$\phi = \phi_{ref} \cdot \frac{I}{I_{ref}} \cdot \frac{A_{ref}}{A} \cdot \frac{n^2}{n_{ref}^2} \tag{4.4}$$

where I is the integral of intensities in the fluorescence spectrum, n is the index of refraction for the solvent, and A is the absorbance at the excitation wavelength. The index of refraction was considered for glycerol solutions of varying concentrations.

4.3.2 Cellular contribution

Within the context of the DNA duplex, Cy3 reports cell-substrate interaction as a function of intensity. In solution, intensity changes are primarily a consequence of environmental rigidity. Increase in viscosity, and thus rigidity, of the environment increases the fluorescence intensity of Cy3. When Cy3 is conjugated to DNA, the increased viscous drag increases Cy3 quantum yield for both single stranded and duplex DNA. Somewhat surprisingly, the enhancement in quantum yield is larger for ssDNA than dsDNA. As a result, from the perspective of Cy3-ssDNA, Cy3-dsDNA complexes show a decreased quantum yield. Similarly, one might expect that cells would induce more rigidly structured micro-environments upon Cy3 molecules, which

are already confined to the surface at one end via their DNA backbones. Such increase in rigidity should then correspond to an increase in fluorescence intensity. In turn, the areas occupied by cells should appear brighter, but this is not the case.

Our results from imaging cells on fluorescent surfaces indicate a decrease in fluorescence intensity. The unexpected result in DNA has been attributed to a Cy3-oligonucleotide interaction within a single strand that is disrupted upon annealing to complementary strand. In the duplex, Cy3 interacts with the first few nucleotides on the opposite strand[72, 65, 69]. In the case of cells, a similar structural readjustment may be key. In our constructs, the Cy3 dye is directly opposite a series of Thymidines. The interactions between Cy3 and nucleotides is thermodynamically unfavorable [80]. As a result, unlike many dyes that are quenched by nucleotides on the complementary strand, Cy3 shows enhanced fluorescence, in particular when opposite Thymidines. Consequently, one explanation for the observed result is that cells partially denature the duplex at its ends, which situates Cy3 farther from the opposing Thymidines. Accordingly, from the perspective of Thymidine-enhanced fluorescence intensities, the cell coincident areas of the sensor-coated surface show a decreased fluorescence intensity. One report[56], suggests that Cy3-DNA experiences a structure-dependent intensity increase upon binding by polymerase. Thus, the structural sensitivity is conserved but the relationship is reversed.

The intensity decrease has relatively binary sensitivity. The profile of intensities characterizing the cell-induced quenching is narrow and shifted from the brighter intensities contributed by the background-control signal. This narrow distribution suggests a threshold quenching sensitivity to cell-coincidence. For the sensor complex this means that the proximity of the cell imposes a new structural minimum to the DNA and thus the micro-environment of Cy3 at some threshold distance. As for the cells, considering that in this configuration, Cy3 is confined to the surface via the DNA duplex, the distance of sensitivity is limited to about 10nm from the Cy3 location. Consequently, the binary response suggests that within this surface-proximal, 10nm range, one proximity mode is dominant.

The cell-based mechanism yielding Cy3 quenching may be a result of a number of

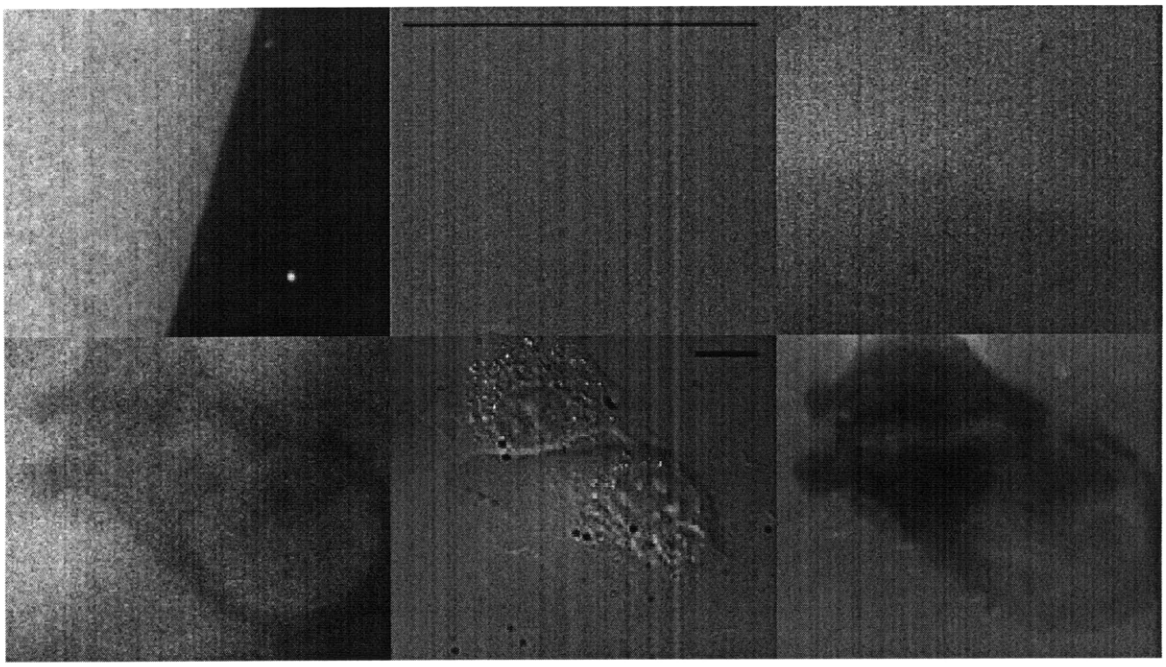

Figure 4-12: Fluorescence emission and reflection are independent. Edge of fluorescent feature show in the top panel (Cy3, DIC, Reflection). In the bottom panel, a cell's contribution to the fluorescence (left) and reflection (right) image shows similar features.

homogeneous proximity-based processes. As examples, the repulsive negative charge of the glycocalyx on the underside of the cell contributes to electrostatic repulsion, the density of intramembrane structures generates steric repulsion, hydrophobic confinement leads to more highly structured water molecules interacting with the sensor complex, or some combination of these. In solution, introducing a similar perturbation is likely to populate a continuum of states between the initial equilibrium and and the final lowest energy configuration. Confined molecules, however, have fewer degrees of freedom and thus have access to fewer available states. If the populations are monitored as a function of Cy3 fluorescence intensity, the continuum of intensities (populations) narrows significantly. Projected onto an image, a Cy3 quenching in response to cell-coincidence maps extent of cell-surface interaction. It is important to note that the quenching response we describe here is completely reversed upon cell disengagement form a particular area.

To further test the hypothesis that cell-mediated quenching is a measure of cell-

surface proximity, we compared our results against another proximity measurement: reflection microscopy. Reflection microscopy operates along a similar light path as fluorescence microscopy, with the most significant modification that the dichroic mirror in the fluorescence path is replaced with a half mirror. The result of this modification is that the topography of the underside of the cell is imaged. The interference image is a result of optical path differences between light reflecting from surfaces of varying heights and indices of refraction. We alternated between the two modes of imaging (reflection and fluorescence) and show the distinct images they form in Figure 4-12. The top panel shows the edge of an area coated with fluorescent sensor. The Cy3 emission appropriately only forms an image in the fluorescence image and is invisible in the DIC and reflection images. The bottom panel shows contribution of cells to the intensities of the fluorescent surface and reflection image.

The fluorescence images and the proximity images from reflection microscopy, report similar features. Intensity histograms for cell-engaged vs cell-free regions show a similar intensity changes in the two very different detection schemes:reflection and fluorescence (bottom left, Figure 4-14). The spatial correlation coefficient between background corrected and normalized images varies between 0.1 and 0.6 depending on surface preparation conditions. The maximum correlation between the two types of images is most likely limited by the axial resolution of the two imaging techniques. Reflection microscopy has about 150nm axial resolution and the range of intensities for a reflection image is wide. The fluorescence image has a much narrower range of intensities. Figure 4-13 compares the two normalized distributions. The Cy3 image resembles a binary version of the reflection image. This observation further confirms that our reporter is sensitive within a much finer axial range.

Proximity response is not distance-dependent. The high degree of similarity between IRM and Cy3 images in conjunction with the binary nature of the Cy3 signal led us to consider the possibility that the duplex reporter is sensitive to a range of distances about 0-10nm from the cover slip surface. Because reflection microscopy is least sensitive in this range, sensing proximity at these smaller distances would supplement the range of information available to reflection imaging. We addressed the

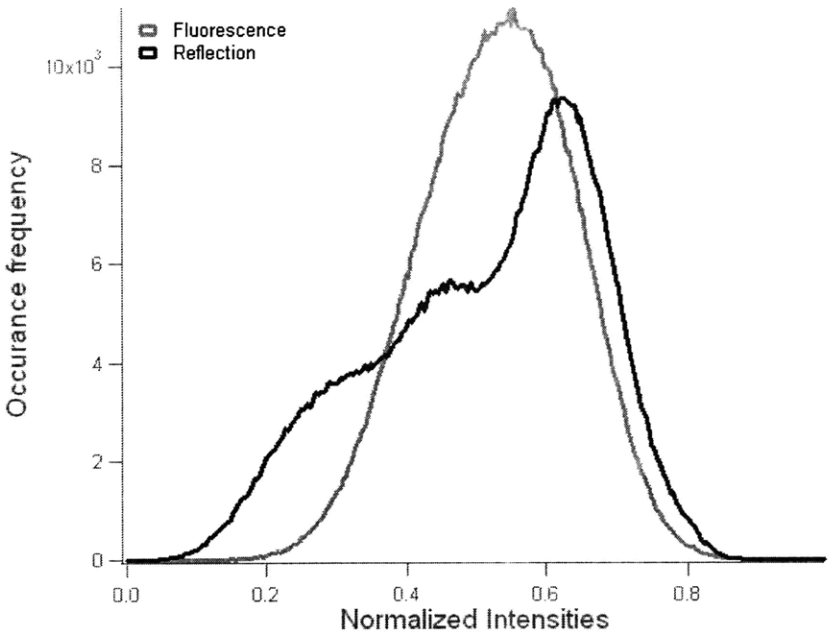

Figure 4-13: Normalized distributions of intensities for the reflection and fluorescence images. Compared to the reflection image, the Cy3 fluorescence covers a narrower range of intensities and resembles a binary version of the reflection

endpoints of this range by varying the location of Cy3 within the duplex and yielding a Cy3 nearest the surface at about 1nm displacement (limited by the length of linkers involved in DNA attachment chemistry) and a Cy3 farthest from the surface at about 9nm. This 1-9nm Cy3-surface separation did not yield significant differences in the Cy3 images. Quenching profiles showed the same relatively binary character at both endpoints and the degree of quenching localized to similarly within the cell. Given that cell-surface separation is fixed at a distance where the attractive and repulsive forces between the cell and the surface are balanced, our results suggest that within the 10nm proximity to the surface (and corresponding 16nm sensing proximity accessible to the Cy3 in the distance-variation experiments) , only one optimal separation satisfies the balance.

4.3.3 Discussion

The Cy3-DNA complex activates a cover slip surface to sense cell-surface adhesion. Upon engaging with the highly fluorescent surfaces, cells partially quench the fluores-

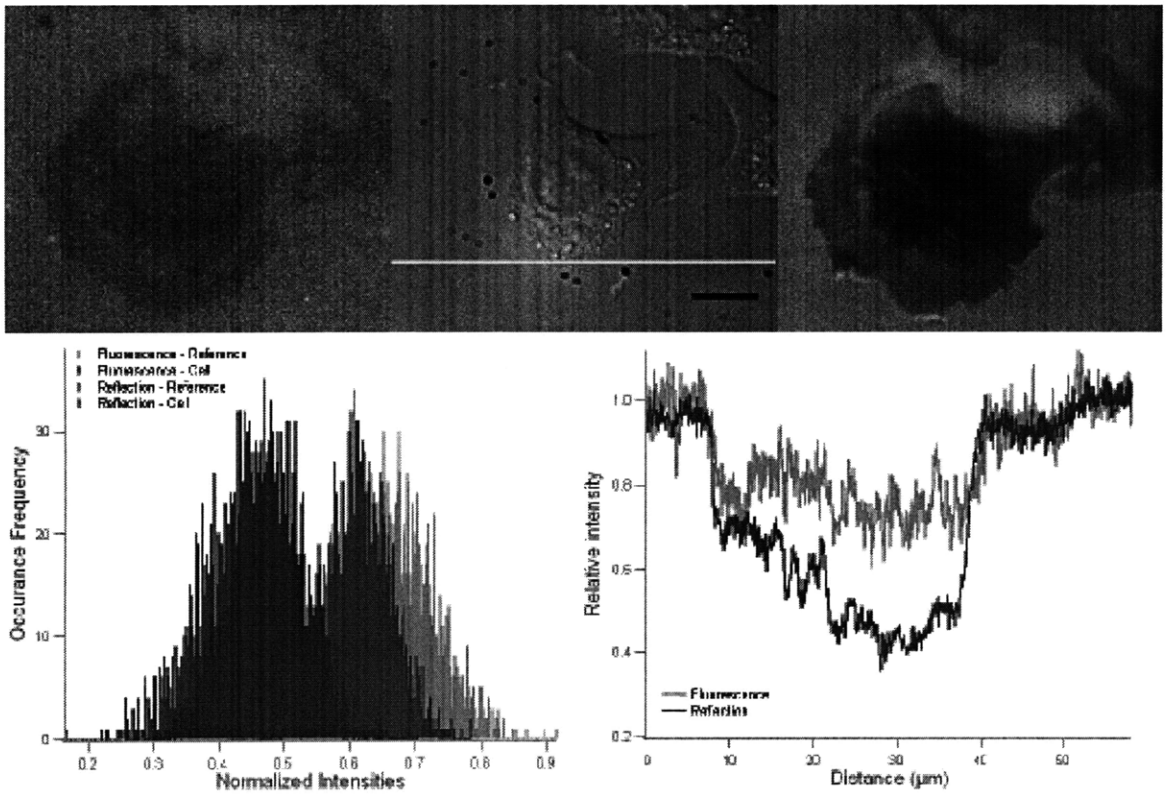

Figure 4-14: The reflection and Cy3 fluorescence images show similar features relative to an adherent cell. Top panel compares Cy3 image (left), DIC (center), and reflection image (right). The bottom panel show that normalized images show similar shifts between the leading edge and the of the cell and the background. Profile plot (bottom right) shows the increased with larger axial resolution within the reflection images.

cence intensity. The intensity changes thus map the relationship between the cell and surface. In the previous section, we quantified various sources of fluorescence intensity changes to isolate fluorescence quenching. Here, we evaluated several sources of Cy3-DNA sensitivity, potential contributions from cell adhesion-mediated confinement of fluorescent sensor molecules, and compared with reflection microscopy to asses/define the sensor system's capability.

Surface-immobilized Cy3-DNA molecules report cell-induced structural deviations via fluorescence intensity readout. Initially, the DNA duplexes in buffer solution, interact with Cy3 in a particular favorable structural relationship that yields the reference signal. Environmentally-induced deviations from the molecular contacts Cy3 makes with its initial environment affect the intensity. We record this relative

intensity change in response to cell-surface interaction. Steady state fluorescence experiments tested environmental sensitivity to rigidity and pH. The results showed that only viscosity has a strong effect on the intensity, and none of the tested conditions showed a decrease in fluorescence. Molecules with confined degrees of freedom likely report these changes differently. As for the cell's capability to alter the sensor's immediate micro-environment, we considered structural and charge mediated quenching. Unfavorable structure or charge induced conformations can decrease Cy3 fluorescence by setting bounds to the electronic relationship between Cy3 and nearby molecules to an interaction that competes for the excitation energy or fluorescence emission relaxation.

Reflection microscopy, used to image the distance between a cell and surface, provided a good imaging control. Reflection images confirmed that the changes in intensity map the proximity of the cell to the cover slip surface. The intensity histograms of reflection and fluorescence suggest that the fluorescence response is relatively binary. Some variation is evident in the extent of quenching within the cell, but significantly less than for the reflection images. This difference suggests that our fluorescence method is sensitive on a much finer axial resolution than the reflection method. Furthermore, fluorescent images from Cy3 at surface separations between 0 and 10nm from the surface, did not show a change. This observation confirms that only one cell-surface separation minimum exists within approximately 15nm from the cover slip surface.

Up to this point, we evaluated only potential chemical contributions to the observed quenching. Experiments with only dye coating the surface did not show the significant change observed for dye within DNA. We considered quenching as either a cell-induced or dye-sensitive phenomenon that is associated with deviations from the more favorable initial micro-environment experience by the dye within the DNA. Upon recommendation[48], we assessed the effect of cell-induced optical changes: fluorescence intensity change with index of refraction.

The refractive index of solvent affects the fluorescence intensity. An optical consequence of cell-surface adhesion is a change in index of refraction introduced upon

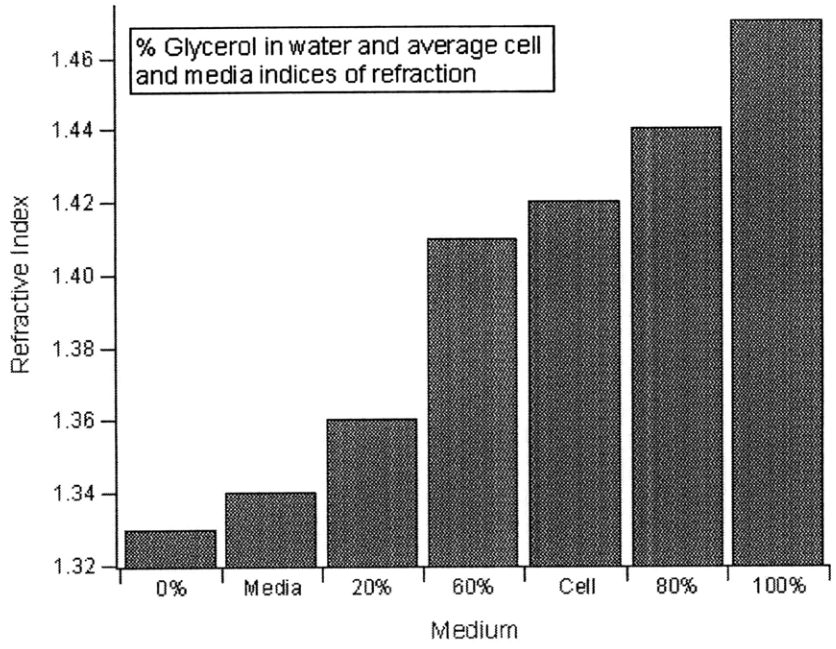

Figure 4-15: Range of refractive indices relevant to cell-imposed environments. Refractive index increases with increasing glycerol concentration. Glycerol solutions were prepared at 0, 20, 60, 80, and 100% glycerol to span the range of indices measured for cells: 1.36 (cytoplasm) – 1.48 (lipid membrane). Average index reported for cell is 1.42. These prepared samples were used for all subsequent index experiments to minimize preparation error for the highly viscous samples.

the immediate environment of the dye (cell-surface separations are on nanometer length-scales). We measured the effect of index of refraction on the sensor molecule-coated surface. The average index of refraction of a cell is about 1.42, with lower refractive index within the cytoplasm and higher for the lipid membrane. The range of indices relevant to cells matches well with the range of refractive indices spanned by glycerol dilutions. We prepared sensor coated surfaces and introduced glycerol solutions to determine the relationship between index of refraction and fluorescence intensity of the sensor surface. The relationship can be seen in Figures 4-16 and 4-17. For reference, the refractive index for the cell and cellular media is shown in Figure 4-15. Intensities for reflection images were included as a control for refractive index independence. While refractive index plays a role in the optical path difference experiences by two beams traversing different parts of the sample, reflected image formation is an otherwise distinct process and thus unaffected by solutions of varying

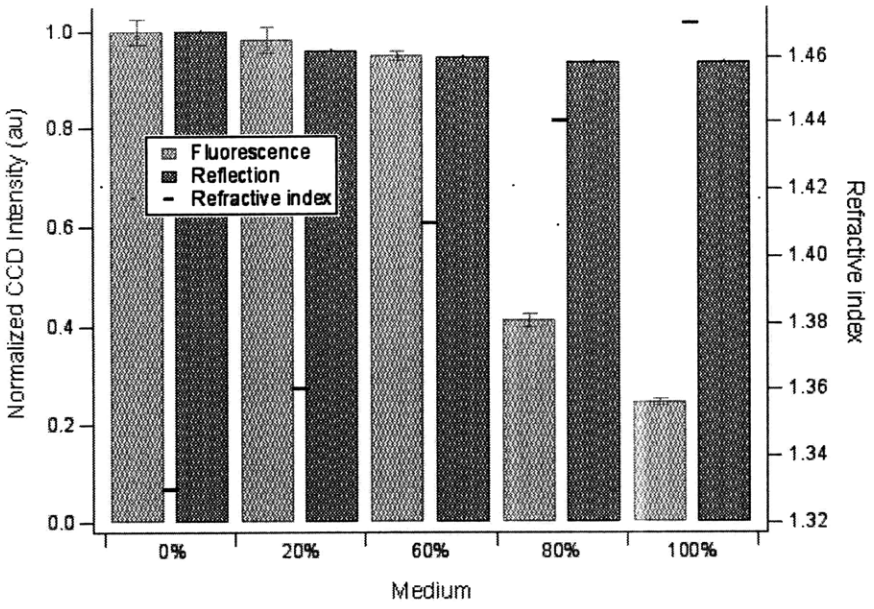

Figure 4-16: The effect of glycerol concentration on fluorescence intensity and reflection. Intensity decreases with increasing glycerol concentrations showing an opposite trend from the bulk observation (strong increase in fluorescence with higher viscosity). This result shows that surface-confined molecules are more sensitive to index of refraction, while sensor molecules free in solution are more sensitive to the viscosity. The corresponding refractive indices are plotted as red dashed on the right axis to show the reverse relationship. Intensities from the reflection image are shown as a control. Reflection image is generated by an independent process and is thus insensitive to the different solutions (unlike with cells, where very similar features were observed).

indices.

We observed intensity decreases with higher refraction index. We previously showed in bulk solution that the the intensity of the DNA-dye sensor molecules is strongly dependent on viscosity. The intensity increases with with increasing concentrations of glycerol and thus with higher viscosity. It is important to note that this relationship is reversed for sensor molecules that are confined to the surface. This result may relate to the reduced degrees of freedom available to surface confined molecules. Molecules immobilized on a cover slip surface are less sensitive to increases in viscosity which, in bulk solution experiments, increase the activation energy of the cis-trans isomerization and consequently the fluorescence lifetime and quantum yield. The sensitivity to index of refraction dominates at the surface. The surface fluo-

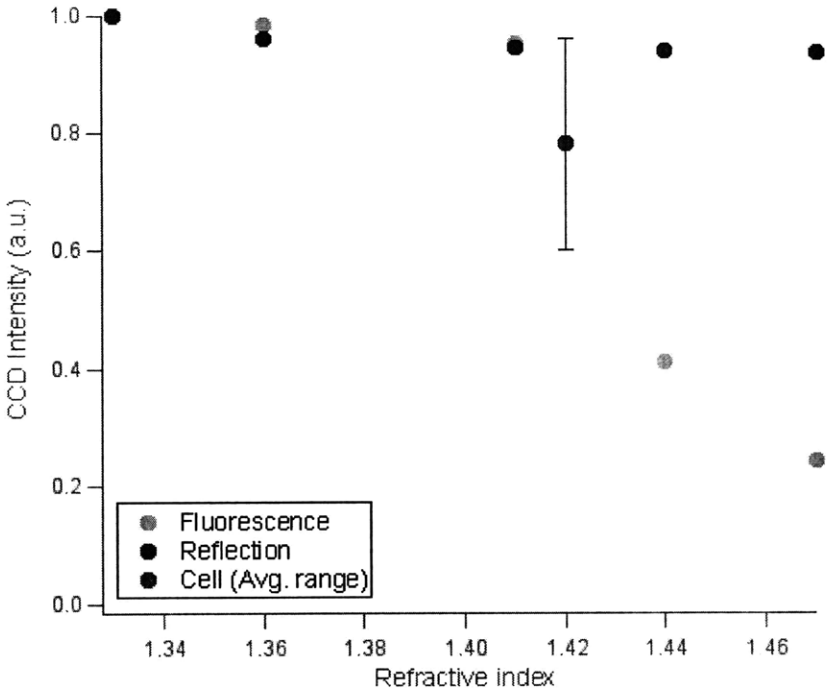

Figure 4-17: Fluorescence intensity decreases with increasing refractive index. The refractive index of glycerol increases non-linearly with glycerol concentration. Intensity also experiences a stronger decrease with higher glycerol concentrations (indices of refraction). Gray circles show the reflection control, unaffected by index. Orange circles show fluorescence intensities decreasing with increasing index, and the red circle shows the average index of a cell with the range representing percent decrease in surface intensity we observe for regions occupied by adhered cells.

rescence sensitivity to refractive index is likely the most significant reporter of cell proximity.

The enhanced environmental sensitivity of DNA-Cy3 reporter complex provides several advantages to measuring the cell-substrate interface. The most significant of these is the ability to access cell-biomaterial interactions at thin layers further from the surface. Confinement to the cover slip surface is also not critical. In the case of reflection microscopy and TIRF, measurements are restricted to 150 and 200nm from the coverslip surface, respectively. Our molecular sensor approach falls in the range available to epi-illumination. It is not limited to the cover slip surface and, with a comparably high magnification objective, and imaging range of several millimeters. Similarly, distance sensitive techniques, such as FRET and quenching report on a shorter range with high sensitivity within that dynamic (not surface-limited) range.

The geometry of this reporter system is well controlled. The assay is prepared independently of the experiment, and the probability of a match between the fluorescent and quenching entities is good. Furthermore, the high initial signal serves as an excellent internal reference for the system. These properties, offer an advantage over fluorescence methods that are limited by statistical probability of an interaction occurring to register a response signal. The high sensitivity at several nanometer length scales is comparable to FRET but not restricted to an acceptor of specific spectral overlap. Furthermore, no special optical reconfiguration is necessary and the chemistry is straightforward to adapt. As a result, the cell-surface interaction for thicker materials (e.g. with different compliances) can be examined through fairly simple extension of the assay we described.

Bibliography

[1] Tahsin Oguz Acarturk, Margaret M. Peel, Patricia Petrosko, William LaFramboise, Peter C. Johnson, and Paul A. DiMilla. Control of attachment, morphology, and proliferation of skeletal myoblasts on silanized glass. *Journal of Biomedical Materials Research*, 44(4):355–370, 1999.

[2] Christian Albrecht, Kerstin Blank, Mio Lalic-Multhaler, Siegfried Hirler, Thao Mai, Ilka Gilbert, Susanne Schiffmann, Tom Bayer, Hauke Clausen-Schaumann, and Hermann E. Gaub. DNA: A Programmable Force Sensor. *Science*, 301(5631):367–370, 2003.

[3] Erich Sackmann Ana-Sunana Smith. Progress in mimetic studies of cell adhesion and the mechanosensing. *ChemPhysChem*, 10(1):66–78, 2009.

[4] Ebbe S. Andersen, Morten M. Dong, Mingdongand Nielsen, Kasper Jahn, Ramesh Subramani, Wael Mamdouh, Monika M. Golas, Bjoern Sander, Holger Stark, Cristiano L. P. Oliveira, Jan Skov Pedersen, Victoria Birkedal, Flemming Besenbacher, Kurt V. Gothelf, and Jorgen Kjems. Self-assembly of a nanoscale DNA box with a controllable lid. *Nature*, 459:73–76, 2009.

[5] Yusuke Arima and Hiroo Iwata. Effects of surface functional groups on protein adsorption and subsequent cell adhesion using self-assembled monolayers. *Journal of Materials Chemistry*, 17(38):4079–4087, 2007.

[6] Nathalie Q. Balaban, Ulrich S. Schwarz, Daniel Riveline, Polina Goichberg, Gila Tzur, Ilana Sabanay, Diana Mahalu andSam Safran, Alexander Bershadsky, Lia Addadi, and Benjamin Geiger. Force and focal adhesion assembly: a close relationship studied using elastic micropatterned substrates. *Nature*, 3, 2001.

[7] Andrs J. Garca Benjamin G. Keselowsky, David M. Collard. Surface chemistry modulates fibronectin conformation and directs integrin binding and specificity to control cell adhesion. *Journal of Biomedical Materials Research Part A*, 66A(2):247–259, 2003.

[8] SC. Blanchard, HD. Kim, RL. Jr. Gonzalez, JD. Puglisi, and Chu S. tRNA dynamics on the ribosome during translation. *Proc Natl Acad Sci U S A.*, 101(35):12893–12898, August 2004.

[9] Steven M. Block, Charles L. Asbury, Joshua W. Shaevitz, and Matthew J. Lang. Probing the kinesin reaction cycle with a 2d optical force clamp. *PNAS*, 100, 2003.

[10] Steven M. Block, Charles L. Asbury, Joshua W. Shaevitz, and Matthew J. Lang. Probing the kinesin reaction cycle with a 2D optical force clamp. *Proceedings of the National Academy of Sciences of the United States of America*, 100(5):2351–2356, 2003.

[11] S. Brasselet and W. E. Moerner. Fluorescence Behavior of Single Molecule pH -Sensors. *Single Molecules*, 1(1), 2000.

[12] R. R. Brau, J.M. Ferrer, P. B. Tarsa, P. Lee, D.C. Appleyard, and M.J. Lang. Reducing enhanced photobleaching forcombined, coincident optical weezers and single molecule fluorescence. *Biophysical Journal*, 91(3), 2006.

[13] Jeffrey S. Burmeister, Lauri A. Olivier, W. M. Reichert, and George A. Truskey. Application of total internal reflection fluorescence microscopy to study cell adhesion to biomaterials. *Biomaterials*, 19(4-5):307 – 325, 1998.

[14] Kevin Burton and Lansing Taylor. Traction forces of cytokinesis measured with optically modified elastic substrata. *Nature*, 385, 1997.

[15] Carlos Bustamante, Yann R. Chemla, Nancy R. Fode, and David Izhaky. Mechanical processes in biochemistry. *Annual Reviews of Biochemistry*, 73, 2004.

[16] Carlos Bustamante, Jed Macosko, and Gijs Wuite. Grabbing the cat by the tail: Manipulating molecules one by one. *Nature Reviews Moleclar Cell Biology*, 1(2), 2000.

[17] Ciro Cecconi, Elizabeth A. Shank, Carlos Bustamante, and Susan Marqusee. Direct Observation of the Three-State Folding of a Single Protein Molecule. *Science*, 309(5743):2057–2060, 2005.

[18] Yann R. Chemis, K. Aathavan, Jens Michaelis, Shelley Grimes, Paul J. Jardine, Dwight L. Anderson, and Carlos Bustamante. Mechanism of Force Generation of a Viral DNA Packaging Motor. *Cell*, 122, 2005.

[19] Liaohai Chen, Duncan W. McBranch, Hsing-Lin Wang, Roger Helgeson, and David G. Whitten Fred Wudl. Highly sensitive biological and chemical sensors based on reversible fluorescence quenching in a conjugated polymer. *PNAS*, 96(22), 1999.

[20] Yu Chen, Dehong Hu, Erich R. Vorpagel, and H. Peter Lu. Probing single-molecule t4 lysozyme conformational dynamics by intramolecular fluorescence energy transfer. *The Journal of Physical Chemistry B*, 107:7947–7956, 2003.

[21] A. S. G Curtis. Cell reactions with biomaterials: The microscopies. *European Cells and Materials*, 1:59–65, 2001.

[22] A.S.G. Curtis and C.D.W. Wilkinson. Reactions of cells to topography. *Journal of Biomaterials Science*, 9:1313–1329, 1998.

[23] Olivia du Roure, Alexandre Saez, Axel Buguin, Robert H. Austin, Philippe Chavrier, Pascal Silberzan, and Benoit Ladoux. Force mapping in epithelial cell migration. *PNAS*, 102(7):2390–2395, 2005.

[24] B. Essevaz-Roulet, U. Bockelmann, and F. Heslot. Mechanical separation of the complementary strands of DNA. *PNAS*, 94, 1997.

[25] Yoshio Fukui, Taro Q. P. Uyeda, Chikako Kitayama, and Shinya Inoue. How well can an amoeba climb? *PNAS*, 97(18):10020–10025, 2000.

[26] Catherine G. Galbraith and Michael P. Sheetz. A micromachined device provides a new bend on fibroblast traction forces. *PNAS*, 94(17):9114–9118, 1997.

[27] Jeff Gore, Zev Bryant, Michael D. Stone, Marcelo Nöllmann, Nicholas R. Cozzarelli, and Carlos Bustamante. Mechanochemical analysis of DNA gyrase using rotor bead tracking. *Nature*, 439, 2006.

[28] Wei-Hui Guo, Margo T. Frey, Nancy A. Burnham Burnham, and Yu-Li Wang. Substrate rigidity regulates the formation and maintenance of tissues. *Biophysical Journal*, 90(6), 2006.

[29] T. Ha, T. Enderle, DF. Ogletree, DS. Chemla, PR. Selvin, and S. Weiss. Probing the interaction between two single molecules: fluorescence resonance energy transfer between a single donor and a single acceptor. *Proc Natl Acad Sci U S A.*, 93(13):6264–8, 1996.

[30] Bjorn M. Reinhard Hari Shroff, Merek Siu, Harish Agarwal, Andrew Spakowitz, and Jan Liphardt. Biocompatible force sensor with optical readout and dimensions of 6 nm^3. *NanoLetters*, 5(7), 2005.

[31] AK Harris, P Wild, and D Stopak. Silicone rubber substrata: a new wrinkle in the study of cell locomotion. *Science*, 208(4440):177–179, 1980.

[32] Thomas Heinlein, Jens-Peter Knemeyer, Oliver Piestert, and Markus Sauer. Photoinduced Electron Transfer between Fluorescent Dyes and Guanosine Residues in DNA-Hairpins. *The Journal of Physical Chemistry B*, 107(31):7957–7964, 07 2003/07/04/.

[33] Sungchul Hohng and Taekjip Ha. Single-molecule quantum-dot fluorescence resonance energy transfer. *ChemPhysChem*, 6(5):956–960, 2005.

[34] Sungchul Hohng, Chirlmin Joo, and Taekjip Ha. Single-Molecule Three-Color FRET. *Biophysical Journal*, 87(2):1328–1337, 2004.

[35] Jonathon Howard. *Mechanics of Motor Proteins and the Cytoskeleton.* Sinauer Associates, February 2001.

[36] Akihiko Ishijima, Hiroaki Kojima, Takashi Funatsu, Makio Tokunaga, Hideo Higuchi, Hiroto Tanaka, and Toshio Yanagida. Simultaneous observation of individual ATPase and mechanical events by a single myosin molecule during interaction with actin. *Cell*, 92(2):161–171, 1998.

[37] Akira Katsumi, A. Wayne Orr, Eleni Tzima, and Martin Alexander Schwartz. Integrins in mechanotransduction. *Journal of Biological Chemistry*, 279(13), 2004.

[38] Ben-Zion Katz, Eli Zamir, Alexander Bershadsky, Zvi Kam, Kenneth M. Yamada, and Benjamin Geiger. Physical state of the extracellular matrix regulates the structure and molecular composition of cell-matrix adhesions. *Mol. Biol. Cell*, 11(3):1047–1060, 2000.

[39] Mikls S. Z. Kellermayer, Steven B. Smith, Henk L. Granzier, and Carlos Bustamante. Folding-unfolding transitions in single titin molecules characterized with laser tweezers. *Science*, 276, 1997.

[40] Philip E. Hockberger Kevin E. Healy, Barbara Lom. Spatial distribution of mammalian cells dictated by material surface chemistry. *Biotechnology and Bioengineering*, 43(8):792–800, 1994.

[41] Harold D. Kim, G. Ulrich Nienhaus, Taekjip Ha, Jeffrey W. Orr, James R. Williamson, and Steven Chu. Mg2+-dependent conformational change of RNA studied by fluorescence correlation and FRET on immobilized single molecules. *Proceedings of the National Academy of Sciences of the United States of America*, 99(7):4284–4289, 2002.

[42] Efrosini Kokkoli, Sarah E. Ochsenhirt, and Matthew Tirrell. Collective and single-molecule interactions of 51 integrins. *Langmuir*, 20:2397 – 2404, 2004.

[43] H. J. Kong, T.R. Polte, E. Alsberg, and D.J. Mooney. FRET measurements of cell-traction forces and nanoscale clustering of adhesion ligands varied by substrate stiffness. *PNAS*, 102(12), 2005.

[44] Hyun Joon Kong, Tanyarut Boontheekul, and David J. Mooney. Quantifying the relation between adhesion ligandreceptor bond formation and cell phenotype. *Proceedings of the National Academy of Sciences*, 103(49):18534–18539, 2006.

[45] Joseph R. Lakowicz. *Principles of Fluorescence Spectroscopy.* Springer 2nd edition, 1999.

[46] Matthew J Lang, Polly M Fordyce, Anita M Engh, Keir C Neuman, and Steven M Block. Simultaneous, coincident optical trapping and single-molecule fluorescence. *Nat Meth*, 1:133–139, 2004.

[47] Douglas A. Lauffenburger and Alan F. Horwitz. Cell migration: A physically integrated molecular process. *Cell*, 84, 1996.

[48] C. A. Leatherdale, W.-K. Woo, F. V. Mikulec, and M. G. Bawendi. On the absorption cross section of CdSe nanocrystal quantum dots. *The Journal of Physical Chemistry B*, 106(31):7619–7622, 2002.

[49] Mark H. Lee, David A. Brass, Ronit Morris, Russell J. Composto, and Paul Ducheyne. The effect of non-specific interactions on cellular adhesion using model surfaces. *Biomaterials*, 26(14):1721 – 1730, 2005.

[50] P. P. Lehenkari and M. A. Horton. Single integrin molecule adhesion forces in intact cells measured by atomic force microscopy. *Biochemical and Biophysical Research Communications*, 259(3):645 – 650, 1999.

[51] Hongbin Li, Mariano Carrion-Vazquex, Andres F. Oberhauser, Piotr E. Marszalek, and Julio M. Fernandez. Point mutations alter the mechanical stability of immunoglobulin modules. *Nature Structural Molecular Biology*, 7(12), 2000.

[52] Song Li, Jun-Lin Guan, and Shu Chien. Biochemistry and biomechanics of cell motility. *Annual Review of Biomedical Engineering*, 7(1):105–150, 2005.

[53] Wolfgang A. Linke, Marc Ivemeyer, Peter Mundel, Marc R. Stockmeier, and Bernhard Kolmerer. Nature of pevk-titin elasticity in skeletal muscle. *PNAS*, 95(14):8052–8057, 1998.

[54] Jan Liphardt, Bibiana Onoa, Steven B. Smith, Jr. Tinoco, Ignacio, and Carlos Bustamante. Reversible Unfolding of Single RNA Molecules by Mechanical Force. *Science*, 292(5517):733–737, 2001.

[55] Julie C. Liu and David A. Tirrell. Cell response to rgd density in cross-linked artificial extracellular matrix protein films. *Biomacromolecules*, 9(11):2984–2988, 2008.

[56] Guobin Luo, Mina Wang, William H. Konigsberg, and X. Sunney Xie. Single-molecule and ensemble fluorescence assays for a functionally important conformational change in T7 DNA polymerase. *Proceedings of the National Academy of Sciences*, 104(31):12610–12615, 2007.

[57] Rief M., Pascual J., Saraste M., and Gaub H.E. Single molecule force spectroscopy of spectrin repeats: Low unfolding forces in helix bundles. *Journal of Molecular Biology*, 286, 1999.

[58] John F. Marko and Eric D. Siggia. Stretching DNA. *Macromolecules*, 28, 1995.

[59] S.A.E. Marras, F.R. Kramer, and S. Tyagi. Efficiencies of fluorescence resonance energy transfer and contact mediated quenching in oligonucleotide probes. *Nucleic Acids Research*, 30(21), 2002.

[60] Melissa Massey, W. Russ Algar, and Ulrich J. Krull. Fluorescence resonance energy transfer (fret) for dna biosensors: Fret pairs and forster distances for various dye-dna conjugates. *Analytica Chimica Acta*, 568(1-2):181 – 189, 2006. Molecular Electronics and Analytical Chemistry.

[61] Sean A. McKinney, Alasdair D. J. Freeman, David M. J. Lilley, and Taekjip Ha. Observing spontaneous branch migration of Holliday junctions one step at a time. *Proceedings of the National Academy of Sciences of the United States of America*, 102(16):5715–5720, 2005.

[62] Atusshi Miyawaki, Juan Liopis, Roger Heim, Michael J. McCaffery, Joseph A. Adams, Mitsuhiko Ikura, and Roger Y. Tsien. Fluorescent indicators for ca^{2+} based on green fluorescent proteins and calmodulin. *Nature*, 388, 1997.

[63] Steven Munevar, Yu-Li Wang, and Micah Dembo. Traction force microscopy of migrating normal and h-ras transformed 3t3 fibrolasts. *Biophysical Journal*, 80, 2001.

[64] Kier C. Neuman and Steven M. Block. Optical trapping. *Review of Scientific Instruments*, 75(9):2787–2809, 2004.

[65] David G. Norman, Richard J. Grainger, Dusan Uhrin, and David M. J. Lilley. Location of Cyanine-3 on Double-Stranded DNA: Importance for Fluorescence Resonance Energy Transfer Studies. *Biochemistry*, 39(21):6317–6324, 05 2000/05/05/.

[66] Aandres F. Oberhauser, Piotr E. Marszaleki, Harold P. Erickson, and Julio M. Fernandez. The molecular elasticity of the extracellular matrix protein tenascin. *Nature*, 393, 1998.

[67] MD Pierschbacher, E Ruoslahti, J Sundelin, P Lind, and PA Peterson. The cell attachment domain of fibronectin. Determination of the primary structure. *J. Biol. Chem.*, 257(16):9593–9597, 1982.

[68] H. Raghuraman and A. Chattopadhyay. Organization and dynamics of melittin in environments of graded hydration: A fluorescence approach. *Langmuir*, 19(24), 2003.

[69] Suman Ranjit, Kaushik Gurunathan, and Marcia Levitus. Photophysics of Backbone Fluorescent DNA Modifications: Reducing Uncertainties in FRET. *The Journal of Physical Chemistry B*, 113(22):7861–7866, 03 2009/03/26/.

[70] Matthia Reif, Hauke Clausen-Schaumann, and Herman E. Gaub. Sequence-dependent mechanics of single DNA molecules. *Nature Structural Biology*, 6(4), 1999.

[71] Matthias Rief, Mathias Gautel, Filipp Oesterhelt, Julio M. Fernandez, and Hermann E. Gaub. Reversible unfolding of individual titin immunoglobulin domains by afm. *Science*, 276, 1997.

[72] Matthew E. Sanborn, Brian K. Connolly, Kaushik Gurunathan, and Marcia Levitus. Fluorescence Properties and Photophysics of the Sulfoindocyanine Cy3 Linked Covalently to DNA. *The Journal of Physical Chemistry B*, 111:11064–11074, 08 2007.

[73] U. S. Schwarz, N. Q. Balaban, D. Riveline, A. Bershadsky, B. Geiger, and S. A. Safran. Calculation of Forces at Focal Adhesions from Elastic Substrate Data: The Effect of Localized Force and the Need for Regularization. *Biophys. J.*, 83(3):1380–1394, 2002.

[74] N. C. Seeman. An overview of structural DNA nanotechnology. *Mol. Biotechnol.*, 37:246–257, 2007.

[75] Torsten Strunz, Krisztina Oroszlan, Rolf Schfer, and Hans-Joachim Gntherodt. Dynamic force spectroscopy of single DNA molecules. *Proceedings of the National Academy of Sciences of the United States of America*, 96(20):11277–11282, 1999.

[76] John L. Tan, Joe Tien, Dana M. Pirone, Darren S. Gray, Kiran Bhadriraju, and Christopher S. Chen. From the Cover: Cells lying on a bed of microneedles: An approach to isolate mechanical force. *PNAS*, 100(4):1484–1489, 2003.

[77] Peter B. Tarsa, Ricardo R. Brau, Mariya Barch, Jorge M. Ferrer, Yelena Freyzon, Paul Matsudaira, and Matthew J. Lang. Detecting Force-Induced molecular transitions with fluorescence resonant energy transfer13. *Angewandte Chemie International Edition*, 46(12):1999–2001, 2007.

[78] Olivier Thoumine, Albrecht Ott, Olivier Cardoso, and Jean-Jacques Meister. Microplates: a new tool for manipulation and mechanical perturbation of individual cells. *Journal of Biochemical and Biophysical Methods*, 39(1-2):47 – 62, 1999.

[79] A.Y. Ting, K. H. Klemke, and R. Y. Tsien. Genetically encoded fluorescent reporters of protein tyrosine kinase activities in living cells. *PNAS*, 98, 2001.

[80] Masaki Torimura, Shinya Kurata, Kazutaka Yamada, Toyokazu Yokomaku, Yoichi Kamagata, Takahiro Kanagawa, and Ryuichiro Kurane. Fluorescence-quenching phenomenon by photoinduced electron transfer between a fluorescent dye and a nucleotide base. *Analytical Sciences*, 17(1):155–160, 2001.

[81] GA Truskey, JS Burmeister, E Grapa, and WM Reichert. Total internal reflection fluorescence microscopy (TIRFM). II. Topographical mapping of relative cell/substratum separation distances. *J Cell Sci*, 103(2):491–499, 1992.

[82] L. Tskhovrebova, J. Trinick, J. A. Sleep, and R. M. Simmons. Elasticity and unfolding of single molecules of the giant muscle protein titin. *Nature*, 387, 1997.

[83] Ching-Hsuan Tung, Jonathan Rudolph, and Stanley Stein. Preparation of oligonucleotide-peptide conjugates. *Bioconjugate Chemistry*, 2, 1991.

[84] Meindert A. van Dijk, Lukas C. Kapitein, Joost van Mameren, Christoph F. Schmidt, and Erwin J. G. Peterman. Combining optical trapping and Single-Molecule fluorescence spectroscopy: Enhanced photobleaching of fluorophores. *The Journal of Physical Chemistry B*, 108(20):6479–6484, May 2004.

[85] M. P. I. Vandamme, J. Tiglias, N. Nemat, and B. N. Preston. Determination of the charge content at the surface of cells using a colloid titration technique. *Analytical Biochemistry*, 223(1):62 – 70, 1994.

[86] Stuart L. Cooper Vassiliki A. Tegoulia. Leukocyte adhesion on model surfaces under flow: Effects of surface chemistry, protein, adsorption, and shear rate. *Journal of Biomedical Materials Research*, 50(3):291–301, 2000.

[87] Natarajan Venkatesan and Byeang Hyean Kim. Peptide conjugates of oligonucleotides: Synthesis and applications. *Cemistry Reviews*, 106, 2006.

[88] Jerker Widengren and Petra Schwille. Characterization of Photoinduced Isomerization and Back-Isomerization of the Cyanine Dye Cy5 by Fluorescence Correlation Spectroscopy. *The Journal of Physical Chemistry A*, 104(27):6416–6428, 06 2000/06/17/.

[89] Michael T. Woodside, Peter C. Anthony, William M. Behnke-Parks, Kevan Larizadeh, Daniel Herschlag, and Steven M. Block. Direct measurement of the full, sequence-dependent folding landscape of a nucleic acid. *Science*, 314(5801):1001–1004, 2006.

[90] Michael T. Woodside, William M. Behnke-Parks, Kevan Larizadeh, Kevin Travers, Daniel Herschlag, and Steven M. Block. Nanomechanical measurements of the sequence-dependent folding landscapes of single nucleic acid hairpins. *PNAS*, 103(16), 2006.

[91] Ahmet Yildiz, Joseph N. Forkey, Sean A. McKinney, Taekjip Ha, Yale E. Goldman, and Paul R. Selvin. Myosin v walks hand-over-hand: Single fluorophore imaging with 1.5-nm localization. *Science*, 300, 2003.

[92] Xiaowei Zhuang, Laura E. Bartley, Hazen P. Babcock, Rick Russell, Taekjip Ha, Daniel Herschlag, and Steven Chu. A Single-Molecule Study of RNA Catalysis and Folding. *Science*, 288(5473):2048–2051, 2000.